81 p.

LG85ER0012

NASA CONTRACTOR REPORT CR-174845

PTA Testbed Aircraft Engine Inlet Model Test Report

(NASA-CR-174845) PTA TEST BED AIRCRAFT ENGINE INLET MODEL TEST REPORT, REVISED (Lockheed-Georgia Co., Marietta.) 81 p
CSCL 21E G3/07

N87-10866
Unclas
43843

Contract NAS3-24339
January 1985
Revised: May 1985

NASA

[redacted]

LG85ER0012

NASA CONTRACTOR REPORT CR-174845

PTA Testbed Aircraft Engine Inlet Model Test Report

Contract NAS3-24339
January 1985
Revised: May 1985

NASA

LIMITED DISTRIBUTION
This document is released under distribution limitations until

TABLE OF CONTENTS

PRECEDING PAGE BLANK-NOT FILMED

LIST OF FIGURES

PRECEDING PAGE BLANK NOT FILMED

LIST OF FIGURES (CONTD)

NASA CR-174845

PTA TESTBED AIRCRAFT ENGINE INLET MODEL TEST REPORT

SUMMARY

The PTA inlet duct test program was completed in November 1984. The basic test duct was designed using the Lockheed QUADPAN computational code. Test objectives were to experimentally evaluate, modify as required, and eventually verify satisfactory performance, as well as duct/engine compatibility. Two design refinements, a shaft-to-duct fillet fairing and compressor face hub fairing, were combined in various combinations to create a total of four test configurations. Maximum swirl was simulated by inserting a 30-degree wedge between the incoming flow and the duct entrance. Measured data included duct wall pressures, compressor face total and static pressures, and duct airflow. These data were reduced to obtain total pressure recovery for performance evaluation and circumferential, radial, and harmonic distortion for engine compatibility determination. Compressor face, isobar contour maps were also constructed to permit rapid, visual assessment of flow patterns delivered to the engine.

In correlating the duct wall surface pressures, the measured trends were reasonably well predicted by the analytical data. Absolute values of pressure coefficients, however, did not correlate as well as had been hoped, as the negative values of the measured coefficients tended to be underpredicted.

Measured total pressure recovery for the basic duct was 0.993 with no swirl and 0.989 for inflow with a 30-degree simulated swirl angle. This compared to a predicted recovery of 0.979 with no swirl. Measured circumferential distortion with swirl, based on a least-square curve fit of the data, was 0.204 compared to a maximum allowable value of 0.550. Other measured distortion parameters did as well or better relative to their respective maximum allowable values.

Small incremental performance improvements were measured for various combinations of the fillet and hub fairings. Among the combinations examined, the shaft-to-duct fillet fairing alone provided the best overall performance. It delivered a recovery of 0.996 relative to 0.993 for the basic duct and a circumferential distortion of 0.046 compared to 0.128 for the basic duct. Because these differences are small and because the basic duct performance levels are well above target values, the basic duct configuration with no refinements is recommended for the PTA inlet as a minimum cost installation.

INTRODUCTION

It has been demonstrated with small-scale aeroperformance models that the advanced turboprop, or propfan, can deliver propulsive efficiencies close to 20-percent higher than equivalent technology turbofans at cruise Mach numbers in the 0.75 to 0.80 range. These efficiency gains can be translated into fuel savings of the same order of magnitude. Attainment of these benefits, however, depends on efficient installations. To achieve this goal, research on propfans has been underway for about 10 years. Recognizing the importance of inlet and duct performance to this objective, a test program to evaluate inlet ducts designed specifically for propfans was initiated in 1981. Results were published in Reference 1 and were used as input to inlet design for studies under NAS Contract NAS3-22751. Results from this effort were applied to the design of models for testing in the cooperative research program GUN (Gelac/United Technologies/NASA). This program eventually extended into three phases, and a substantial amount of pressure, drag, and propeller blade stress data were obtained. These data, as they became available, were applied to the design of the inlet configuration for the Propfan Test Assessment (PTA) Program.

Analysis of blade stress data from the GUN program indicated that the inlet entry should be moved aft about 10 inches in the full-scale PTA configuration. This resulted in a higher relative duct offset ratio than had been tested in the Reference 1 program, due to other considerations dictating that the engine position be fixed. When the PTA contract was awarded, an inlet duct test was specifically identified as a required task to be performed early in the program. Its purpose was to assure that performance

would be adequate and that compatibility of the inlet duct with the engine could be demonstrated.

TEST OBJECTIVES

The objectives of this test program were to experimentally evaluate, modify as required, and eventually verify satisfactory performance and engine compatibility for the PTA inlet "S" duct configuration. The criteria to be met were based on predicted total pressure recovery and Allison specified limits for engine distortion parameters. Compatibility was to be demonstrated at the extreme combination of maximum engine corrected airflow and maximum anticipated propeller induced swirl angle.

TEST HARDWARE

Engineering drawings for the inlet duct model, test rig, and instrumentation are listed by title and drawing number in Appendix 1. The general arrangement of the model test assembly is shown in Figure 1. The 0.338-scale fiberglass inlet duct is fed by a bellmouth and discharges into the rig entrance, which is a simulated compressor face. Section A-A illustrates the cross-section shape of the inlet throat. Configuration test variables included a shaft-to-duct fillet fairing and an optional new hub fairing, as shown in the figure. A summary of the major dimensions and design features for the basic duct configuration is presented in Figure 2.

The complete test rig with model installed is shown in the photo of Figure 3. Downstream of the simulated compressor face, there is a diffuser followed by a screen. The screen protects the suction fan from foreign object damage and helps smooth out the flow for entrance into the flow measuring section. This section consists of a large diameter, constant area pipe followed by an ASME long radius flow nozzle. The throat of the flow nozzle provides an entrance into the 8.0-inch TD376 fan pumping unit. Aft of the fan exit is a second diffuser to help efficiently discharge the flow to ambient pressure. Power for the TD376 fan is transmitted through a tip turbine which admits air around the periphery of the unit. Approximately two pounds per second of drive air at 150 psig are required to operate the fan at rated capacity.

Details of the model installation itself can be seen in the closeup side view of Figure 4. In a similar view, Figure 5 shows the model installation with a 30-degree turning duct (wedge) inserted between the bellmouth and duct throat. The wedge is designed to simulate a 30-degree swirl angle induced by the propeller at the anticipated worst case operating condition. The photo of Figure 6 shows a right hand, 3/4 front view of the basic installation. Finally, in Figure 7, a view down the entrance to the duct shows total pressure rake installation and the basic hub hardware.

INSTRUMENTATION SUMMARY/DATA ACCURACY

A summary of the test instrumentation and estimated accuracies is included in Figure 8. The primary measurements were made at the compressor face plane. The basic total pressure instrumentation consisted of six, equally spaced rakes with five area weighted probes each. In addition, there were six single probes interspersed between rakes at the Ring No. 2 radius (see Figure 9). This layout is detailed in the drawing entitled "Rake - D and A" (Appendix 1). A simplified illustration of the layout is presented in Figure 9.

Just forward of the compressor face, on the duct surface, there were six equally spaced static pressure taps. In order to avoid possible interference with the readings, these taps were displaced circumferentially to lie between the total pressure rakes. The "S" duct diffuser model was instrumented with top, side, and bottom rows of static pressure taps. Both the compressor face and duct wall static pressure tap patterns are detailed in the drawing entitled "Pressure Tube Instl" (Appendix 1). The key details regarding the installation of the static pressure taps are presented in Figure 10. There was also an inspection window with a wide angle lens installed just aft of the first bend in the duct.

The flow measuring section in the inlet test rig was instrumented as normally done for a standard ASME flow nozzle. There were two static taps in the constant area section and two taps in the nozzle throat. There was also one thermocouple in the upstream constant area section for use as a check on flow total temperature.

Miscellaneous additional instrumentation included ambient pressure, ambient temperature, and fan drive pressure. The latter pressure was the actual means by which fan rpm/airflow was set for test purposes. A curve of duct airflow versus fan drive pressure was generated for use in setting a series of prescribed test conditions.

DATA ACQUISITION AND REDUCTION EQUIPMENT

Pressure data were acquired in the standard manner using a scanivalve, pressure transducer arrangement. A TI990 computer was utilized for on-line processing of the acquired data. In conjunction with this computer system, a plotter was set up to generate a limited number of plots for initial assessment of duct performance.

Data from the static pressure taps in the flow-measuring section were processed in the same manner as the total pressure data from the compressor face. To obtain the delta pressures in the flow nozzle, however, a very sensitive, low-range pressure transducer was utilized to assure maximum accuracy.

TEST FACILITIES

Testing was conducted in the outdoor test area adjacent to the Lockheed Pneumatics Laboratory test facility. Drive air was available at the required pressure and temperature to operate the fan up to and well above its rated capacity. Experienced personnel permanently assigned to the Pneumatics Laboratory supported the test effort and assured the timely delivery of data tapes.

TEST TECHNIQUES

A proven, calibrated test rig powered by a pneumatically driven, 8.0-inch diameter TD376 fan was employed to pump air through a 0.338-scale PTA "S" duct model. Forward of the inlet throat, a bellmouth was utilized in place of the standard PTA inlet lip. This arrangement delivered essentially 100-percent recovery airflow to the duct entry and permitted evaluation of the

duct itself in isolation. A 30-degree turning duct, or wedge, was fabricated for installation between the bellmouth and the throat in order to simulate peak swirl induced by worst case operation of the propeller.

Data from the total pressure rakes, as described earlier, provided the input for the computation of total pressure recovery and the various distortion parameters defined by Allison in Reference 2. When used in conjunction with the compressor face static pressure taps, Mach number and flow rate could also be determined. Three longitudinal rows of static pressure taps along the key duct surfaces provided data for correlation with theoretical pressures already generated. One strategically placed peephole with a high-angle lens was installed in the duct wall. This provided a means of observing tuft behavior and confirming the locations of separated regions.

TEST PROCEDURES AND VERIFICATION OF MEASUREMENTS

The general procedure for a given configuration arrangement was to run a series of airflows in both ascending and descending order to define the performance characteristic curves. A basic set of duct performance/distortion characteristics was defined by running with a minimum diameter shaft cover and no lower surface, shaft-to-duct fillet fairing. Other geometric combinations included runs with the fillet fairing installed, and also with an improved hub fairing at the compressor face, and then, with both new fairings simultaneously.

A summary of the entire run program is presented in Figure 11. The first four runs covered all combinations of the internal design refinements. The fifth run was made with the 30-degree wedge for swirl simulation. Run No. 7 was a repeat of Run No. 5 after a complete teardown and reassembly of the test setup. Run Nos. 6 and 8 were contingency runs made to examine the potential of either vortex generators or a vane to control throat separation. As it turned out, this problem did not materialize, so the data for Runs 6 and 8 were not reduced and evaluated.

Most of the planning of test procedures had been concerned with the diagnosis and solving of problems, when and if they occurred. After the testing began,

it soon became evident that duct performance would exceed expectations by a generous margin. The primary problem, then, became one of verifying the validity of the better-than-predicted test results. Three approaches were taken to accomplish this objective. These approaches, listed below, are described in the paragraphs that follow.

1. Verify pressure data accuracy by recalibration against a known source.
2. Verify airflow data accuracy using previous calibrations and different computation methods.
3. Attach a network of tufts to the inside duct surface and visually verify that the flow is attached to the surface.

Pressure Data - Using a calibrated manometer, the pressure transducers were calibrated across the operational range. Incrementally increasing pressures followed by incrementally decreasing pressures were imposed upon the transducers, and a least square curve fit of the results was generated. Suction pressures of 40 inches of water were then imposed on each of the pressure ports in succession. Leakage, when it occurred, was eliminated either by replumbing the lines or servicing the scanivalve itself, as necessary. Reference pressures were recorded and displayed at the beginning and ending of each run. If a zero shift of more than 0.02 inches of water was indicated, the case was rerun.

Airflow Data - A special one-pound per square inch transducer was used to measure differential static pressure data for the ASME long radius flow nozzle that preceded the 8.0-inch fan pumping system. This assured that operation would be at a fairly high percentage of maximum range. A total of four methods was used to calculate airflow--three of these were based on the ASME flow nozzle data and the fourth was based on compressor face pressure readings. The cornerstone of the methodology was the ASME procedure taken directly from Reference 3. The second and third methods were calibrations against standard orifice plate measuring sections as performed by different teams at different times in the past. Compressor face Mach number, obtained from the totals and statics at that station, was used to compute the fourth value of airflow. The compressor face and ASME computed airflows agreed almost exactly. Airflows from the calibrations ran from 3- to 4-percent

higher than the ASME and compressor face calculated values. Because of the time that had passed since the calibrations had been performed and because of the close agreement between the ASME and compressor face computed airflows, the ASME airflows were selected for use in generating the performance plots. Some weight was also given to the fact that, if an error exists, it is desirable that the airflow be on the low side, since low readings of airflow during test will result in higher values being quoted for the pressure loss and distortion parameters at the correct flow conditions.

Flow Visualization - The use of tufting for the purpose of flow visualization is particularly well suited for verifying the kind of high performance level obtained for the PTA duct test configuration. If significant separation existed, it would be hard to define the degree of it by observing tuft behavior. With a high performance configuration, however, it should be a simple matter to verify that the flow is essentially unseparated. For this installation, that is the procedure that was followed. A generous pattern of wool tufts was affixed to the upper, side, and lower surfaces of the duct wall between the throat and compressor face. Runs were made at two airflows--maximum and 50 percent. Observations were made through the wide angle lens in the duct wall as well as through the inlet entry. Both the test engineer and a NASA representative were present for the test.

The conclusions of the observers were that the tuft behavior confirmed the relatively high performance levels measured for the duct. At 50-percent airflow, all tufts except the one located just beneath the shaft were found to be well behaved and appeared to be lying essentially flat against the duct wall surface. At maximum airflow, the result was essentially the same, except that the stability of the tuft directly beneath the shaft had visibly improved.

SUMMARY OF PROBLEMS AND CORRECTIVE ACTIONS

Although there were no problems in meeting the target values for the various performance/distortion parameters, there were some minor operational problems encountered during the conduct of the test. The most serious of these was rake failure that occurred on two separate occasions. On the first occasion,

two rakes failed while the flow was being increased substantially above the PTA installation design value. The rake stiffeners failed at the roots, and the tubes bent backward aft of the compressor face and out of position. As closely as could be determined, the failure occurred while the compressor face Mach number was being increased above 0.48. The two rakes were repaired and were beefed-up substantially from their original design. From that point on, inlet flow was limited to a value slightly below the flow rate at which the failure occurred. On the second occasion, two more rakes failed during the first run being made with the 30-degree wedge in place. This time failure occurred at a compressor face Mach number of just under 0.44. When the fix was performed, the two failed rakes were repaired, and these, plus all the remaining rakes, were beefed-up substantially. No more failures occurred during the testing.

One other structural failure occurred when two of the four attachments for the throat vane, which was being tested as a potential separation fix, broke off at the duct wall surface. Since, by this time, it had become evident that a separation fix would not be required, the vane was not repaired and the test was terminated.

Other problems that occurred during the conduct of the testing were more or less routine in nature. Leaks and/or blockages in the pressure tubes did occur from time to time, but the only significant results were minor delays in the completion of the test program. If the failure occurred in the critical compressor face instrumentation, the policy was to make the repair and repeat the run. If only the duct wall instrumentation was involved, then the repair was made after the run was completed, and the particular probe involved was simply deleted before the data was plotted.

SUMMARY OF TEST RESULTS

The basic PTA duct plus a number of design refinements were examined during the test program. A design point ($M_{cf} = 0.36$) comparison of total pressure recovery and circumferential distortion for each of the important test configurations is shown in the following table:

Configuration	Recovery	Cir Dist
Basic Duct + Fillet	0.996	0.046
BD + Fillet + New Hub	0.995	0.102
Basic Duct + New Hub	0.994	0.117
Basic Duct	0.993	0.128

As the table shows, the tested refinements resulted in small improvements in performance. The basic PTA inlet duct with no additions met or exceeded all objectives established prior to conduct of the test. The comparison of measured to target levels for key parameters that describe the performance of the basic inlet duct design is shown below:

Parameter	Measured (No Swirl)	Measured (30-Deg Swirl)	Target
Recovery	0.993	0.989	0.979
Circum. Distortion	0.128	0.204	0.550
Radial Distortion	0.017	0.050	0.375
Harmonic Distortion	0.12	0.17	1.6
(A1 thru A4)	0.08	0.16	0.32
	0.04	0.12	0.20
	0.03	0.05	0.20

For recovery with no swirl, the target level of 0.979 was established based on a duct loss analysis conducted using SAE Handbook data (Reference 4) and an in-house test described in Reference 1. The recovery of 0.993 that was actually measured represents a total pressure loss of one-third the target value.

The target levels for distortion parameters were the acceptable limits specified by Allison in Reference 2. These levels had to be met at all operating conditions, including the extreme case of 30 degrees entry swirl. As shown in the table above, there are no cases where measured distortion parameters exceed 60 percent of the target values.

DISCUSSION

The duct design analysis, correlations of wall pressure data, and test results in terms of both recovery and distortion are discussed in detail in the following paragraphs.

Duct Design Analysis

The starting point for the design analysis was a longer duct with the inlet located close behind the propfan. Wind tunnel tests, however, showed that this inlet location produced unacceptably high blade dynamic stresses. Other tests performed after submission of the PTA proposal to NASA indicated that increasing the separation between the propeller and inlet entry by 10 inches would alleviate the problem. Several methods of doing this were examined, but it was eventually determined that the most practical approach was to shift the inlet throat aft by 10 inches, thereby compressing the duct length by that same amount, since the position of the engine had to remain fixed in the PTA design because of other considerations. The external forebody contour would remain essentially the same, but would be slightly refaired to the nacelle maximum cross-section. No change would be made to the internal lip or throat, either in shape or in area. Because of the gradual expansion of the fairing behind the spinner, however, there would be some reduction in the height of the boundary layer diverter. The decision was made to follow this approach, so the challenge became one of refining the duct design to obtain at least the same or, possibly, better performance than the longer configuration.

The change to a shorter duct rendered the consideration of internal diffusion even less desirable, since a high offset ratio and internal diffusion tend to combine in an unfavorable manner. Earlier in the design process, the decision had been made to go with an essentially constant area duct and accomplish the required diffusion within the pre-entry streamtube. The risk of incurring a serious drag penalty from this approach was believed to be low, based on the findings presented in Figure 15, page 6 of Reference 5. These findings showed that for an installation similar to the PTA, little or no penalty in overall, apparent thrust minus drag results from reducing mass flow ratio well below the design value.

The design analysis of duct geometry was performed using the Lockheed QUADPAN program. This is a panel program for steady subsonic potential flow about arbitrary configurations. It is a small perturbation-type program, which means that as Mach number is increased, the permissible

value of any given perturbation diminishes, if accuracy is to be maintained. Its application is limited to attached flow, but in most cases, it can provide the guidance required to define a shape that has little or no separation.

A panel model of the basic duct design after refinement is shown in Figure 12. This configuration has the basic hub supplied by Allison, but there is a fillet to smooth out the flow below the shaft-duct intersection. Panels normal to the flow direction are shown at both the throat and compressor face stations. These are permeable panels for which the leakage can be specified in order to simulate internal flow. In this case, permeability was specified for the compressor face panels only, and continuity was specified to set the throat panel velocities. This is an accurate simulation of the real case, where compressor face pumping defines the flow characteristics through the front end of the duct.

The internal pressure distributions for the initial, longer configuration are shown in Figure 13. As would be expected, a moderately severe negative pressure peak, followed by an adverse pressure gradient, is seen along the lower surface aft of the throat. The severity of the adverse gradient is due primarily to the proximity of the shaft and is concentrated in the region of the shaft/wall intersection. Substantially higher negative pressure peaks are seen along the upper and sidewall surfaces near the beginning of the second leg of the turn.

When the total duct length was reduced by a total of 10 inches full scale, none of the cross-section coordinates were changed. The increments between stations were merely shrunk by a proportional amount. This change, however, substantially affected the local gradients and associated peak pressures, as shown in Figure 14. Peak negative pressures in key areas increased in absolute value by as much as one-thrid. This shape, without refinement, was plainly unacceptable.

Refinement of the design was an iterative procedure. Initial work was concentrated in the most critical areas and consisted of modifying local curvatures and/or area distributions as appeared to be appropriate. As the worst pressure peaks were reduced, other areas had to be modified as

their associated pressure peaks became the highest levels that remained. The process was continued until no additional improvement could be obtained. The resulting pressure distributions are presented in Figure 15 and show substantially lower gradients plus peak pressures that have been reduced by two-thirds from those measured for the initial, reduced-length configuration. These distributions appear to be significantly improved over the original, longer duct design.

Correlation of Wall Pressure Data

When the test was performed, data obtained from the longitudinal rows of wall pressure taps were compared with the QUADPAN predicted distributions. The basic duct with fillet was chosen for the correlation study because of the reduced possibility of flow separation in the experimental case. The correlations were better in some cases than others, but they were close enough to verify the use of the analytical pressures as design guidelines.

Experimental and analytical pressure distributions for the top surface of the duct are presented in Figure 16. The agreement is very good for the first 35 percent of the duct length, but aft of that point, as the flow begins to expand, the experimental gradient is significantly higher. This continues up to about 90 percent of duct length, where the two curves begin to converge again. It is not entirely clear why the correlation is poor in the 35- to 90-percent region, but it may be partly due to the double vortex pattern, which typically sets up in the second turn of an "S" duct. This type of three-dimensional flow pattern is not handled by the QUADPAN code used for the analytical work. Another possible reason is that viscous effects become more important as the flow moves toward the downstream end of the duct, while QUADPAN performs a purely inviscid analysis.

The side-surface pressure correlation, shown in Figure 17, was only close near the beginning and end of the duct. Deviation was most significant in the 30- to 45-percent range. This is probably due to the fact that viscous effects are amplified in corner regions, such as this. Boundary layers tend to pile up in the corners, so that their combined displacement thickness is high enough to substantially change the effective contour shape. As the

duct transitions to a circular shape, the boundary layer tends to respread itself, and the local impact of the buildup begins to diminish. This partly accounts for the observed reconvergence of the two curves near the end of the duct.

The lower-surface pressure correlation, seen in Figure 18, was the best of the three, with significant deviation occurring only in the region where the flow was locally perturbed near the shaft. In that area, it was difficult to select panel locations that were exactly coincident with experimental pressure tap positions. The better correlation obtained on this surface was likely due to the existence of an initial favorable gradient followed by a relatively mild adverse gradient spread over almost the entire duct length.

Mach Number Effects on Wall Pressures

Even at maximum airflow demand, the peak Mach numbers inside the final duct are not high. They are, however, high enough to observe some effect relative to the purely incompressible case. Measured low-speed distributions for the three rows of model pressure taps are presented in Figure 19. These are contrasted by the pressures for the same locations measured with maximum airflow, shown in Figure 20. In the aft top surface region, the pressure peaks were significantly lower at the higher flow rate. This could possibly result from reduction in viscous effects due to the higher duct Reynolds number. More likely, however, it is primarily due to a readjustment in the double vortex pattern that tends to control the flow in this region of the duct. This is borne out by the fact that, while the upper surface pressure peak is reduced, the negative pressure coefficients along the side surface are slightly higher along most of the duct length.

The effect of a simulated 30-degree swirl at maximum airflow is shown in Figure 21. The side surface pressure taps are located on the upwind side, and, as would be expected, their negative pressure levels are substantially increased. The bottom surface distribution, on the other hand, has been somewhat flattened along the first half of the duct surface. This may indicate that some crossflow persists along a significant part of the duct

length. This conclusion is verified by the contour plots, which will be discussed later and which show that some crossflow even exists for a full 100 percent of the duct length. The duct Mach number distributions for the same data are shown in Figure 22. With peak duct Mach numbers reading only about 0.53, as indicated, no problems should be experienced with loss factor divergence due to criticality or shock-induced separation.

Duct Performance/Distortion Data

The data in this section are presented for five cases--the four basic duct geometries and the 30-degree swirl simulation case. In addition, Run 7, which is a partial repeat and extension of Run 5, is also presented. Run 7 is not an immediate repeat of Run 5 but was performed after a teardown and complete rebuild of the rig test setup.

Total Pressure Recovery - Data for the six area weighted, total pressure rakes at the simulated compressor face were averaged to obtain total pressure recovery. For each of the cases described above, these recoveries, as a function of compressor face Mach number, have been fitted with third-order, least-square curves and are presented in Figure 23. A highly expanded vertical scale was selected for the plot, so that the configuration ranking could be clearly seen. However, this does give the appearance of significant scatter when it was, in fact, quite low as measured by the standards normally applied to this type of test.

At zero swirl angle (Beta), it is apparent that each combination of geometric changes has resulted in some improvement over the basic duct. The highest recovery was obtained with the basic duct plus fillet, but with the original Allison hub design. Although the new hub fairing was an improved design by itself, it possibly had a detrimental effect on the overall area distribution when the fillet was in place. In any case, the percentage reduction in total pressure loss for the fillet alone was substantial, although the absolute value of the increment was relatively small.

Data for the 30-degree swirl case was taken only for the basic duct configuration, so the data represented by x's and diamonds should be compared

only to the circles to obtain the swirl effect alone. As shown in Figure 23, the effect of a 30-degree swirl angle is significant. At design compressor face Mach number of 0.36, the total pressure loss is increased by roughly 50 percent. Although the x's and diamonds are supposed to be data taken for the same configuration, some change did occur as a result of teardown and rebuild of the rig. Most of the difference seen probably occurred as a result of reshaping the relatively low-radius bend on the short side of the 30-degree wedge. This was not a lofted contour, and when it was rebuilt, it was very difficult to exactly duplicate the original shape. Use of the more conservative of the two curves should result in a reasonably good estimate of the worst-case effect of a 30-degree inflow angle.

Circumferential Distortion - As used here, the circumferential distortion term (K-Theta) is as defined by Allison in Reference 4. This parameter is the average pressure for the highest pressure 240-degree sector less the average pressure for the lowest pressure 120-degree sector divided by compressible dynamic pressure at the compressor face.

In a similar type of presentation to that used for total pressure recovery, the circumferential distortion (K-Theta) data are shown in Figure 24. All of the data recorded for the test configurations were well within the allowable distortion limit of 0.55 specified by Allison. The configuration ranking based on K-Theta came out the same as the ranking based on recovery, although the percentage changes from one configuration to another were in some cases very different. The worst case, which was the basic duct plus swirl simulation, showed a K-Theta equal to about half the allowable limit. This was close to double the distortion of the same configuration without the swirl simulation.

Radial Distortion - Like circumferential distortion, radial distortion (KR) is evaluated as defined in Reference 4. It is the average pressure in the inner annular area comprising 60 percent of the net compressor face less the average pressure in the outer annular area comprising 40 percent of the net compressor face divided by the average compressor face compressible dynamic pressure.

A presentation of radial distortion (KR) is provided in Figure 25. The apparent scatter is high here, but the vertical scale is expanded to twice that used for circumferential distortion. The maximum allowable limit for KR specified by Allison is 0.375, while the maximum value measured by the test was only about 20 percent of that amount. The relative ranking of configurations is not easy to discern for this parameter. That is probably because the absolute value of the parameter is a large percentage of the width of the scatter band.

In Reference 4, an envelope of KR versus K-Theta has been defined that all measured values for an acceptable inlet duct must fall within. This envelope is presented in Figure 26 with all the measured data points from this test spotted within it. The main point to be considered here is that, at low values of K-Theta, the allowable limit for KR drops down to as low as 0.10. While this does result in KR approaching 50 percent of its limit line, no significant problem is indicated. There were one or two points that, as a result of KR going negative, fell below the bottom of the envelope. No cause for concern is seen here, since this is simply a matter of the way the parameter is defined. It is clear that there would have to be some level of negative radial distortion that would be acceptable. It would appear that this case has not really been considered by Allison.

Harmonic Distortion - Measurements for the computation of this parameter are taken from a series of 12 probes at compressor face ring No. 2, which is the second ring from the outer wall. This ring is composed of six individual probes and six probes that are integral parts of the rakes. The computational methodology is contained in Reference 4. Basically, the computation is set up to yield the first four Fourier Series components for the 12-point, ring 2 circumferential pressure distribution. These components are then ratioed to compressible dynamic pressure at the compressor face to obtain the harmonic distortion components A1 through A4.

The harmonic components measured during this test are plotted versus compressor face Mach number in Figures 27 through 30. The allowable limits for A1 through A4 are 1.6, 0.32, 0.20, and 0.20, respectively. None of the measured components ever closely approached their respective limits.

A1 did not quite reach 15 percent of its allowable limit. A2 and A3, in the course of reaching slightly better than 50 percent of their respective limits, were the closest to critical components that were measured. A4 reached a peak of close to a third of its allowable limit.

In subsequent full-scale testing, components A2, A3, and K-Theta should be tracked more closely than the rest of the parameters. Radial distortion becomes increasingly important as associated K-Thetas drop to extremely low values.

Total Pressure Contour Maps

In order to better visualize the total pressure distributions at the compressor face and understand the actual loss sources, contour plots have been generated for key test points selected from runs being analyzed. These are Runs 1 through 5 plus Run 7. Two test points were selected from the first 4 runs--a nominal compressor face Mach number (MCF) of 0.36, which was the PTA design value, and a nominal MCF of 0.45. The latter was selected as being representative of the MCF for an advanced technology propfan installation. Additionally, one point was selected from Run 5 and one point from Run 7. The contour maps are presented in Figures 31 through 40. Isobars are shown in percent deviation from freestream total pressure. Significant performance/distortion parameters are printed out beneath each of the maps with which they are associated. The dashed contour line is an isobar plotted at zero deviation. That is, the total pressure ratio along the dashed line is equal to the PT2/PT0 listed at the bottom of the figure. One additional parameter that is presented, although not previously discussed, is distortion "Factor." It is defined as maximum individual total pressure less minimum individual total pressure divided by compressor face average total pressure. Reference 4 does not specify any kind of requirement for this parameter.

Contour maps for the basic duct with both the fillet and new hub fairing are presented in Figures 31 and 32. The effect of the shaft wake, even with the fillet, is clearly seen at the six o'clock position. Some slight asymmetry in the wall boundary layer pattern is also evident. It is not

certain why this occurred, although there are at least two possibilities. One is that the model itself may not have been perfectly symmetrical, even though the form for the fiberglass layup was developed using a pre-programmed tape in conjunction with an NC mill. This possibility would seem to be almost eliminated, however, in view of the fact that some of the subsequent patterns were symmetrical. Because this was an outdoor test, a more likely possibility is that wind gusting created the asymmetry rather than any kind of configurational anomaly. This would not normally be a problem, but because the losses measured in this test were so low, gust distortion of the inlet flow could actually create measurable changes in the test results.

The contour plots for the basic duct alone are presented in Figures 33 and 34. In comparison to maps for the duct with both fairings in place, distortion around the hub is substantially increased, while duct wall distortion is noticeably reduced. While the duct wall distortion has now become almost completely symmetrical, some asymmetry now appears in the hub distortion. It is interesting that, when the compressor face Mach number is increased from 0.36 to 0.44, the duct wall distortion is almost entirely eliminated. The basic Allison hub, as compared to the new hub fairing, acts to force the flow away from the center of the duct, thereby increasing distortion near the centerbody while decreasing it near the wall. In view of the Allison definition for radial distortion, it is not surprising that increasing the flow actually reduces KR, as shown, to a very low, slightly negative value. K-Theta increases with higher flow, as would be expected, due to the larger size of the combined low pressure region formed by the centerbody induced and shaft wake distortions.

Figures 35 and 36 provide the contour maps for the basic duct with only the new hub added. These are relatively symmetrical patterns with a fair degree of balance between the duct wall and centerbody distortions. The unfilleted shaft wake forms a fairly clear bridge between the two sources. Even with the new hub, increased flow acts to decrease radial distortion, but from a relatively higher base level. Circumferential distortion increases with flow as expected.

Maps for the best of the tested configurations, the duct with only a new fillet added, are presented in Figures 37 and 38. Even casual inspection

shows that the shaft wake is greatly reduced in magnitude compared to the previous configuration. This is true even for the higher flow rate. What remains is a sort of corner effect, where the duct wall and fillet boundary layers combine at the bottom of the duct. One interesting effect that is not entirely explained is the fact that, with the shaft wake largely filleted out, there is some resurgence of duct wall distortion along the upper perimeter of the duct. Again, this situation is significantly improved by an increase in flow rate.

The last two maps, presented for the basic duct alone as run with a simulated 30-degree swirl, are shown in Figures 39 and 40. A sideflow angle, such as imposed here, causes the duct flow to accelerate on the upwind side and decelerate on the downwind side. The locally accelerated flow magnifies the pressure loss in that region and creates an additional circumferential distortion effect. Looking at Figure 39, this effect tends to combine with the shaft wake generating a comparatively severe depressed sector extending from the 3 o'clock to the 7 o'clock position. Circumferential distortion is seen to be increased substantially relative to the same configuration with no swirl. Because the preponderance of the depressed region is still localized in the hub region, however, radial distortion is slightly negative. At the higher flow rate displayed in Figure 40, radial distortion goes positive and circumferential distortion increases substantially. This appears to be due to a sharp rise in the severity of the separation on the upwind wall and a more complete merging between the shaft wake and the wall separation. Compressor face Mach number was limited to 0.41 for this run, because the danger of rake failure was much greater with the wedge imposed inflow angle.

CONCLUSIONS AND RECOMMENDATIONS

Based on the results of the testing as discussed herein, it is clear that the basic inlet duct design has better than adequate performance and is fully compatible with the selected Allison PTA powerplant. It is reasonable to conclude that all configurations tested are fully compatible with Reference 2, even at compressor face Mach numbers up to 0.45, which is well above the PTA design value of 0.36. It is also reasonable to conclude that an inlet sideflow angle of 30 degrees does not generate distortion levels that are even marginally unsafe, at least to the maximum compressor face Mach number of 0.41 which was imposed in testing with the wedge.

The above conclusions are not meant to imply that all possible problems associated with the inlet duct have been solved. The use of a bellmouth in the test insured a smooth profile entering the duct, while the real installation may have some propeller-induced non-linearity in the profile. Also, the test setup did not simulate the pulsations that are almost certain to be generated by the rotating propeller. If the boundary layer diverter height turns out to be inadequate, the performance will be adversely affected relative to that measured by the model.

Based on the test data obtained and the conclusions drawn above, it is recommended that the basic duct configuration with no refinements be utilized for the PTA inlet installation. The performance is better than expected, the distortion margin to the limit specified by Allison is substantial, and the cost for this choice is minimum. Since the fillet has been tested and proven to provide a performance increment, its design can be held in reserve for possible application later, in the event that performance is compromised for reasons not yet foreseen.

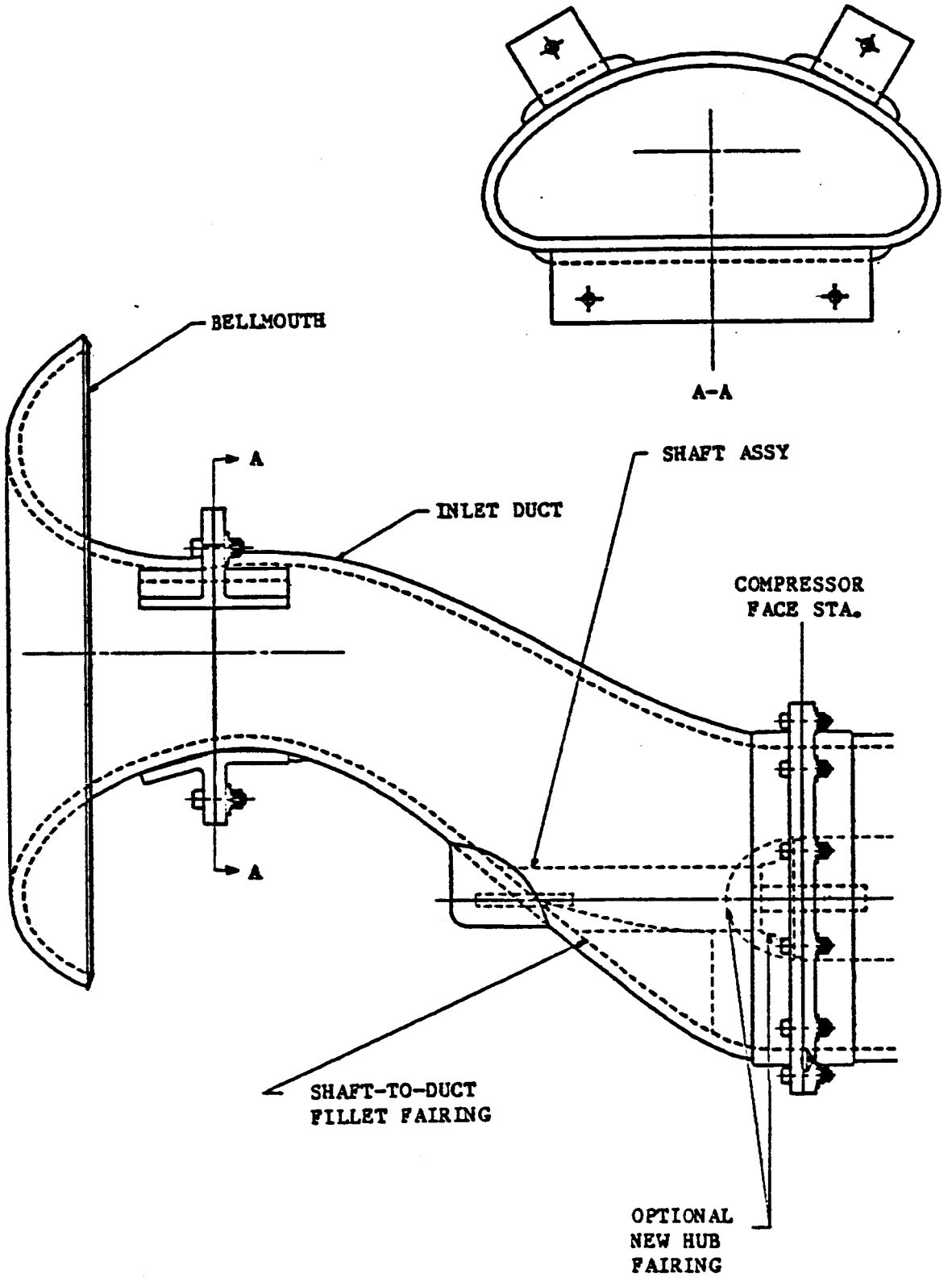

Figure 1. PTA Inlet Duct Assembly - General Arrangement, Fiberglass Test Model

PARAMETER	MODEL SCALE	FULL SCALE
LENGTH (TH. TO C.F.), INCHES	11.945	35.34
OFFSET, DELTA Y, INCHES	5.107	15.11
OFFSET RATIO, DY/DX	0.4275	0.4275
DIAM. OF COMPR. FACE, INCHES	6.220	18.40
DIAMETER OF HUB, INCHES	2.535	7.50
AREA, NET COMPR. FACE, SQ IN	25.331	221.7
AREA RATIO, C.F./THROAT	0.975	0.975
WIDTH/HEIGHT AT THROAT	2.482	2.482
THROAT ASPECT RATIO (AREA/HEIGHT ** 2)	2.131	2.131
MAX FLOW TURNING ANGLE, DEG	29.0	29.0
DESIGN COMPR. FACE MACH NO.	0.36	0.36
PEAK LOCAL MACH NO.	0.46	0.46

Figure 2. PTA Inlet Duct - Summary of Major Dimensions and Design Features

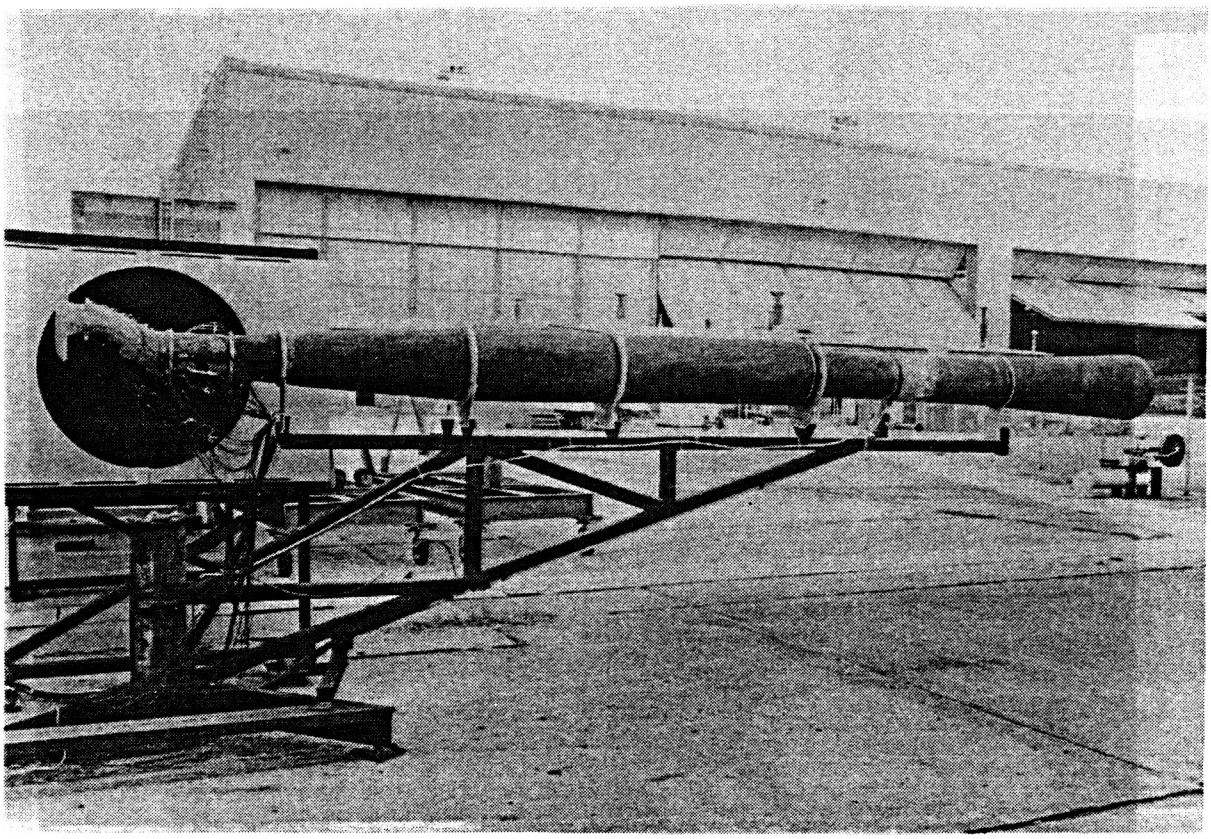

Figure 3. Complete Test Rig with Model, Side View

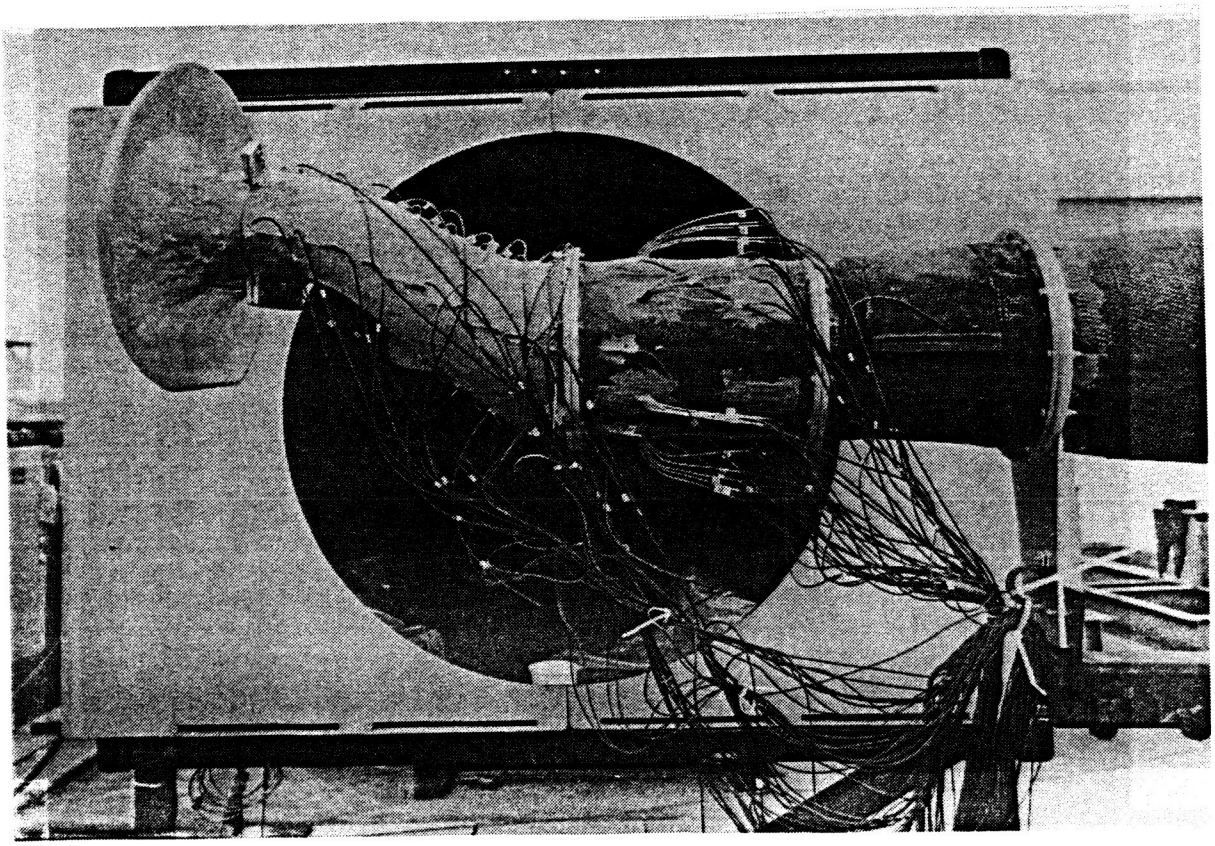

Figure 4. Test Rig with Model, Front End Side View

ORIGINAL PAGE IS
OF POOR QUALITY

ORIGINAL PAGE IS
OF POOR QUALITY

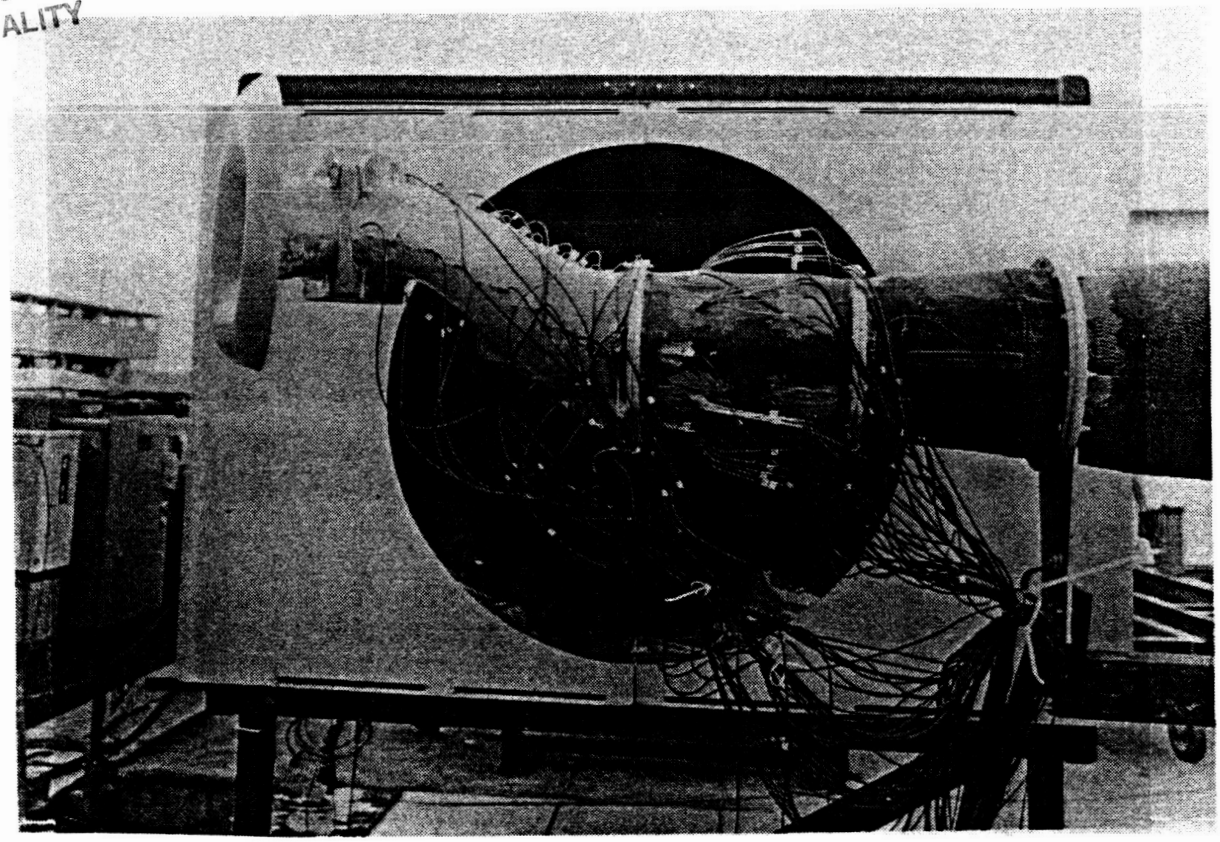

Figure 5. Test Rig with Model plus 30-Degree Wedge, Front End Side View

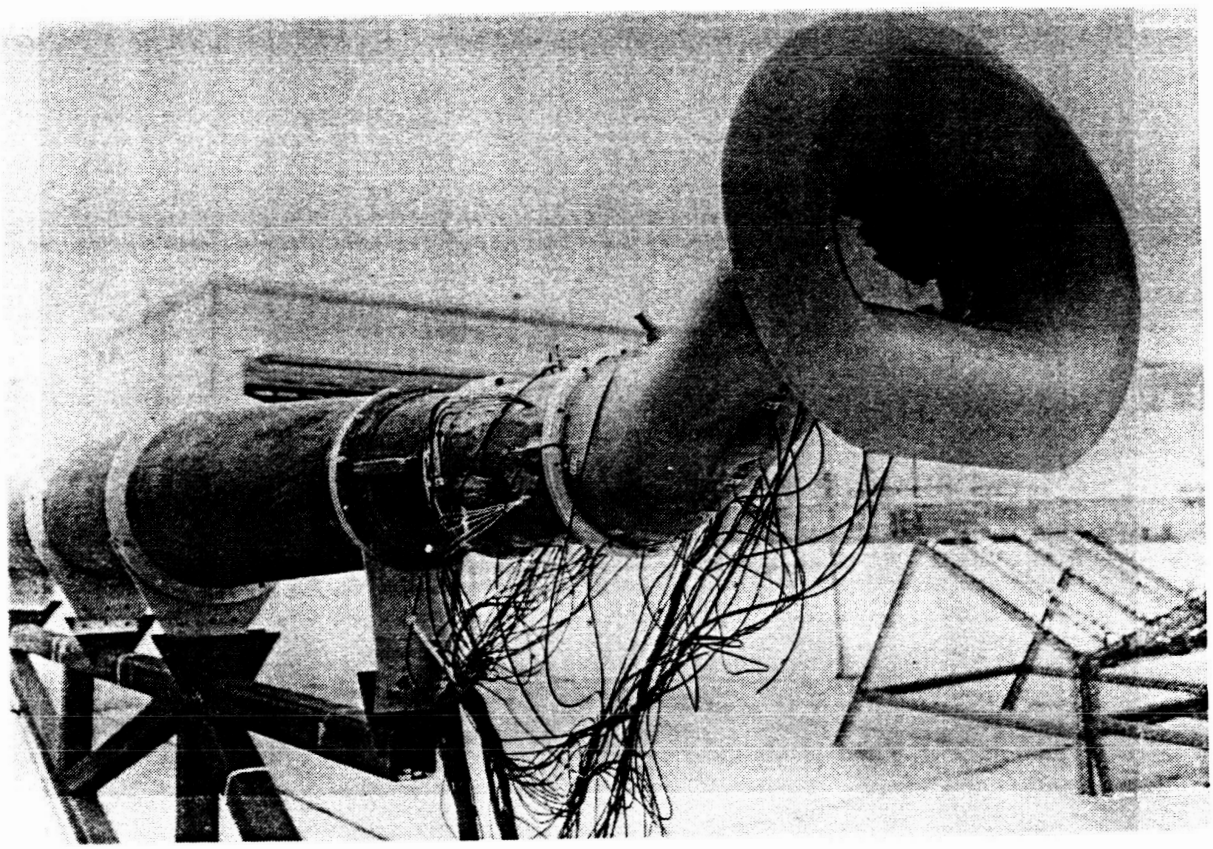

Figure 6. Test Rig with Model, Right 3/4 Front View

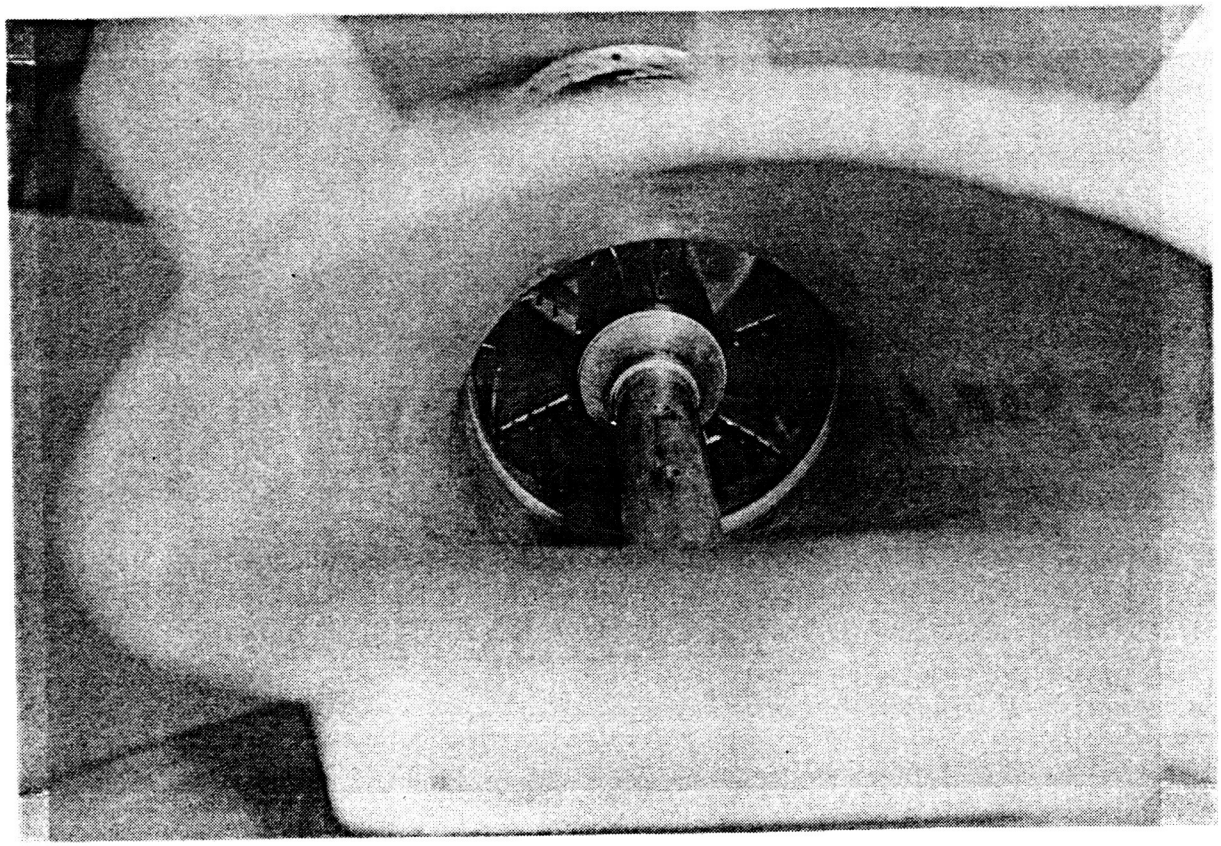

Figure 7. Compressor Face - Hub, Shaft, and Probes

ORIGINAL PAGE IS
OF POOR QUALITY

LOCATION	TYPE	ACCURACY
COMPRESSOR FACE	36 TOTAL PROBES	± 2%
	6 STATIC TAPS	± 2%
"S" DUCT/DIFFUSER ASSY	3 ROWS STATIC TAPS	
	9 TOP	± 2%
	9 SIDE	± 2%
	9 BOTTOM	± 2%
	1 INSPECTION PORT	N/A
FLOW MEASURING SECTION	UPSTREAM	
	1 THERMOCOUPLE	± 1%
	2 STATIC TAPS	± 2%
	DOWNSTREAM	
	2 STATIC TAPS	± 2%
FAN	DRIVE PRESSURE PICKUP	± 2%
MISCELLANEOUS	AMBIENT PRESSURE	± 2%
	AMBIENT TEMPERATURE	± 1%

Figure 8. Summary of Test Instrumentation and Estimated Accuracies.

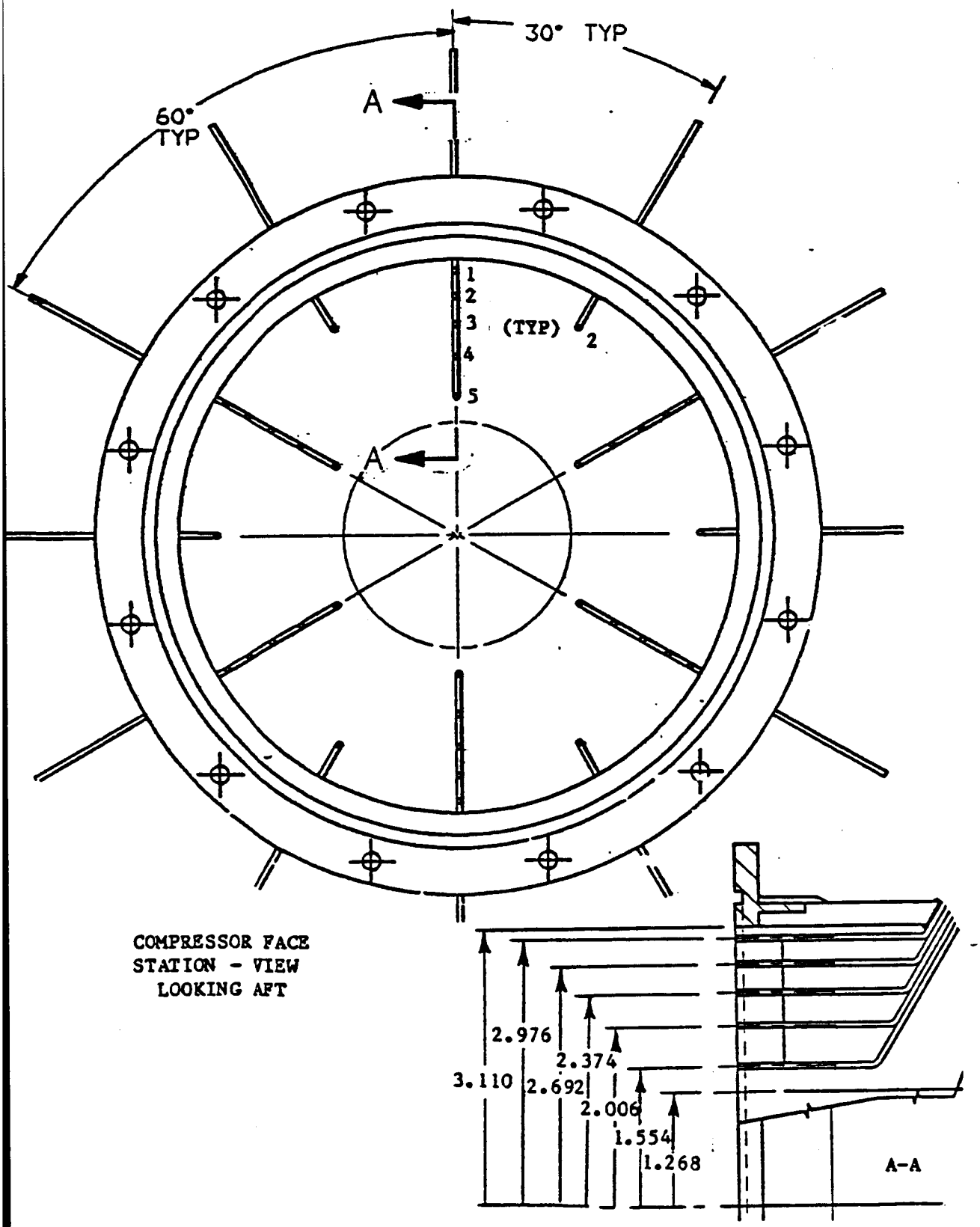

Figure 9. PTA Inlet Duct Test - Total Pressure Instrumentation

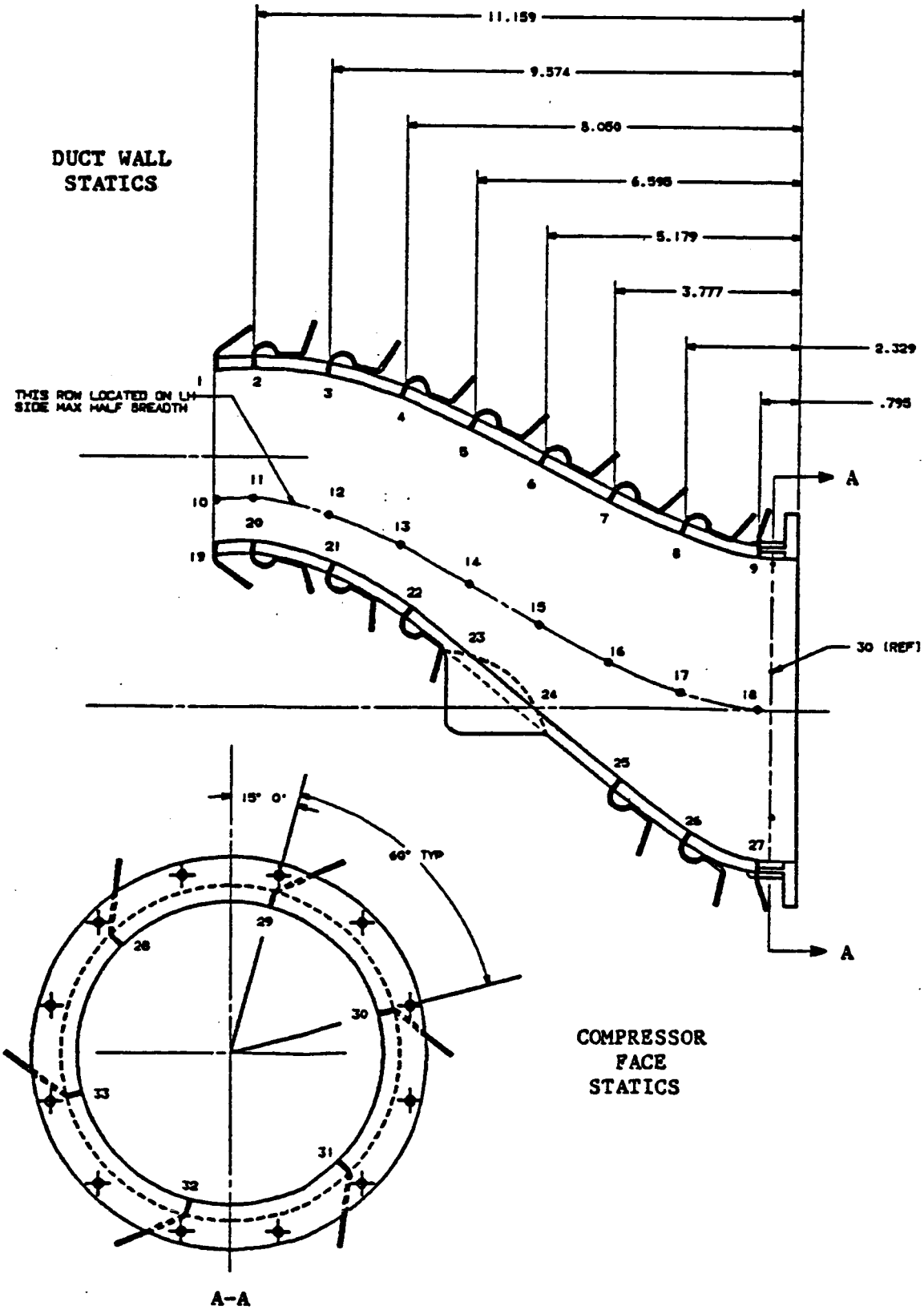

Figure 10. PTA Inlet Duct Test - Static Pressure Instrumentation

RUN	PT	DUCT	SHAFT FILLET	HUB FAIRING	VORTEX GENS	THROAT VANE	WA NOM LB/MIN	YAW DEG	REMARKS
1	1	D-1	YES	NEW	NO	NO	122	0	
1	2	"	"	"	"	"	153	0	
1	3	"	"	"	"	"	183	0	
1	4	"	"	"	"	"	208	0	
1	5	"	"	"	"	"	239	0	
1	6	"	"	"	"	"	271	0	
1	7	"	"	"	"	"	296	0	
1	8	"	"	"	"	"	331	0	
1	9	"	"	"	"	"	360	0	
1	10	"	"	"	"	"	354	0	RAKE FAILURE
1	11	"	"	"	"	"	276	0	(DETECTED AT RUN 13)
1	12	"	"	"	"	"	255	0	" " " "
1	13	"	"	"	"	"	228	0	" " " "
2	1	D-1	NO	OLD	NO	NO	124	0	INCORRECT AIRFLOW
2	1	"	"	"	"	"	159	0	" "
2	1	"	"	"	"	"	125	0	
2	2	"	"	"	"	"	152	0	
2	3	"	"	"	"	"	181	0	
2	4	"	"	"	"	"	210	0	
2	5	"	"	"	"	"	240	0	
2	6	"	"	"	"	"	268	0	
2	7	"	"	"	"	"	299	0	
2	8	"	"	"	"	"	329	0	DROPPED TO 319
2	9	"	"	"	"	"	349	0	
2	10	"	"	"	"	"	304	0	
2	11	"	"	"	"	"	258	0	
2	12	"	"	"	"	"	230	0	
2	13	"	"	"	"	"	198	0	
3	1	D-1	NO	NEW	NO	NO	123	0	
3	2	"	"	"	"	"	154	0	
3	3	"	"	"	"	"	183	0	
3	4	"	"	"	"	"	209	0	
3	5	"	"	"	"	"	243	0	
3	6	"	"	"	"	"	272	0	
3	7	"	"	"	"	"	302	0	
3	8	"	"	"	"	"	330	0	
3	9	"	"	"	"	"	356	0	
3	10	"	"	"	"	"	303	0	
3	11	"	"	"	"	"	264	0	
3	12	"	"	"	"	"	230	0	
3	13	"	"	"	"	"	197	0	

NOTE: DUCT D-1 IS THE BASIC FIBERGLASS DUCT USED FOR ALL RUNS PERFORMED DURING THIS TEST PROGRAM.

Figure 11. PTA Inlet Duct Test Program Run Summary
(Continued on Next Page)

RUN	PT	DUCT	SHAFT FILLET	HUB FAIRING	VORTEX GENS	THROAT VANE	WA NOM LB/MIN	YAW DEG	REMARKS
4	1	D-1	YES	OLD	NO	NO	127	0	
4	2	"	"	"	"	"	146	0	SOME FLOW
4	3	"	"	"	"	"	176	0	UNSTEADINESS
4	4	"	"	"	"	"	209	0	
4	5	"	"	"	"	"	243	0	
4	6	"	"	"	"	"	270	0	
4	7	"	"	"	"	"	300	0	
4	8	"	"	"	"	"	327	0	
4	9	"	"	"	"	"	352	0	
4	10	"	"	"	"	"	304	0	
4	11	"	"	"	"	"	260	0	
4	12	"	"	"	"	"	232	0	
4	13	"	"	"	"	"	199	0	
5	1	D-1	NO	OLD	NO	NO	118	30	
5	2	"	"	"	"	"	153	30	
5	3	"	"	"	"	"	179	30	BAR. .15" HG
5	4	"	"	"	"	"	208	30	LOW, RUN 118
5	5	"	"	"	"	"	240	30	
5	6	"	"	"	"	"	270	30	DUCT TAP NO. 4
5	7	"	"	"	"	"	297	30	BAD PTS 7 THRU 13
5	8	"	"	"	"	"	329	30	2 RAKES FAILED
5	9	"	"	"	"	"	345	30	UNDETECTED THRU 13
5	10	"	"	"	"	"	300	30	" " "
5	11	"	"	"	"	"	265	30	" " "
5	12	"	"	"	"	"	229	30	" " "
5	13	"	"	"	"	"	202	30	" " "
6	1	D-1	NO	OLD	YES	NO	123	30	
6	1	"	"	"	"	"	122	30	RERUN OF PT NO. 1
6	2	"	"	"	"	"	153	30	
6	3	"	"	"	"	"	181	30	
6	4	"	"	"	"	"	208	30	
6	5	"	"	"	"	"	239	30	
6	6	"	"	"	"	"	267	30	
6	7	"	"	"	"	"	298	30	
6	8	"	"	"	"	"	330	30	
6	9	"	"	"	"	"	303	30	
6	10	"	"	"	"	"	260	30	
6	11	"	"	"	"	"	230	30	
7	1	D-1	NO	OLD	NO	NO	238	30	
7	2	"	"	"	"	"	270	30	
7	3	"	"	"	"	"	304	30	
7	4	"	"	"	"	"	328	30	
7	5	"	"	"	"	"	330	30	PT NO. 5 IS A
7	6	"	"	"	"	"	293	30	REPEAT OF PT
7	7	"	"	"	"	"	260	30	NO. 4
7	8	"	"	"	"	"	230	30	

Figure 11. PTA Inlet Duct Test Program Run Summary
(Continued on Next Page)

RUN	PT	DUCT	SHAFT FILLET	HUB FAIRING	VORTEX GENS	THROAT VANE	WA NOM LB/MIN	YAW DEG	REMARKS
8	1	D-1	NO	OLD	NO	YES	119	30	
8	2	"	"	"	"	"	149	30	
8	3	"	"	"	"	"	184	30	
8	4	"	"	"	"	"	208	30	VANE FAILED

Figure 11. PTA Inlet Duct Test Program Run Summary (Concluded)

ORIGINAL PAGE IS
OF POOR QUALITY

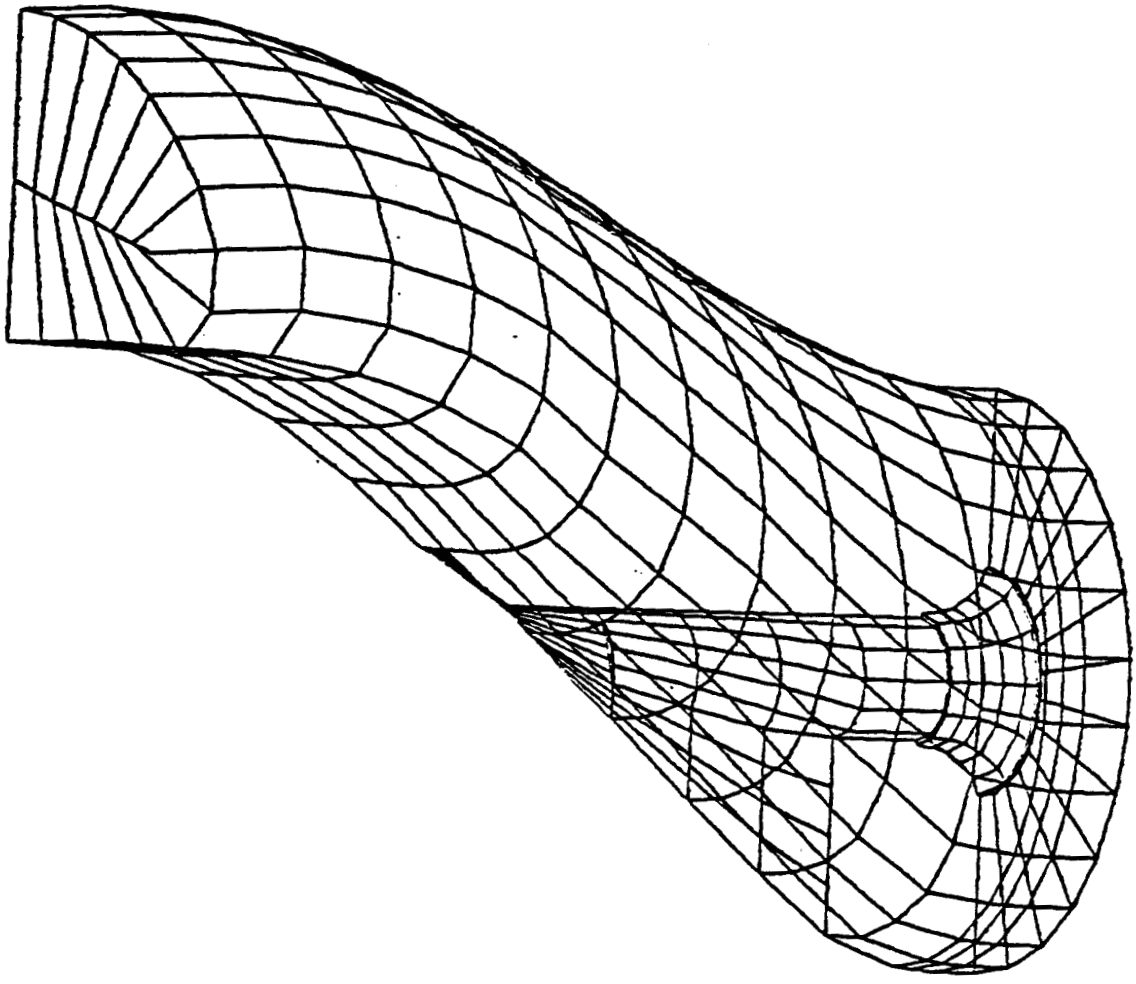

Figure 12. QUADPAN Panel Model, Basic Duct with Fillet

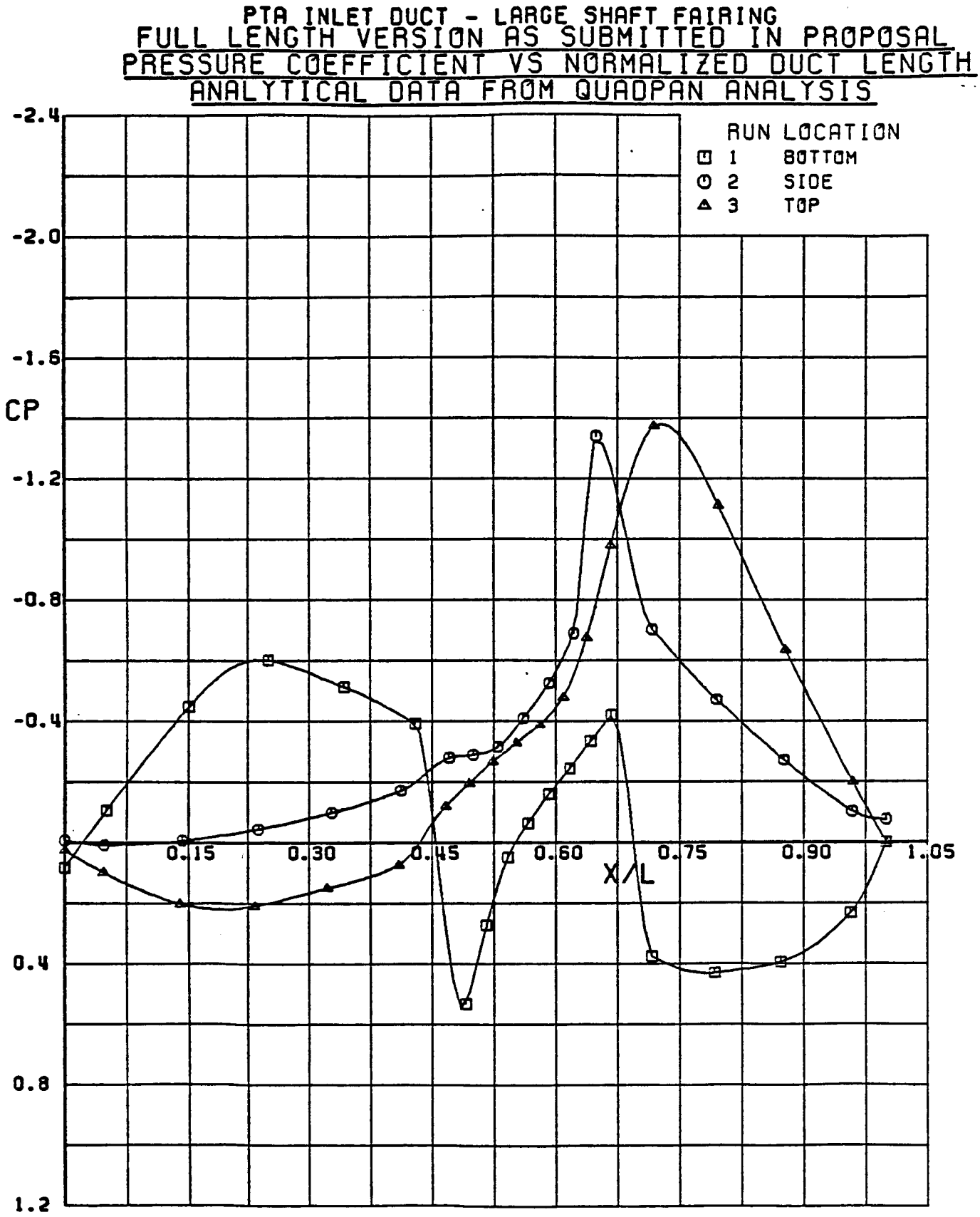

Figure 13. PTA Inlet Duct, Proposal Configuration

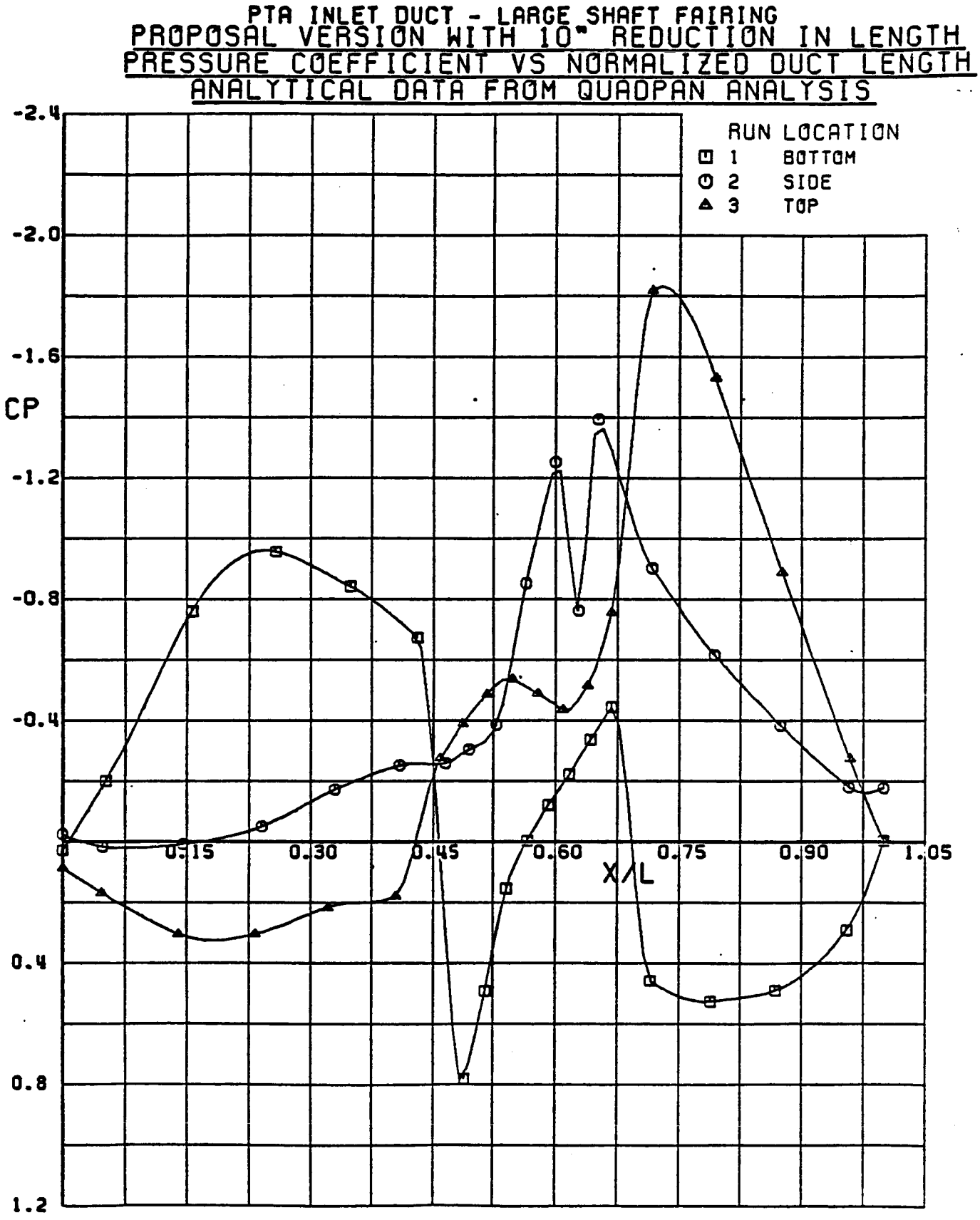

Figure 14. PTA Inlet Duct, Reduced Length Proposal Configuration

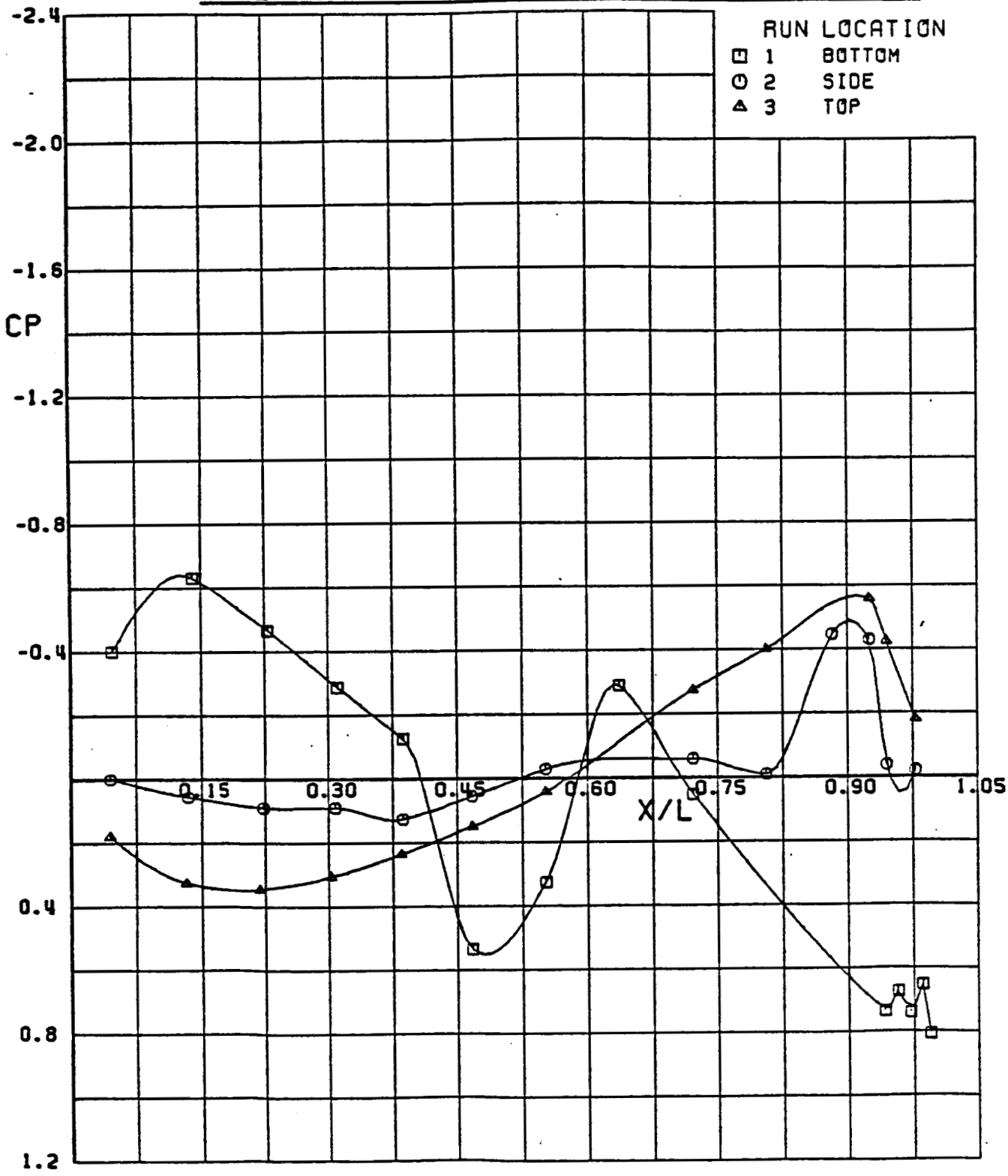

Figure 15. PTA Inlet Duct, Final Configuration

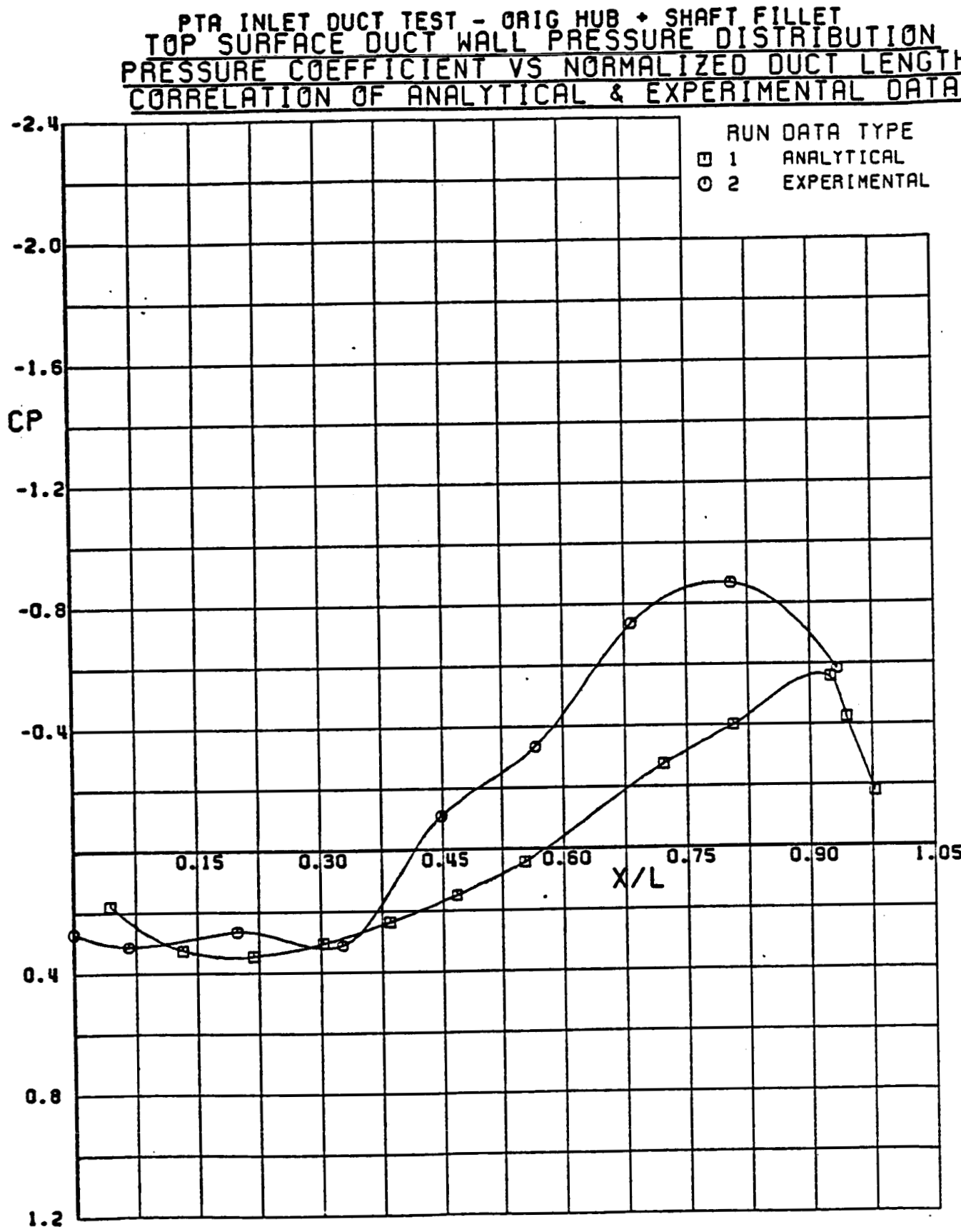

Figure 16. Top Surface Pressure Correlation, Experimental Versus Analytical

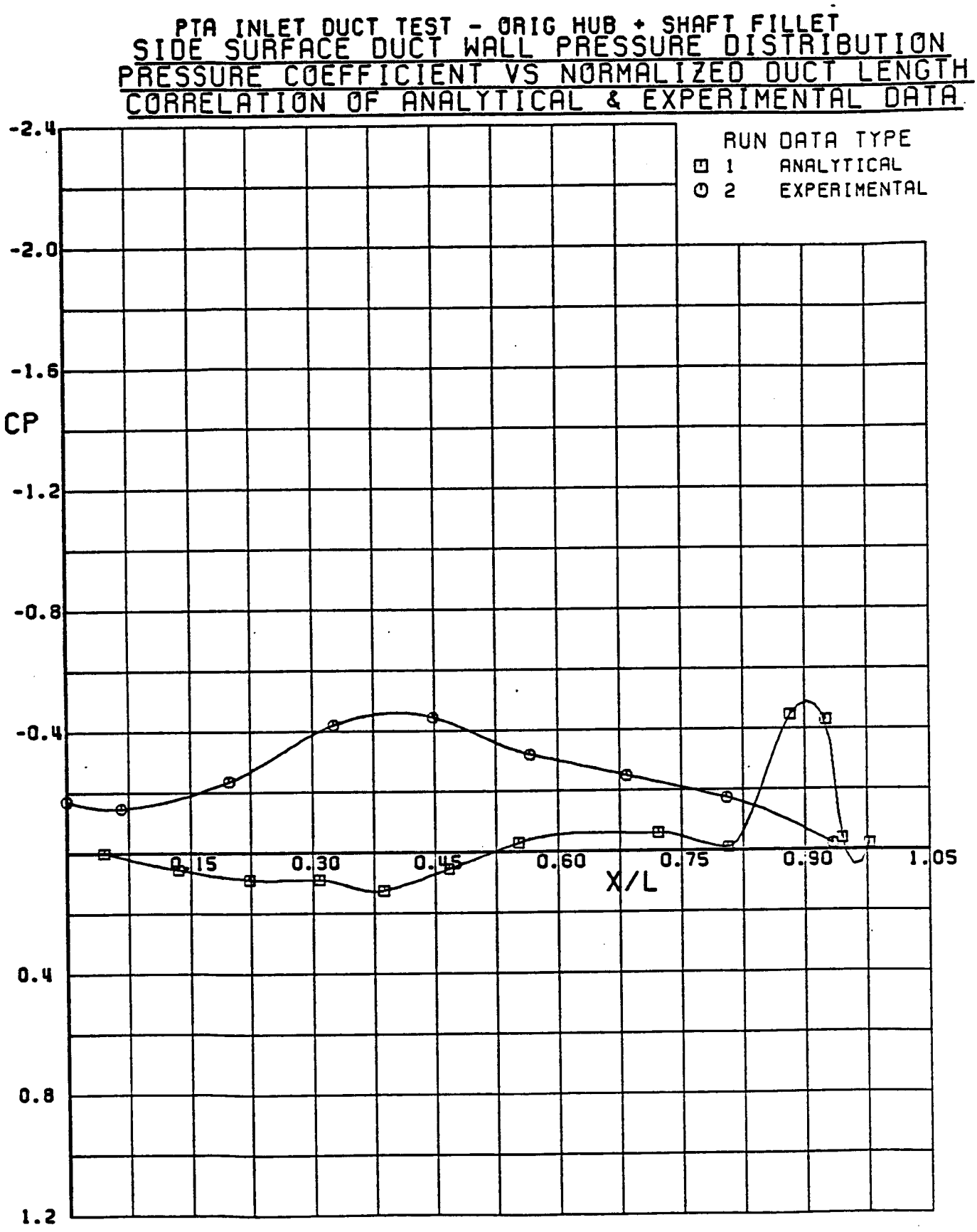

Figure 17. Side Surface Pressure Correlation, Experimental Versus Analytical

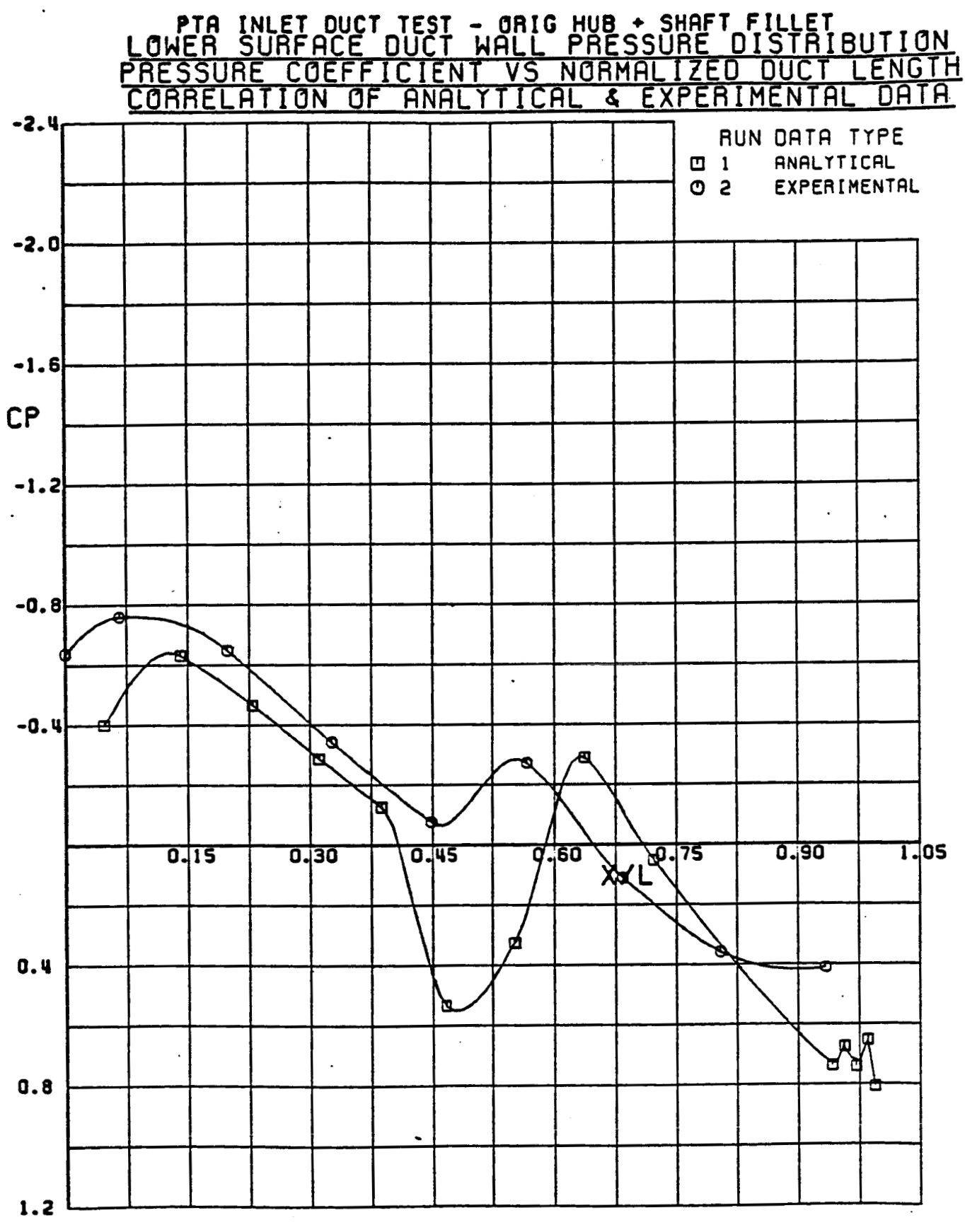

Figure 18. Lower Surface Pressure Correlation, Experimental Versus Analytical

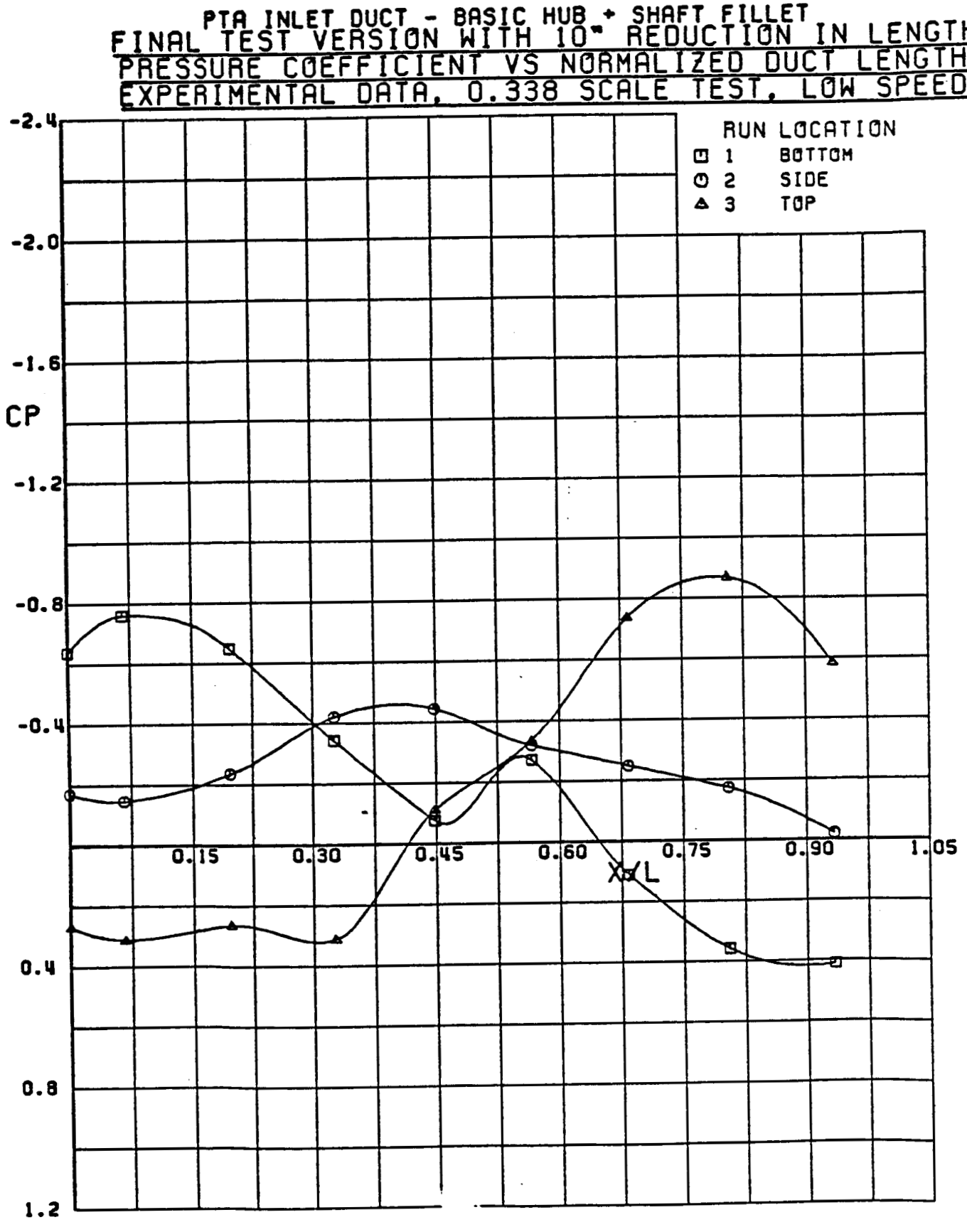

Figure 19. Measured Incompressible Duct Pressure Distribution, MCF < 0.2

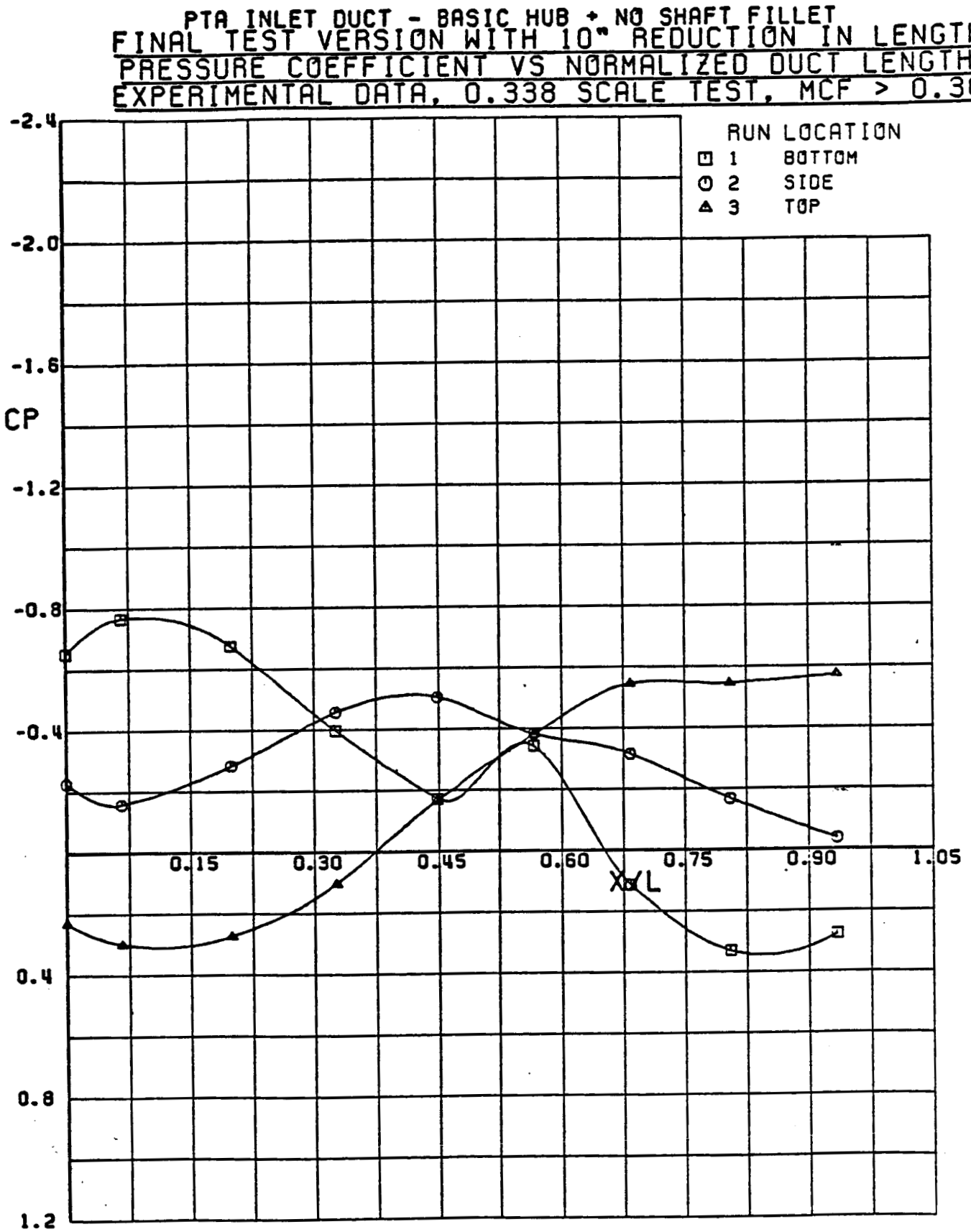

Figure 20. Measured Duct Pressure Distribution, MCF > 0.36

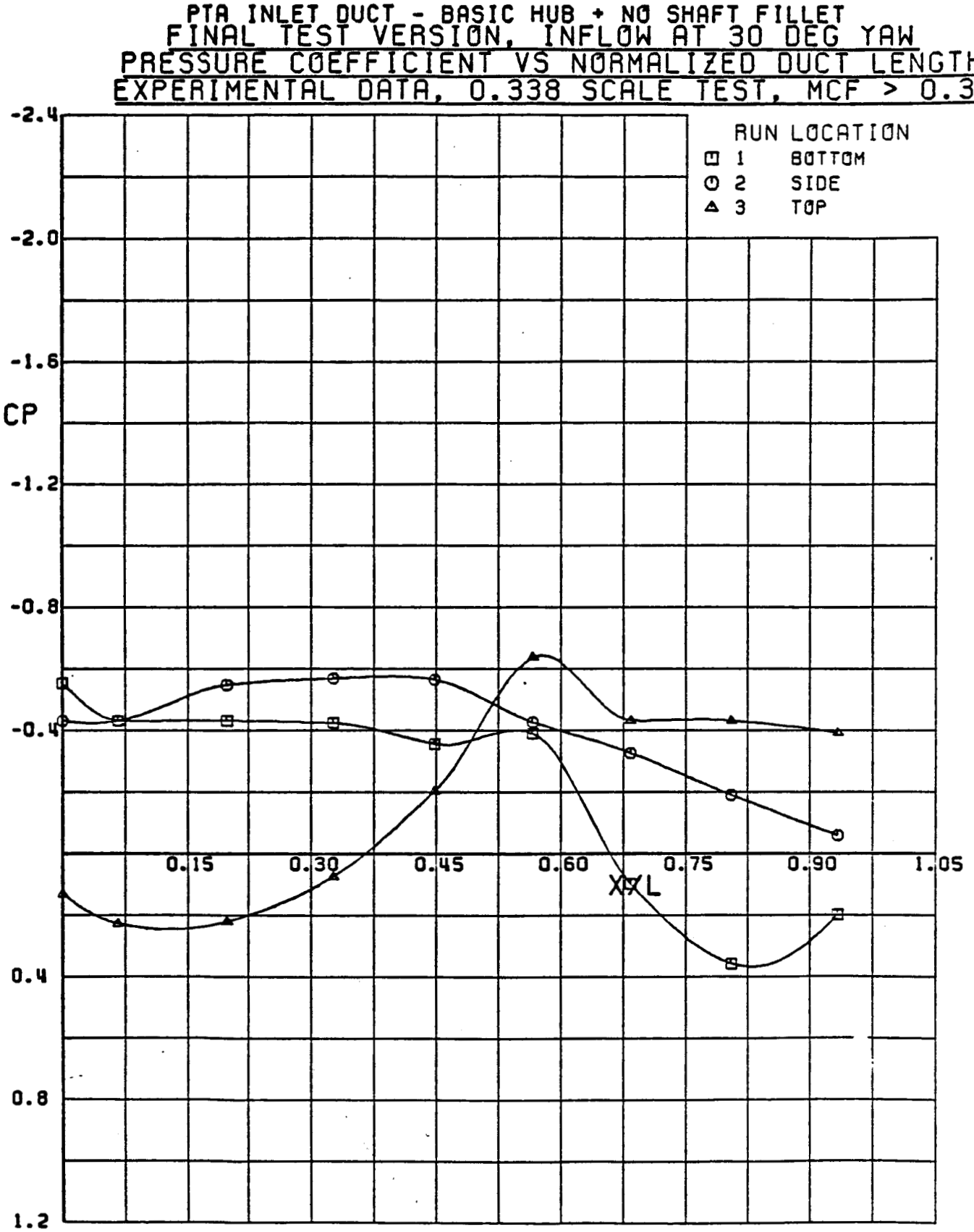

Figure 21. Measured Duct Pressure Distribution with 30-Degree Swirl, MCF > 0.36

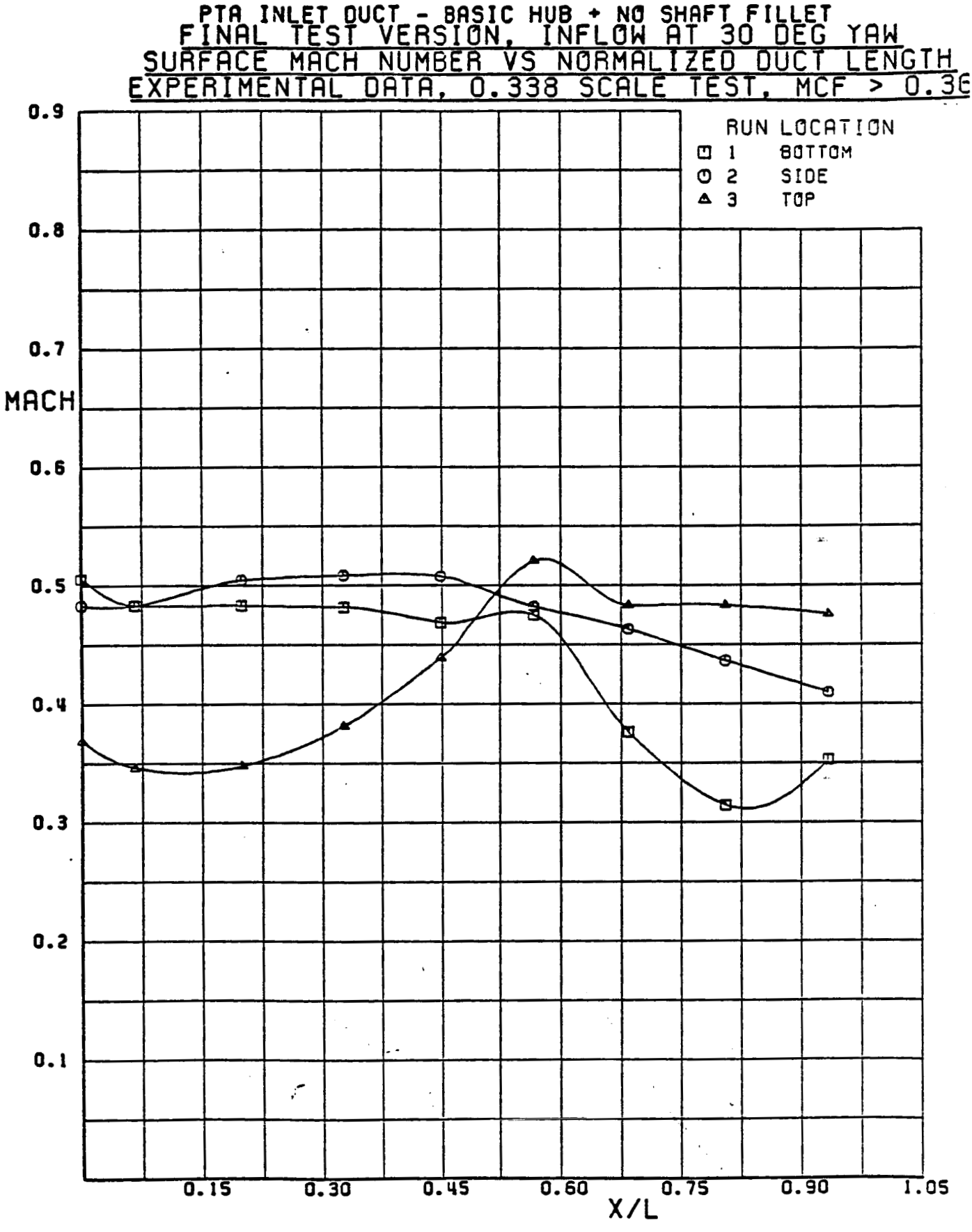

Figure 22. Measured Duct Mach Number Distribution with 30-Degree Swirl, MCF > 0.36

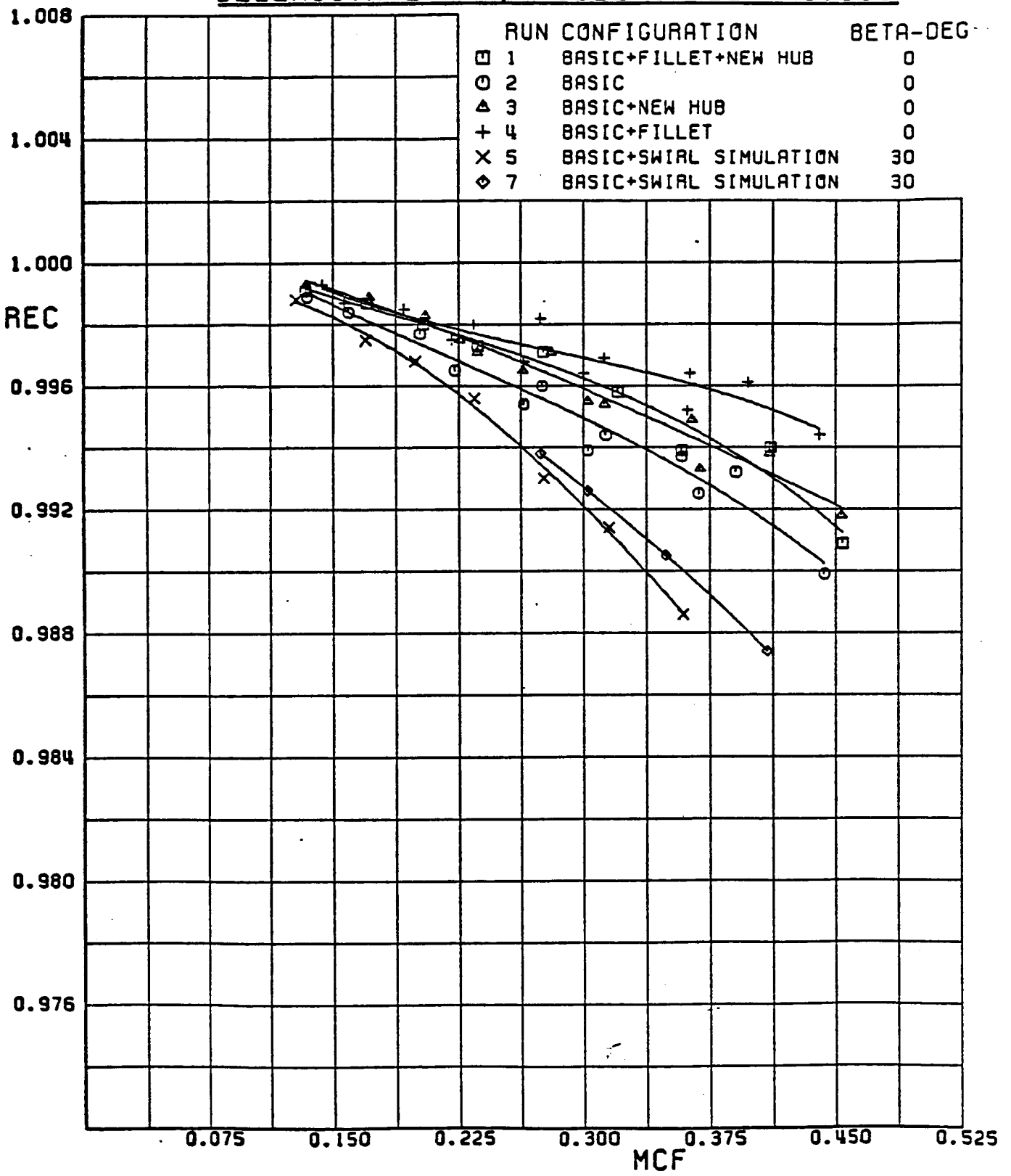

Figure 23. Total Pressure Recovery for Test Configurations

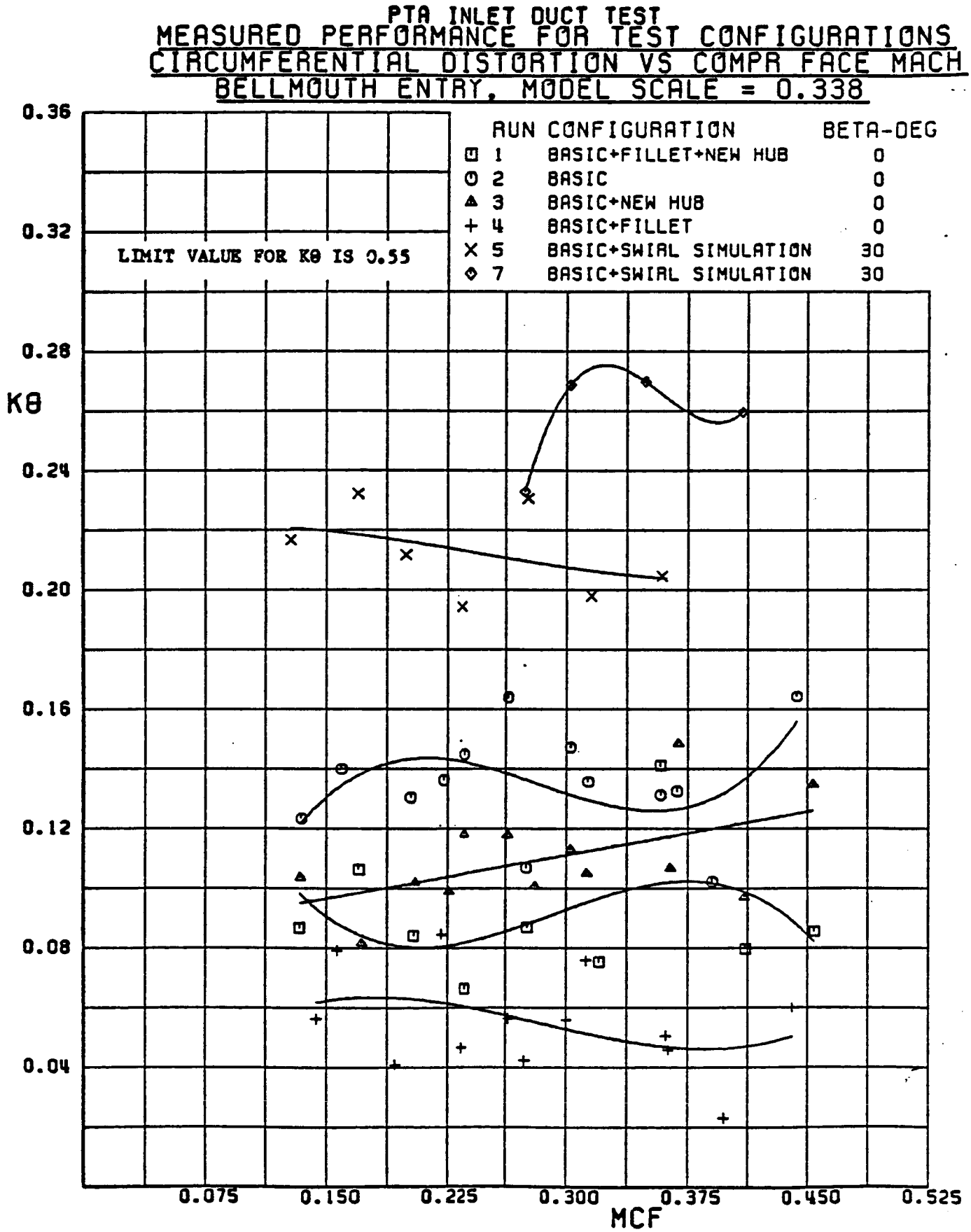

Figure 24. Circumferential Distortion for Test Configurations

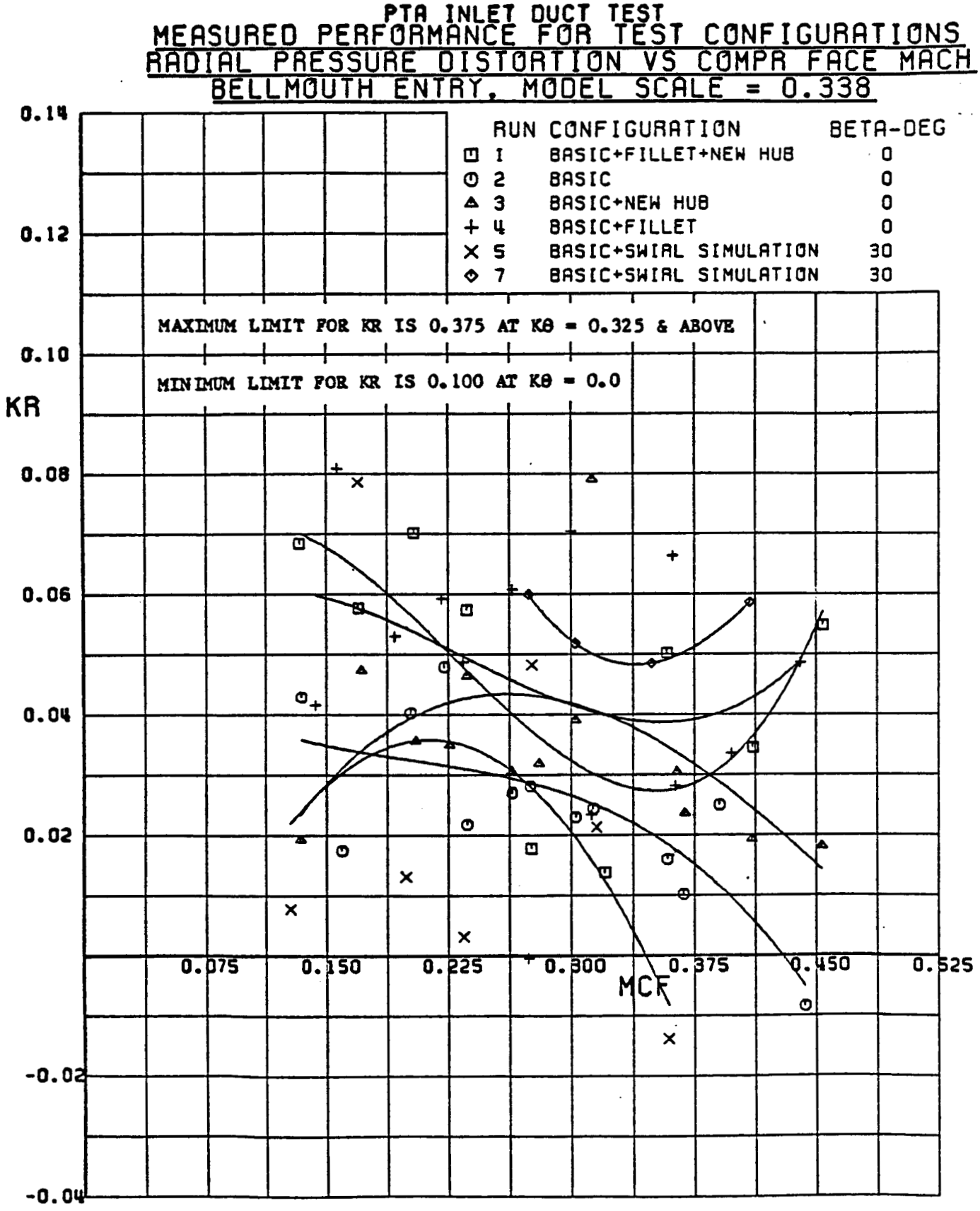

Figure 25. Radial Distortion for Test Configurations

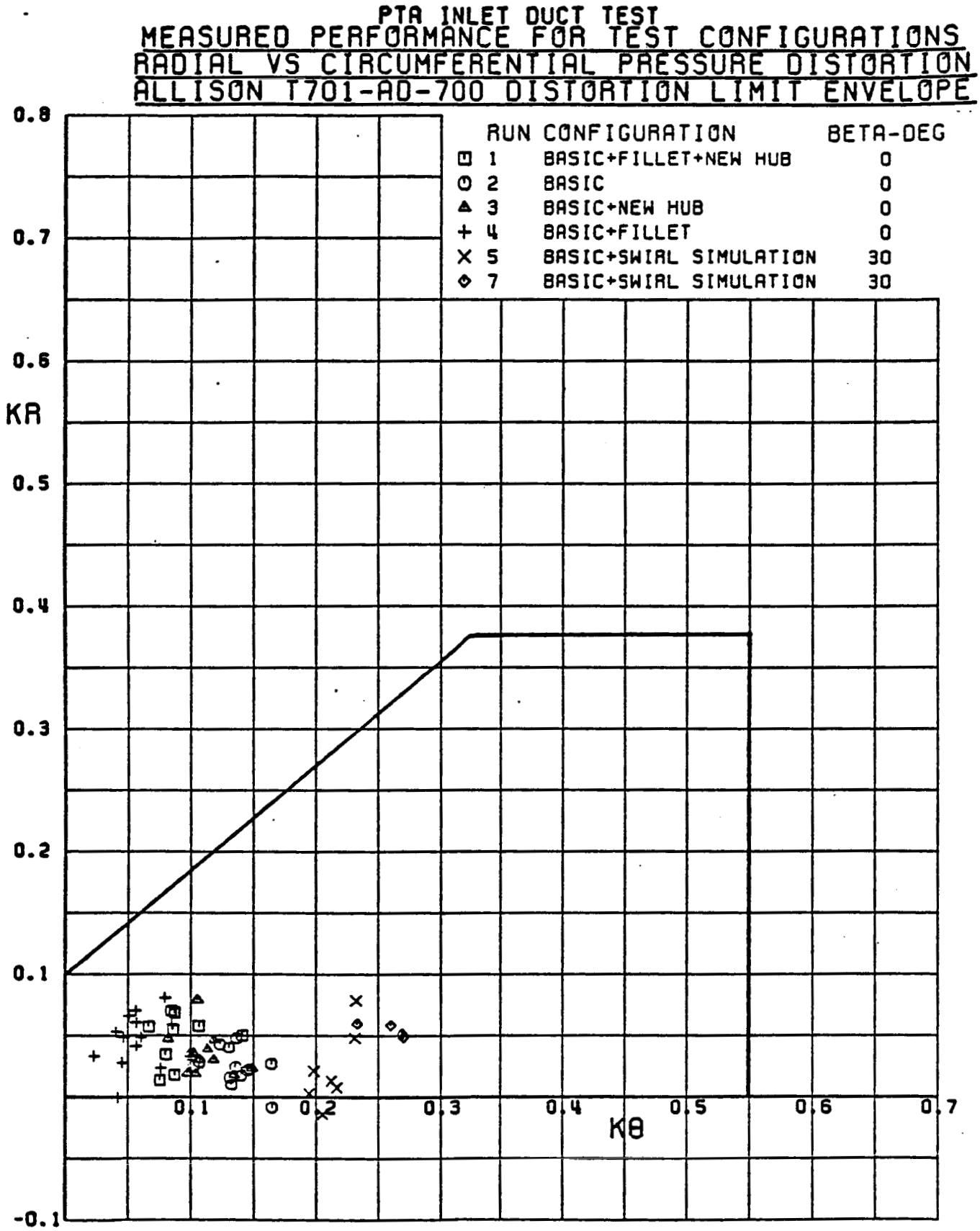

Figure 26. Distortion Relative to Allison Envelope

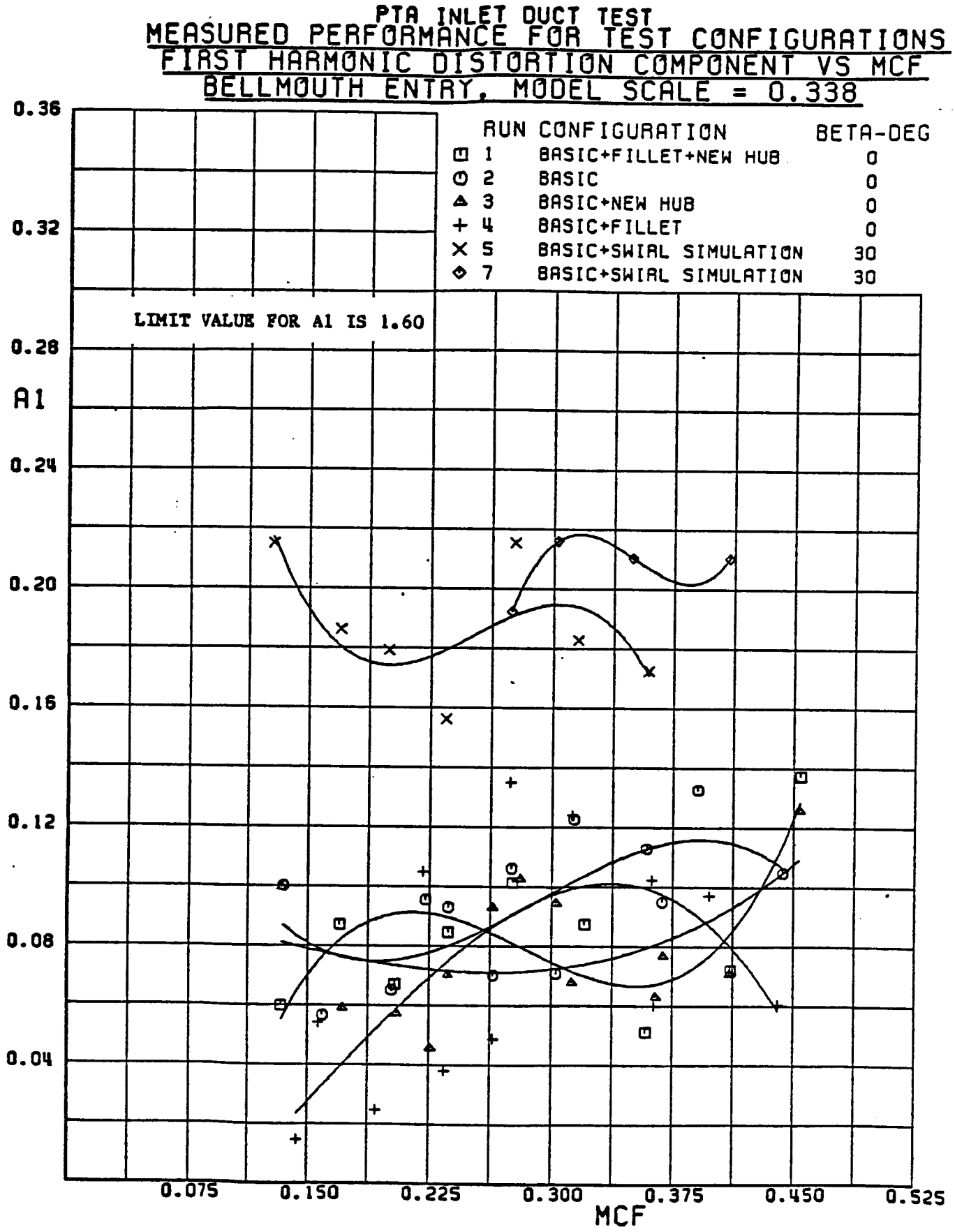

Figure 27. First Harmonic Distortion Component for Test Configurations

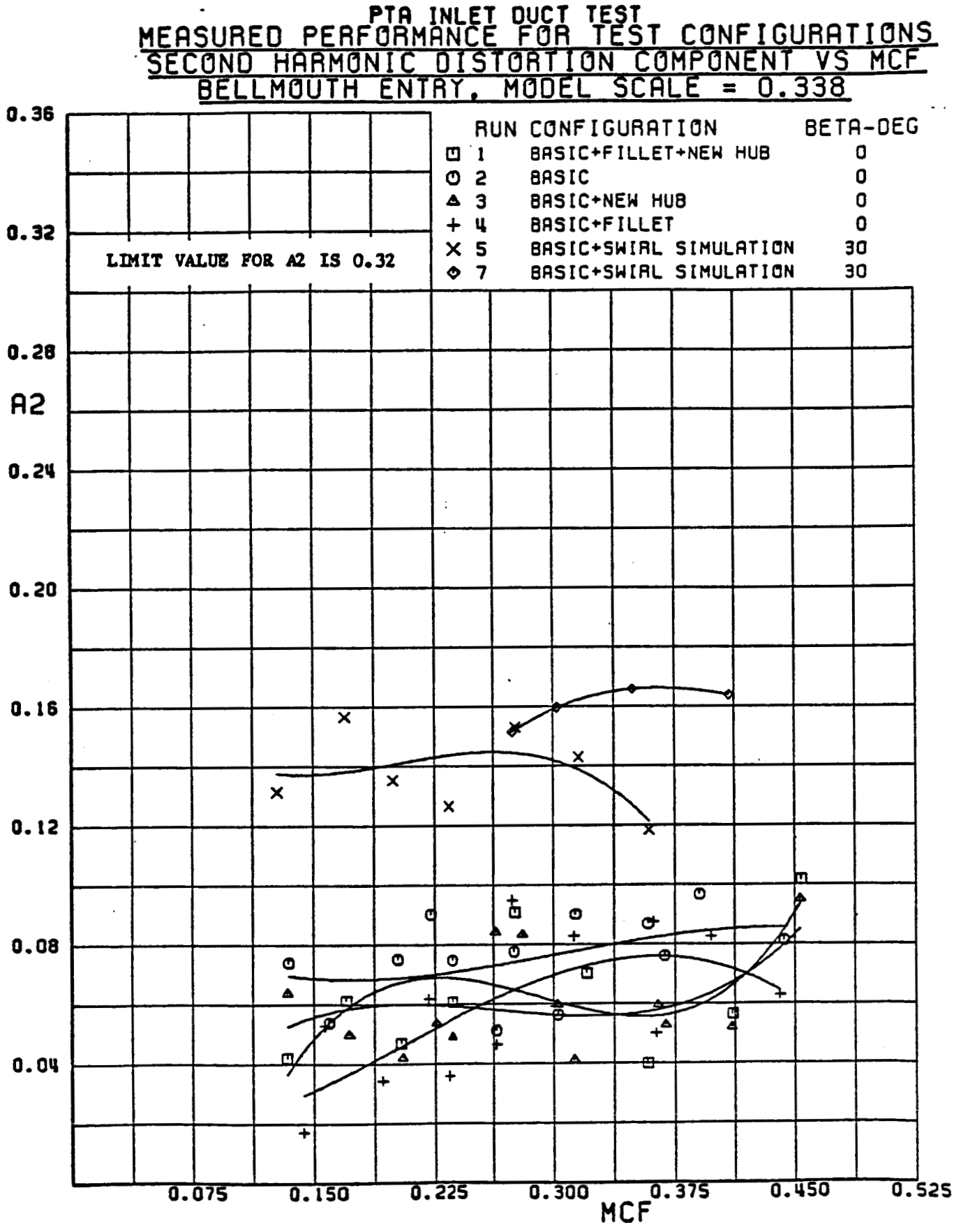

Figure 28. Second Harmonic Distortion Component for Test Configurations

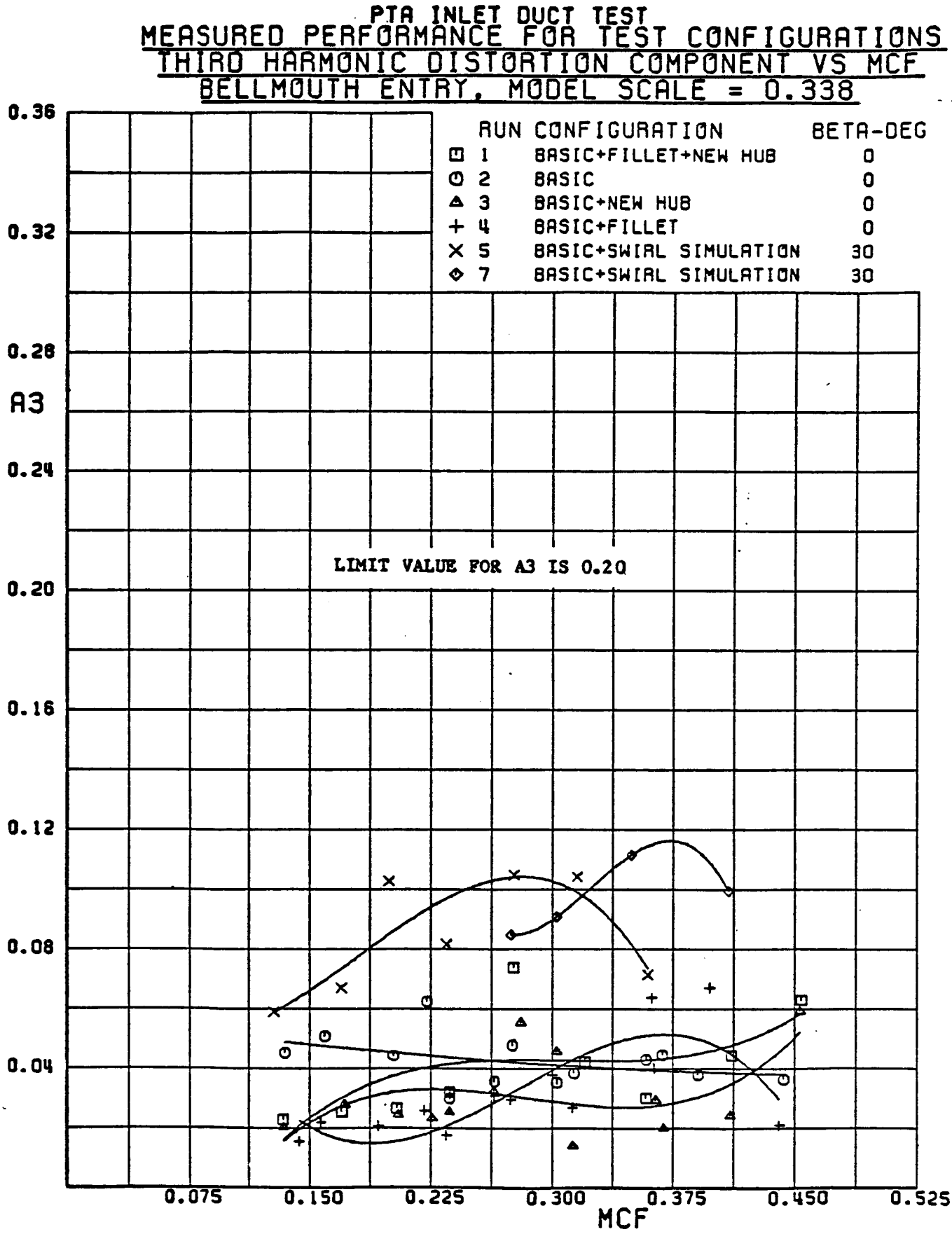

Figure 29. Third Harmonic Distortion Component for Test Configurations

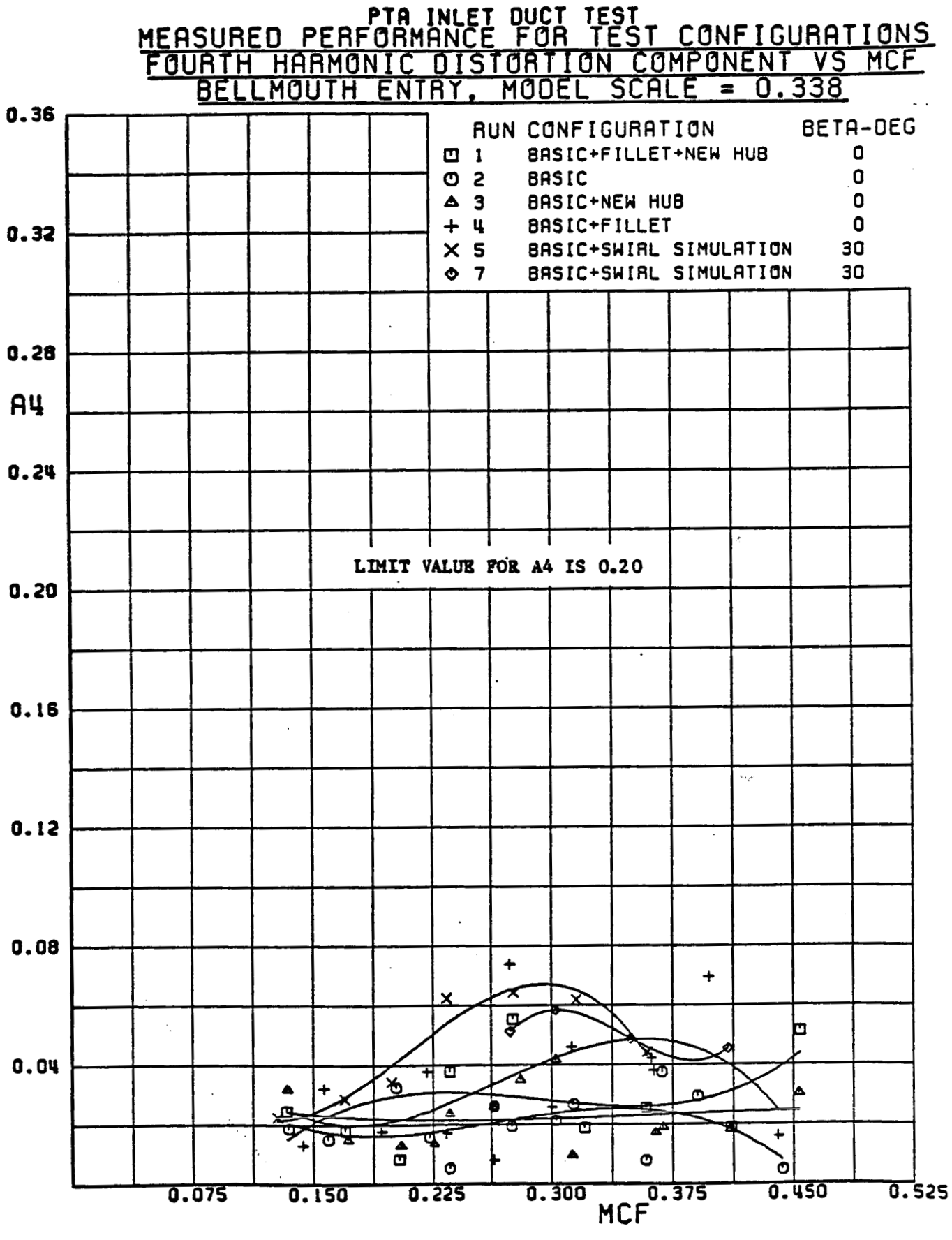

Figure 30. Fourth Harmonic Distortion Component for Test Configurations

PTA DUCT+FILLET+NEW HUB

ENGINE COMPRESSOR FACE
TOTAL PRESSURE CONTOUR MAP
VIEW LOOKING AFT

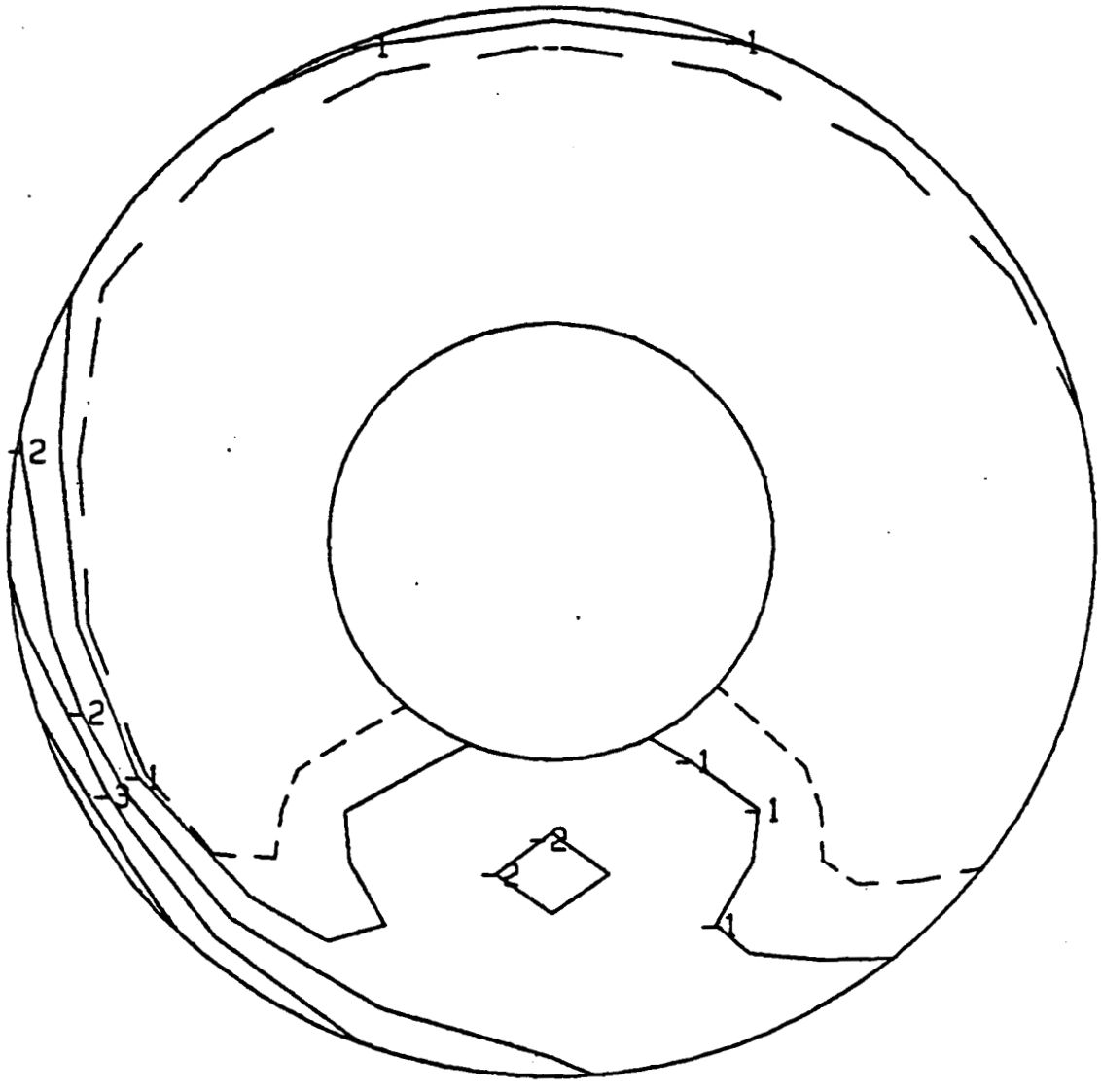

RUN	PT	ALPHA	CFMACH	WA2C
1	7	0.0	0.358	4.99

PT2/PT0	DIST-CIR	FACTOR	DIST-RAD
0.994	0.141	0.032	0.050

Figure 31. Pressure Contour Map, Run No. 1, MCF = 0.36

PTA DUCT+FILLET+NEW HUB

ENGINE COMPRESSOR FACE
TOTAL PRESSURE CONTOUR MAP
VIEW LOOKING AFT

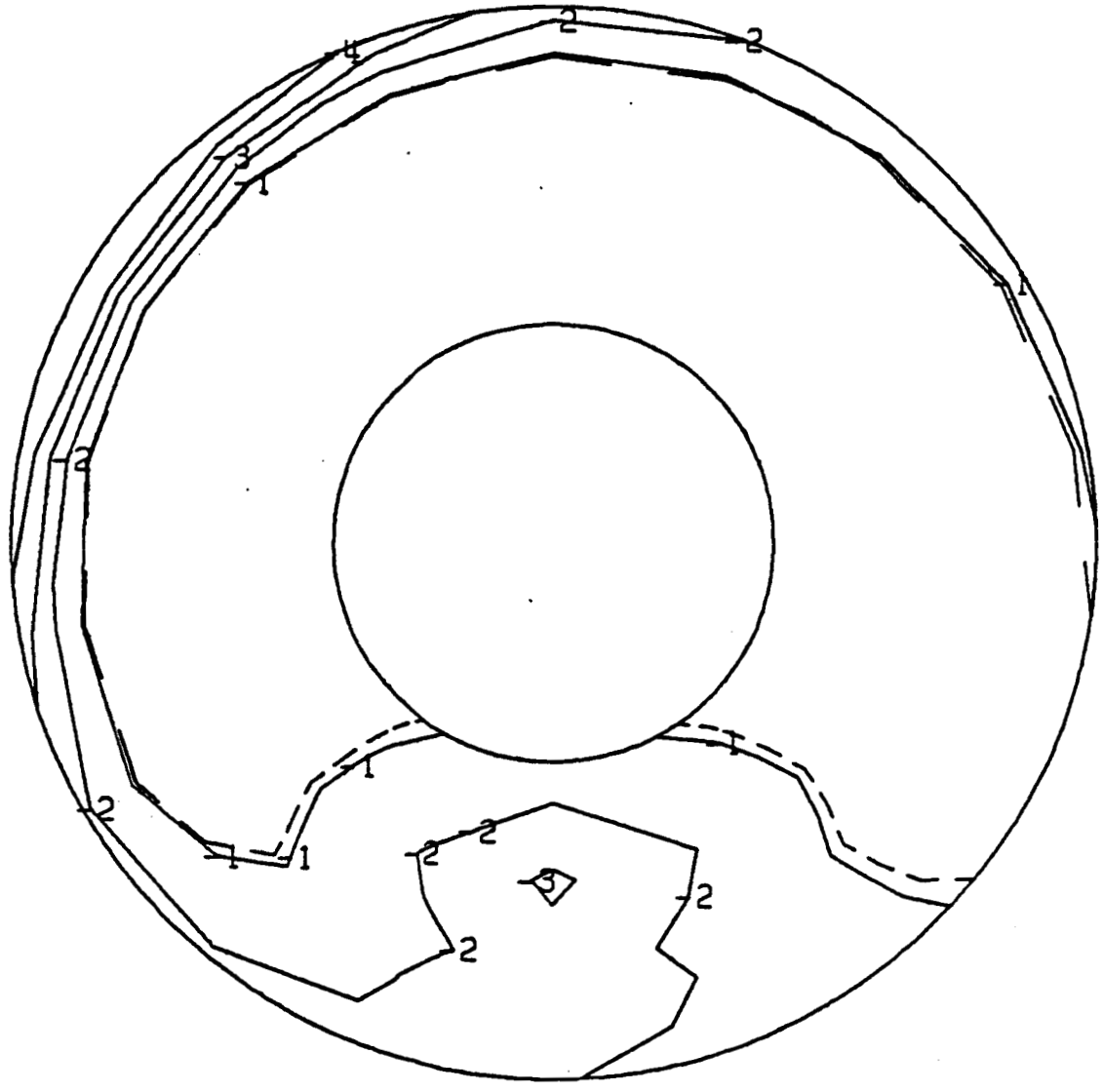

RUN	PT	ALPHA	CFMACH	WA2C
1	9	0.0	0.454	6.05

PT2/PT0	DIST-CIR	FACTOR	DIST-RAD
0.991	0.086	0.043	0.055

Figure 32. Pressure Contour Map, Run No. 1, MCF = 0.45

PTA DUCT+NØ FILLET+ØLD HUB

ENGINE COMPRESSOR FACE
TOTAL PRESSURE CONTOUR MAP
VIEW LOOKING AFT

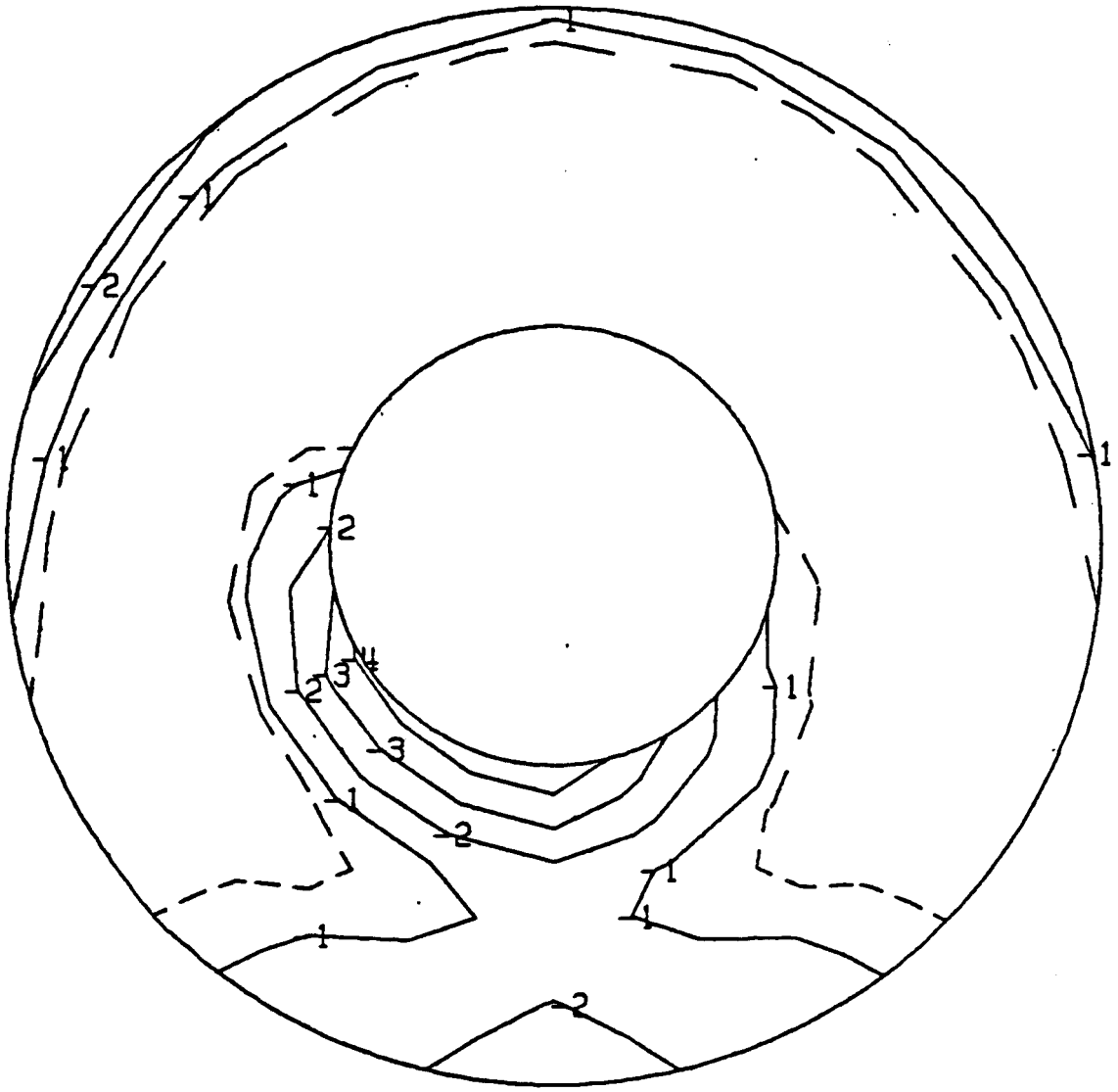

RUN	PT	ALPHA	CFMACH	WA2C
2	7	0.0	0.358	4.99

PT2/PT0	DIST-CIR	FACTOR	DIST-RAD
0.994	0.131	0.034	0.016

Figure 33. Pressure Contour Map, Run No. 2, MCF = 0.36

PTA DUCT+NØ FILLET+ØLD HUB

ENGINE COMPRESSOR FACE
TØTAL PRESSURE CØNTØUR MAP
VIEW LØØKING AFT

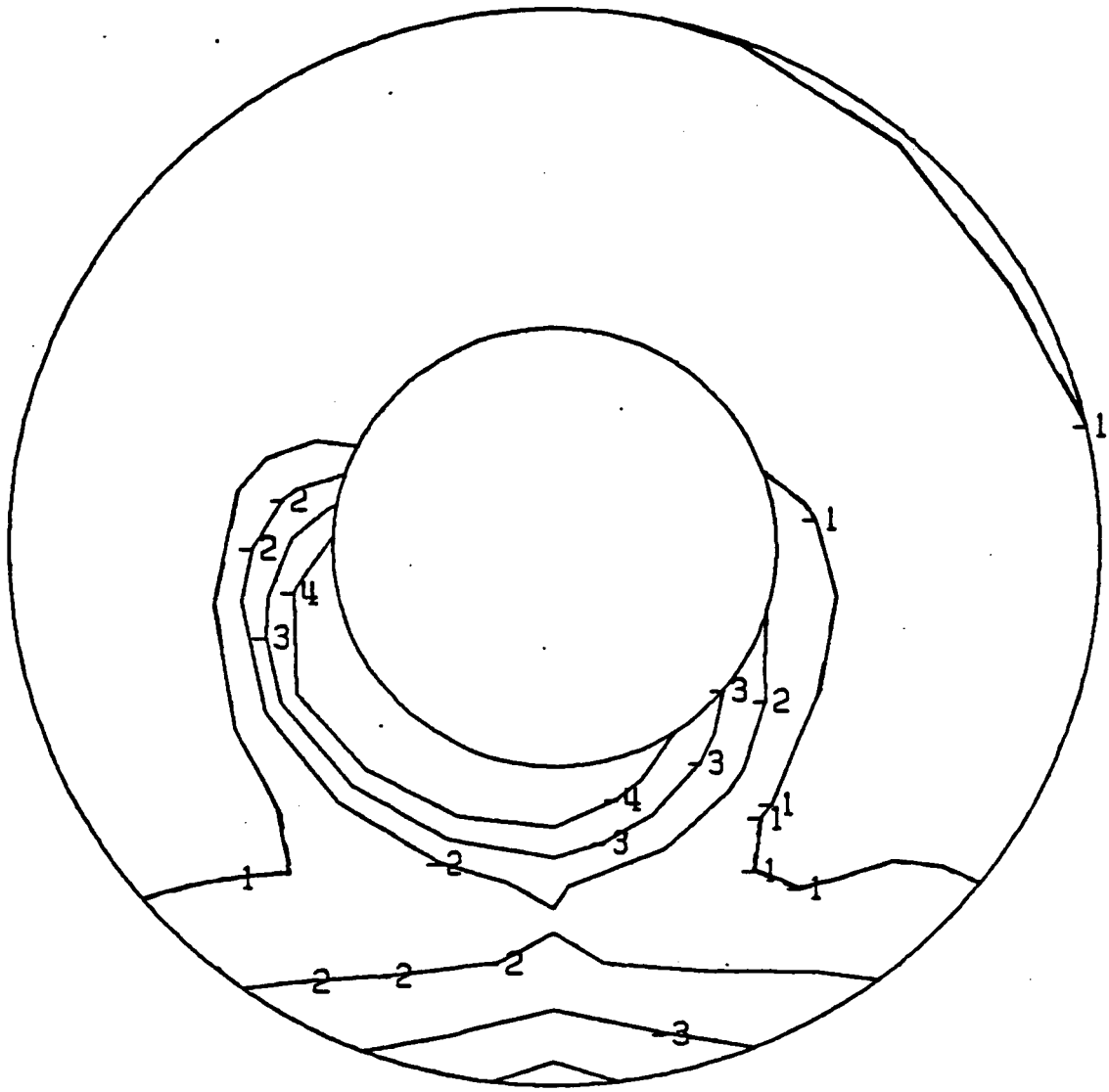

RUN	PT	ALPHA	CFMACH	WA2C
2	9	0.0	0.443	5.93

PT2/PTØ	DIST-CIR	FACTØR	DIST-RAD
0.990	0.164	0.054	-0.008

Figure 34. Pressure Contour Map, Run No. 2, MCF = 0.44

PTA DUCT+NØ FILLET+NEW HUB

ENGINE CØMPRESSØR FACE
TØTAL PRESSURE CØNTØUR MAP
VIEW LØØKING AFT

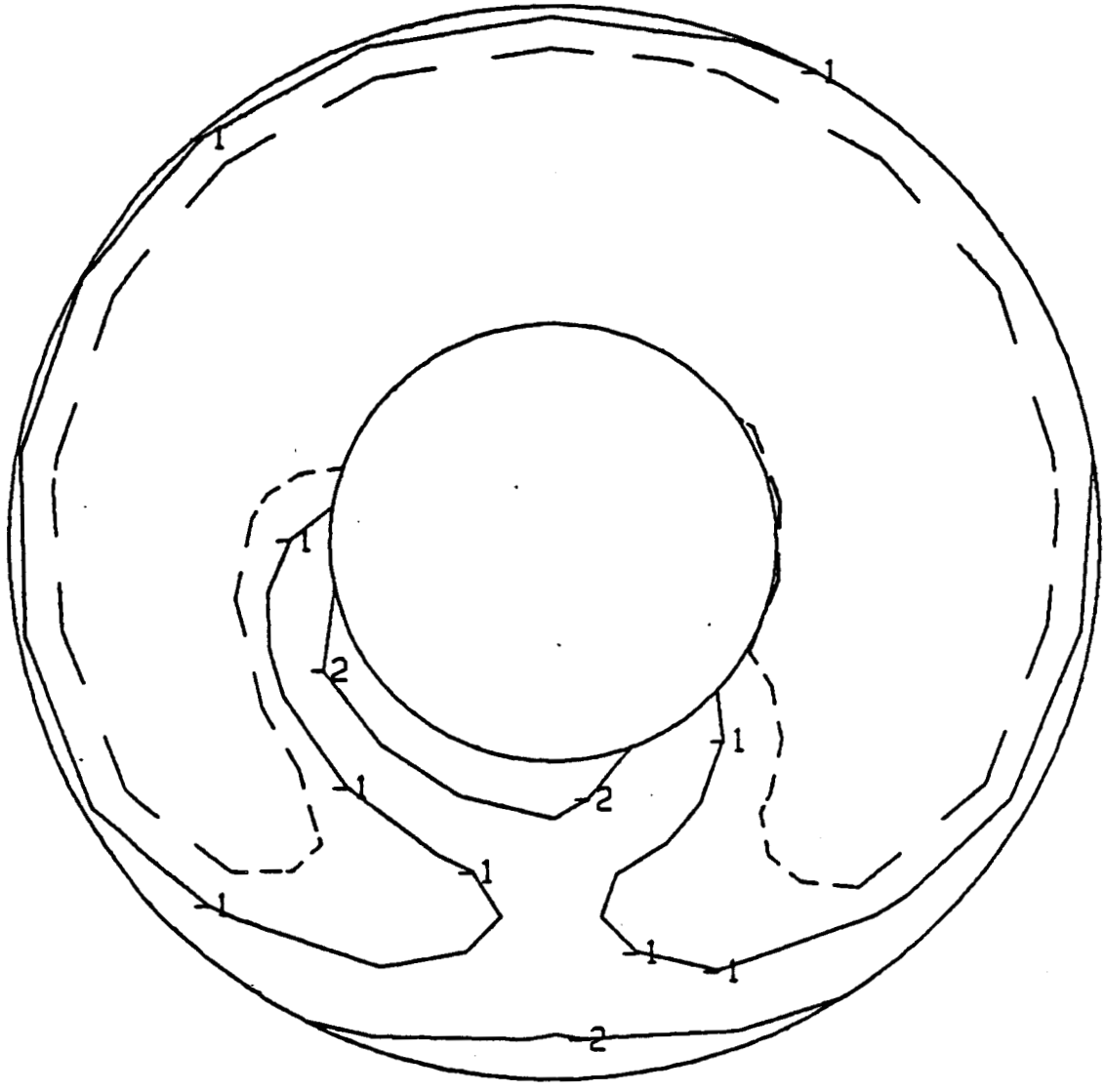

RUN	PT	ALPHA	CFMACH	WA2C
3	7	0.0	0.364	5.06

PT2/PTØ	DIST-CIR	FACTØR	DIST-RAD
0.995	0.107	0.024	0.030

Figure 35. Pressure Contour Map, Run No. 3, MCF = 0.36

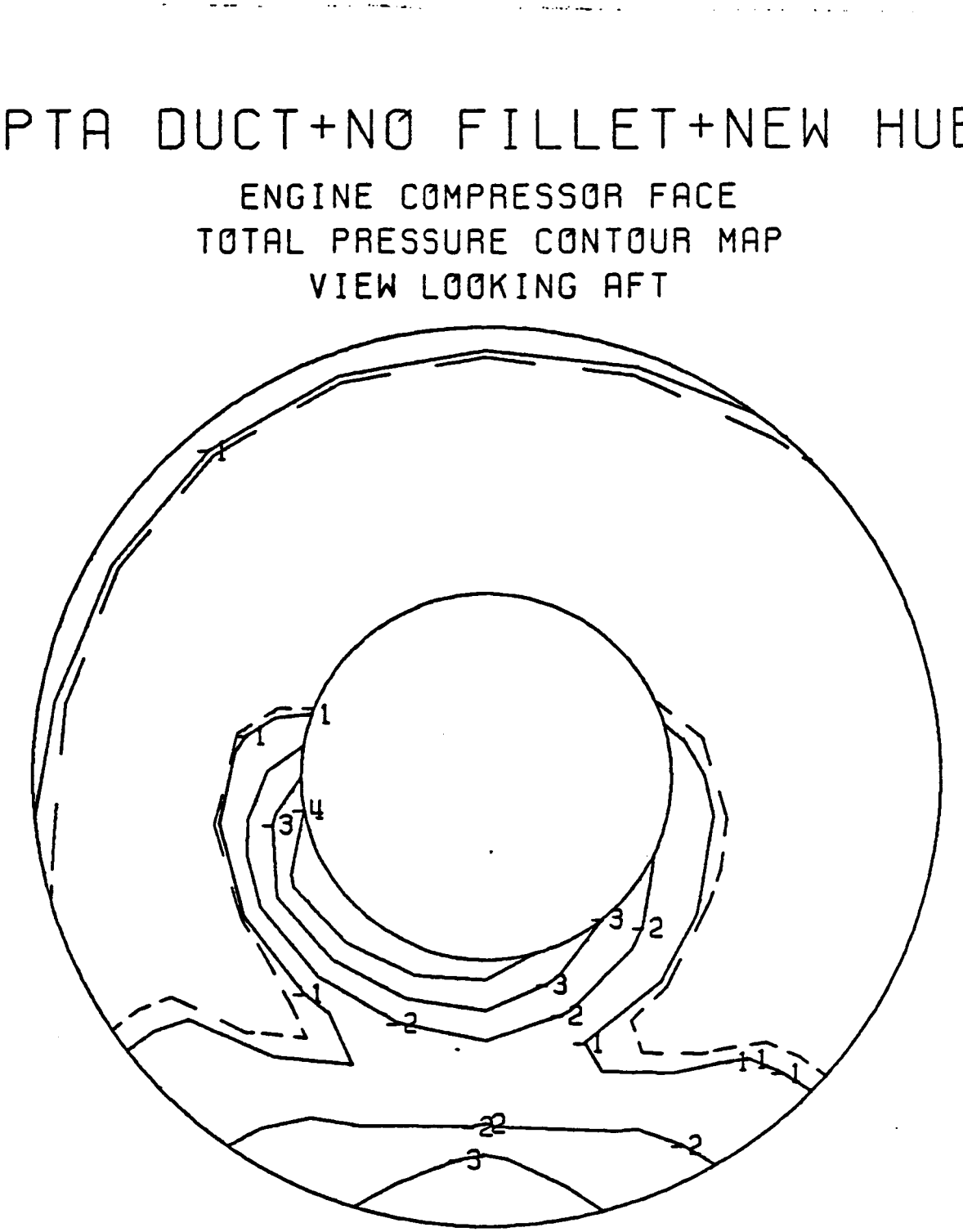

Figure 36. Pressure Contour Map, Run No. 3, MCF = 0.45

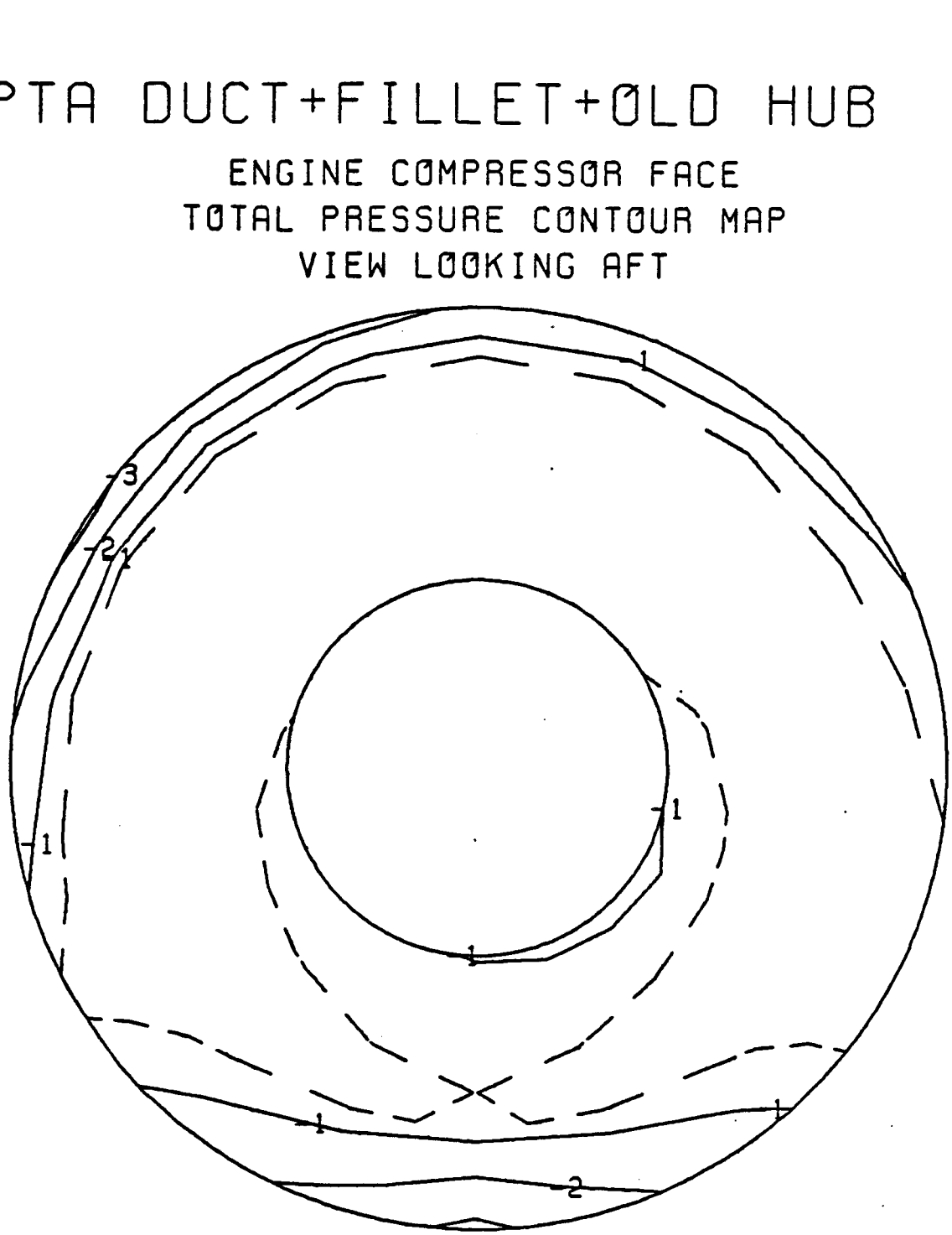

Figure 37. Pressure Contour Map, Run No. 4, MCF = 0.36

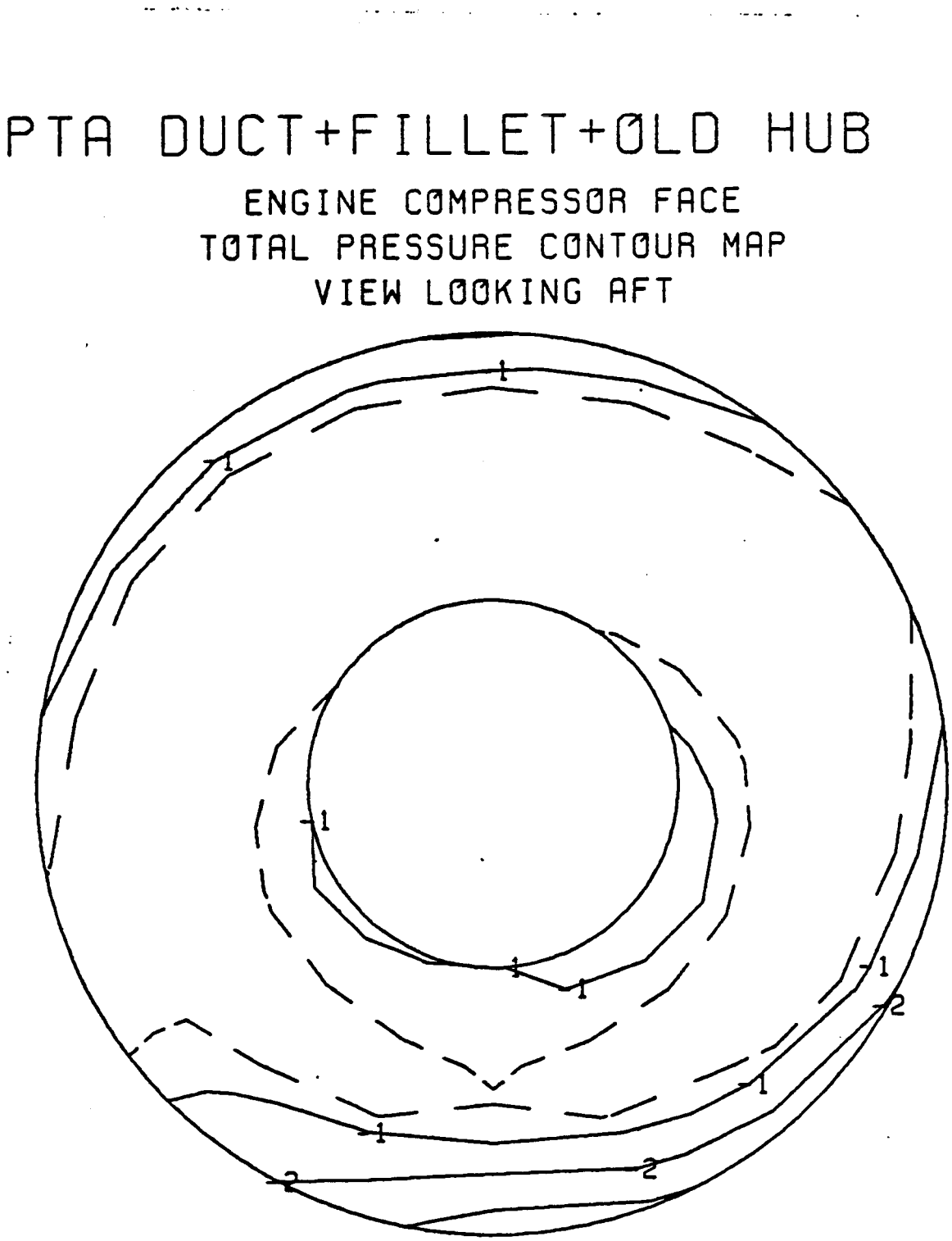

RUN	PT	ALPHA	CFMACH	WA2C
4	9	0.0	0.440	5.90

PT2/PTO	DIST-CIR	FACTOR	DIST-RAD
0.994	0.060	0.032	0.049

Figure 38. Pressure Contour Map, Run No. 4, MCF = 0.44

BASIC PTA DUCT, YAW=30 DEG

ENGINE COMPRESSOR FACE
TOTAL PRESSURE CONTOUR MAP
VIEW LOOKING AFT

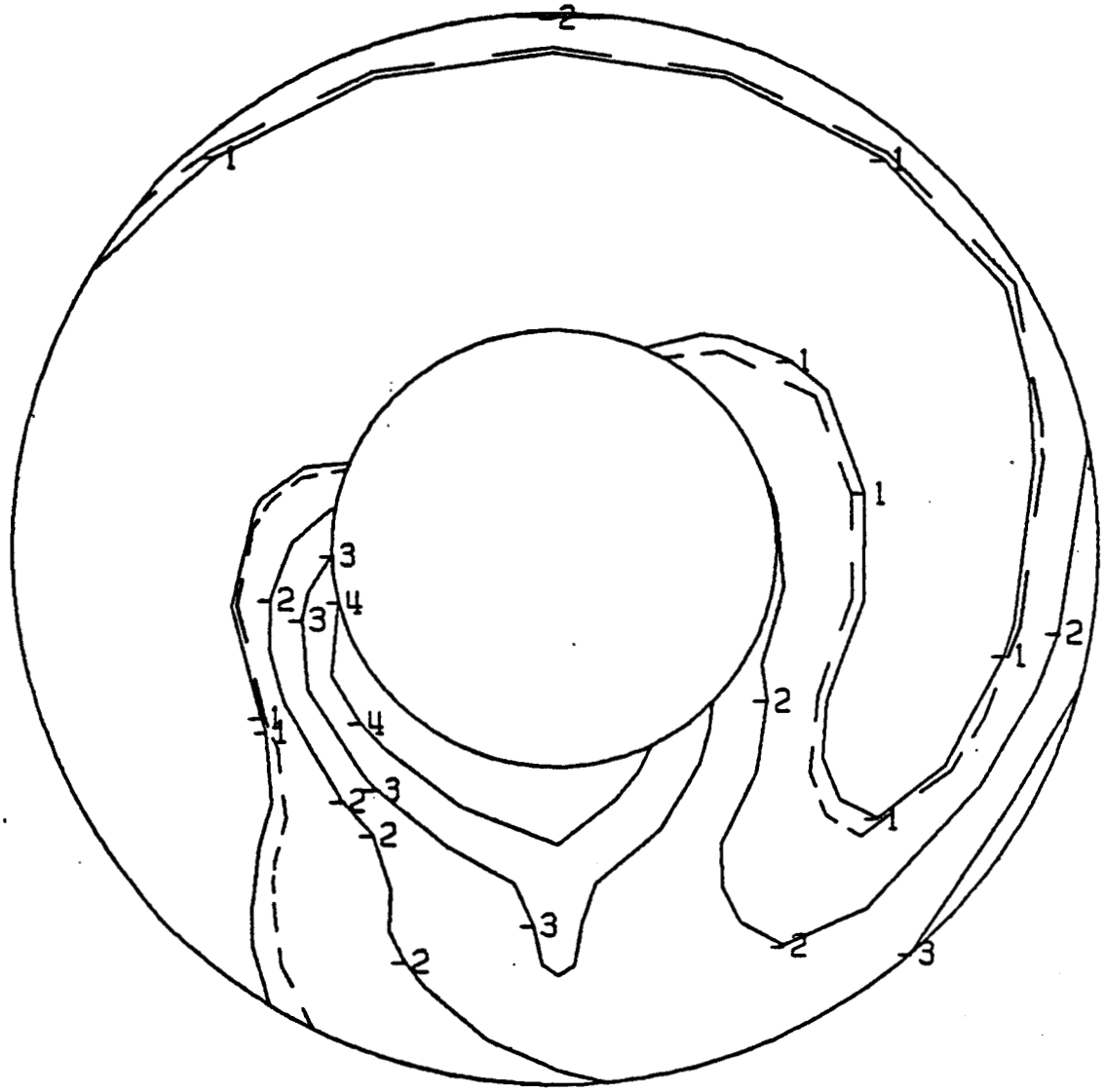

RUN	PT	ALPHA	CFMACH	WA2C
5	7	0.0	0.359	5.00

PT2/PT0	DIST-CIR	FACTOR	DIST-RAD
0.989	0.205	0.045	-0.014

Figure 39. Pressure Contour Map, Run No. 5, MCF = 0.36

BASIC PTA DUCT, YAW=30 DEG

ENGINE COMPRESSOR FACE
TOTAL PRESSURE CONTOUR MAP
VIEW LOOKING AFT

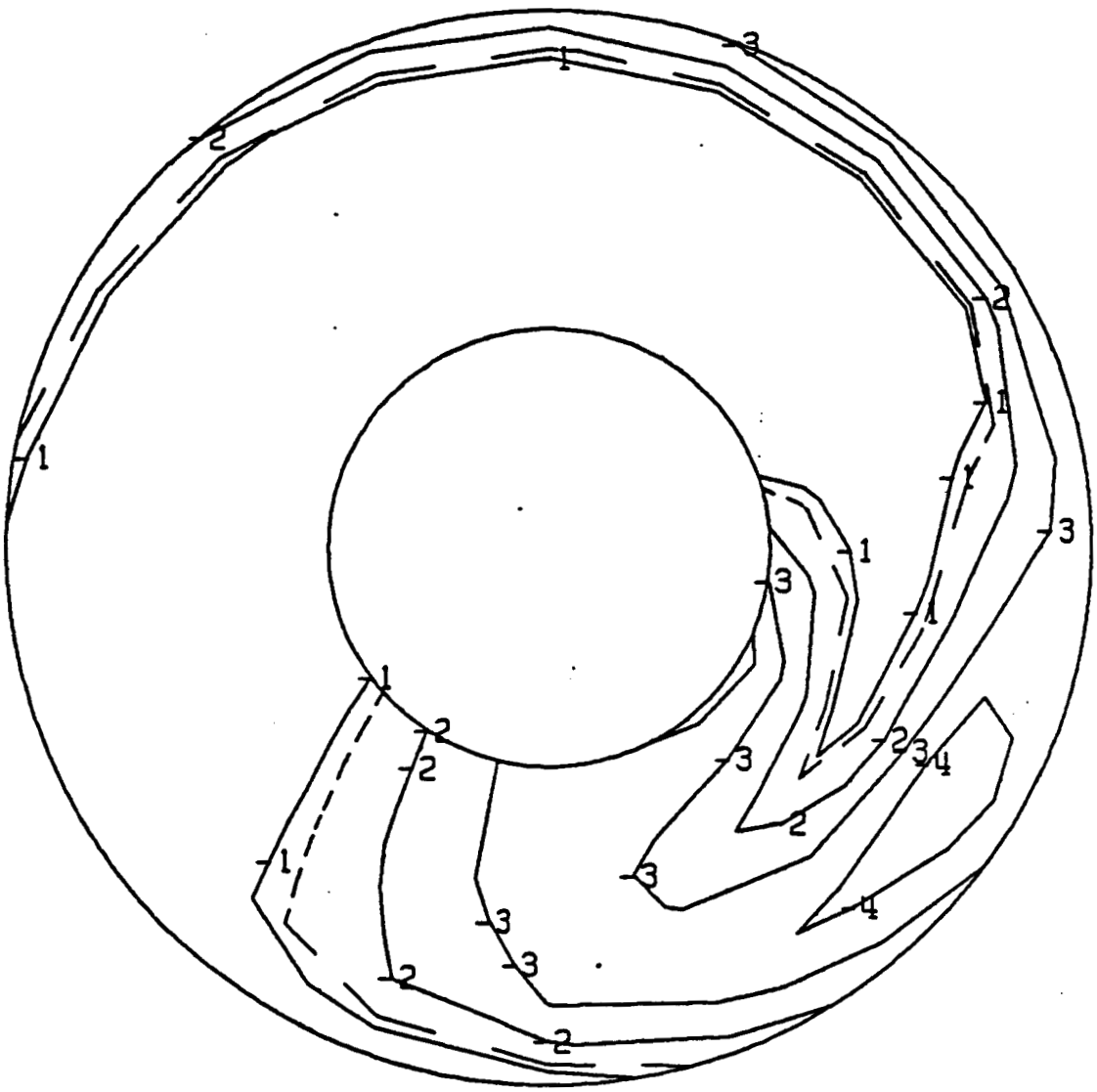

RUN	PT	ALPHA	CFMACH	WA2C
7	5	0.0	0.409	5.57

PT2/PT0	DIST-CIR	FACTOR	DIST-RAD
0.987	0.260	0.052	0.059

Figure 40. Pressure Contour Map, Run No. 7, MCF = 0.41

APPENDIX I

MODEL TEST DRAWINGS

PRECEDING PAGE BLANK NOT FILMED

PRECEDING PAGE BLANK NOT FILMED

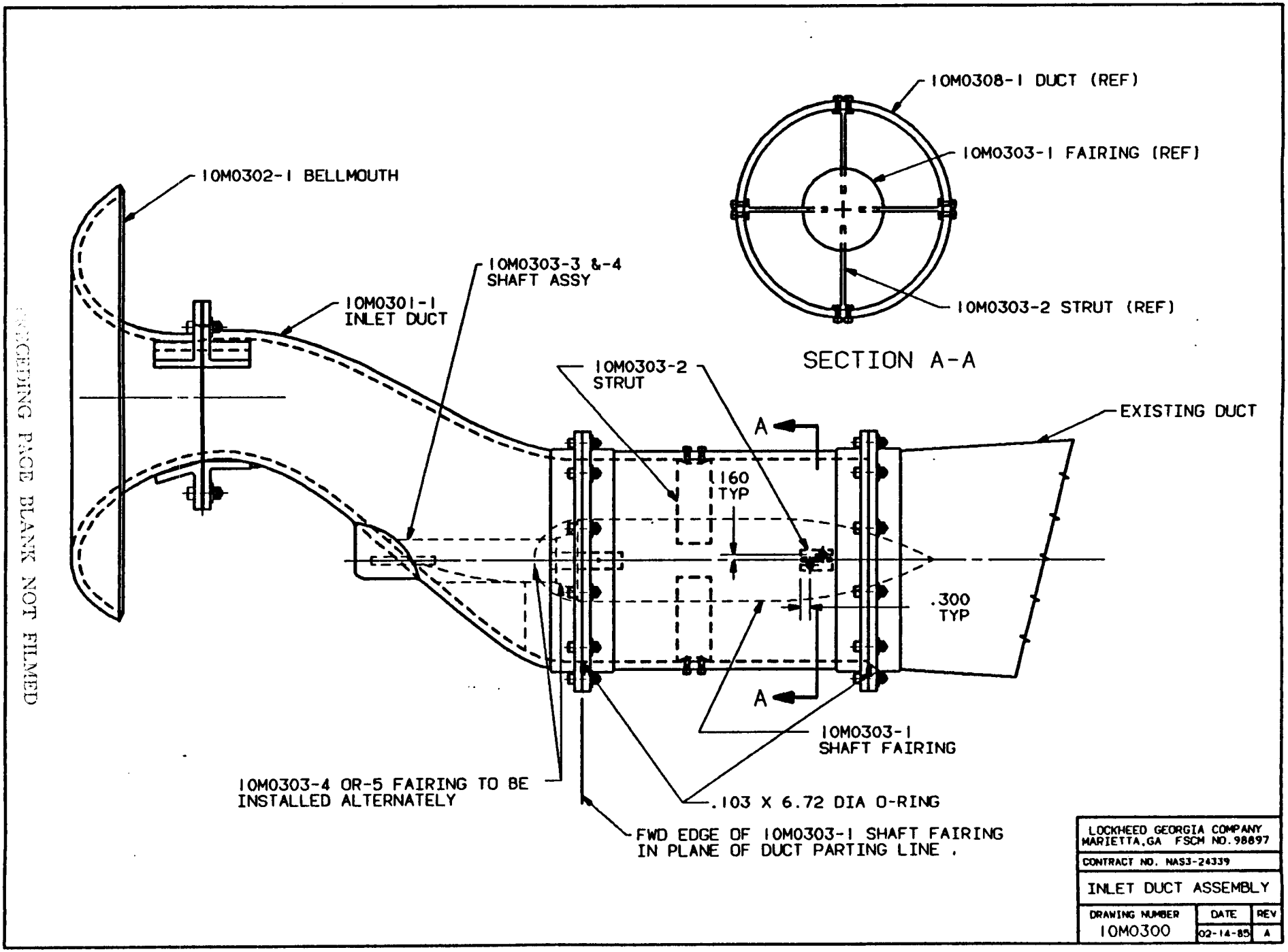

LOCKHEED GEORGIA COMPANY MARIETTA,GA FSCM NO.98897		
CONTRACT NO. NAS3-24339		
INLET DUCT ASSEMBLY		
DRAWING NUMBER	DATE	REV
10M0300	02-14-85	A

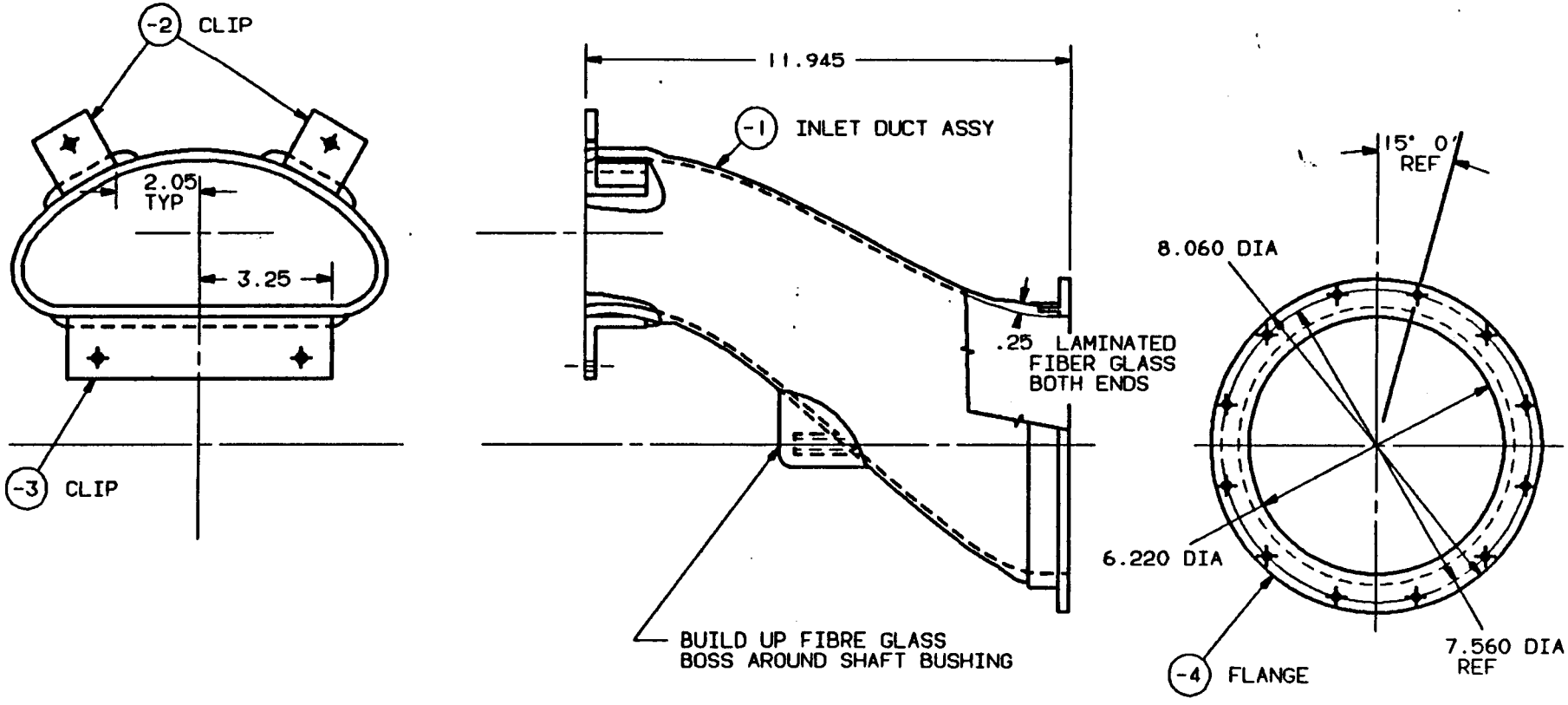

LOCKHEED GEORGIA COMPANY MARIETTA, GA FSCM NO. 98697		
CONTRACT NO. NAS3-24339		
INLET DUCT- D & A		
DRAWING NUMBER	DATE	REV
10M0301	02-14-85	A

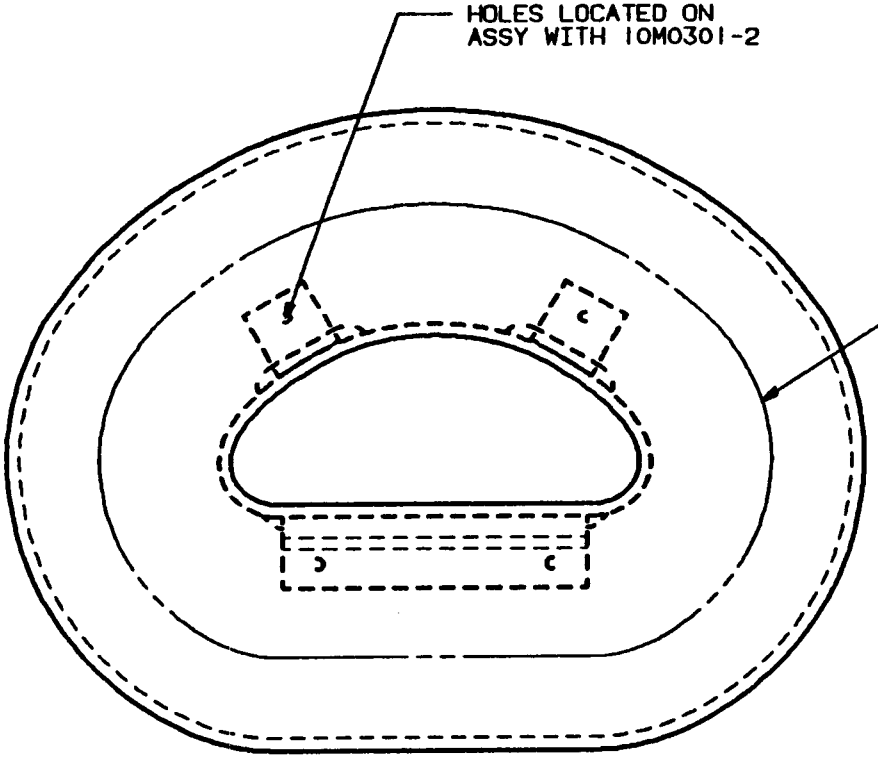

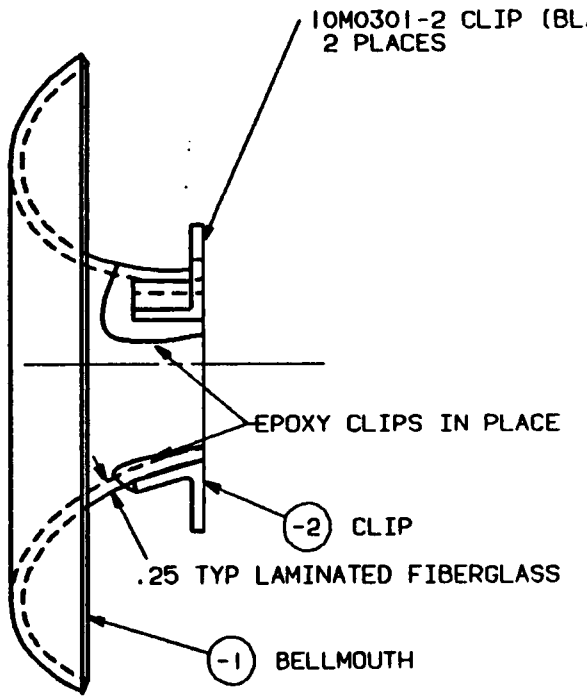

LOCKHEED GEORGIA COMPANY MARIETTA,GA FSCM NO.98897		
CONTRACT NO. NAS3-24339		
BELLMOUTH -D&A		
DRAWING NUMBER 10M0302	DATE 02-14-85	REV A

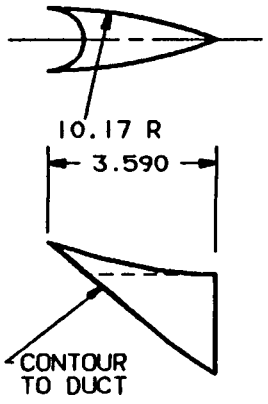

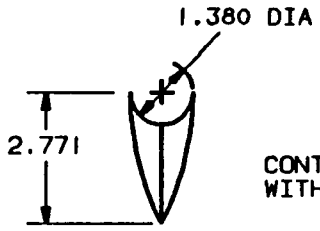

DETAIL-6 FAIRING (SMALL SHAFT)

EPOXY TO -4 SHAFT ON ASSY IN DUCT

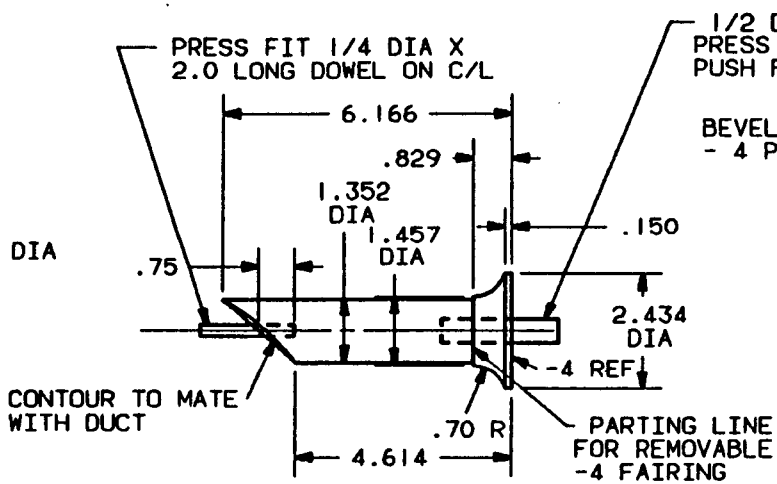

DETAIL -3 SHAFT -4 FAIRING

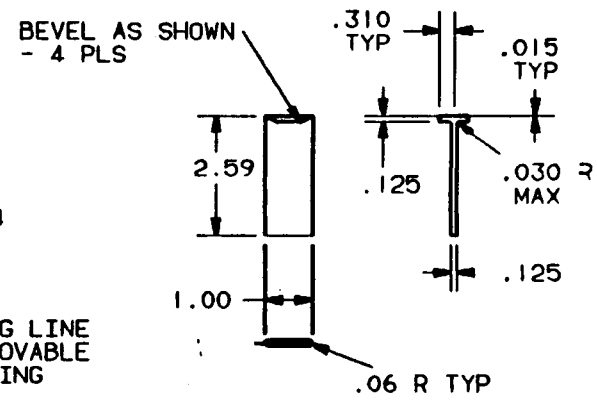

DETAIL -2 STRUT

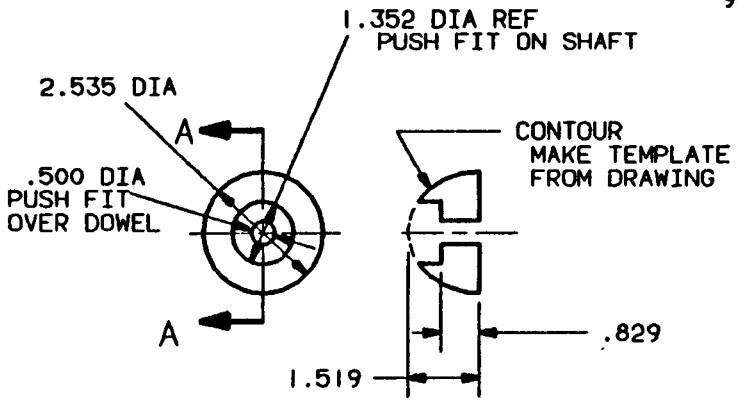

SECTION A-A

DETAIL-5 AFT SHAFT FAIRING

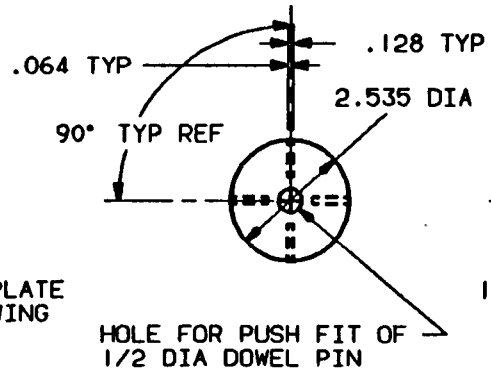

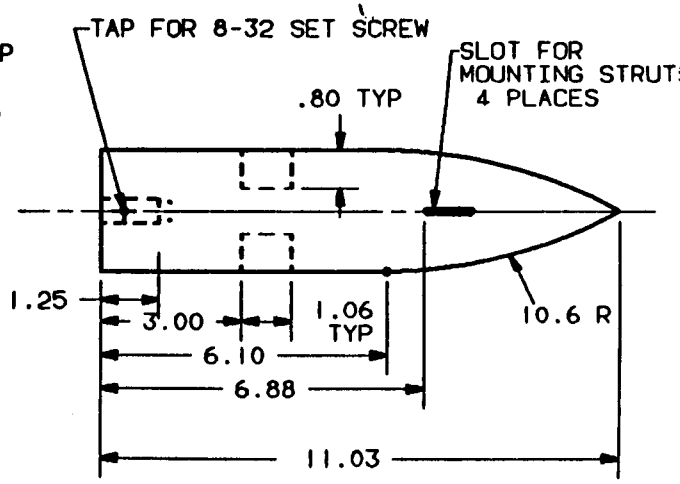

DETAIL -1 SHAFT FAIRING

LOCKHEED GEORGIA COMPANY MARIETTA,GA FSCM NO. 98837		
CONTRACT NO. NAS3-24339		
SHAFT DETAILS		
DRAWING NUMBER 10M0303	DATE 02-14-85	SH. 4

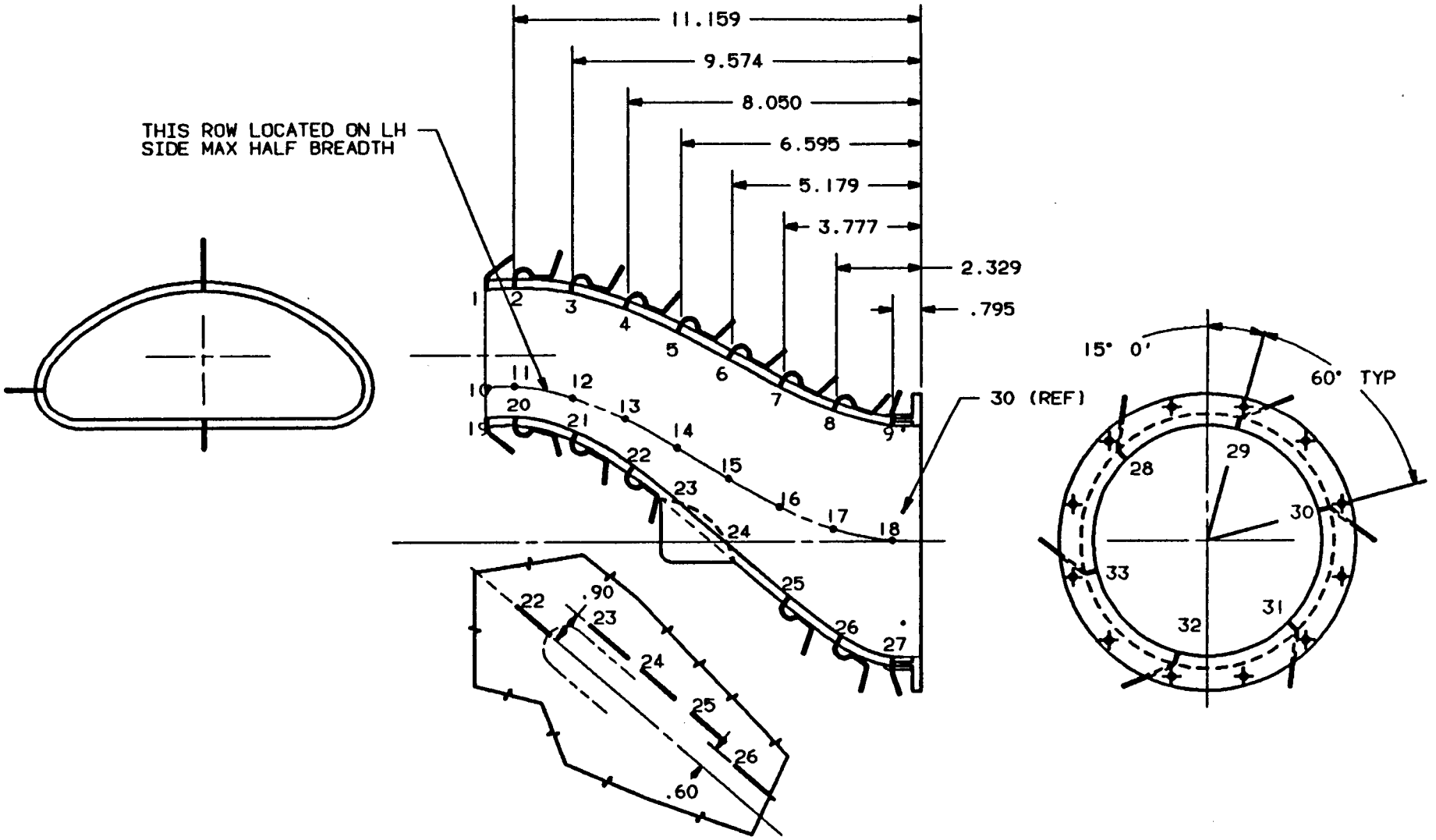

LOCKHEED GEORGIA COMPANY MARIETTA,GA FSCM NO.98897		
CONTRACT NO. NAS3-24339		
PRESSURE TUBE INSTL		
DRAWING NUMBER 10M0304	DATE 02-14-85	REV A

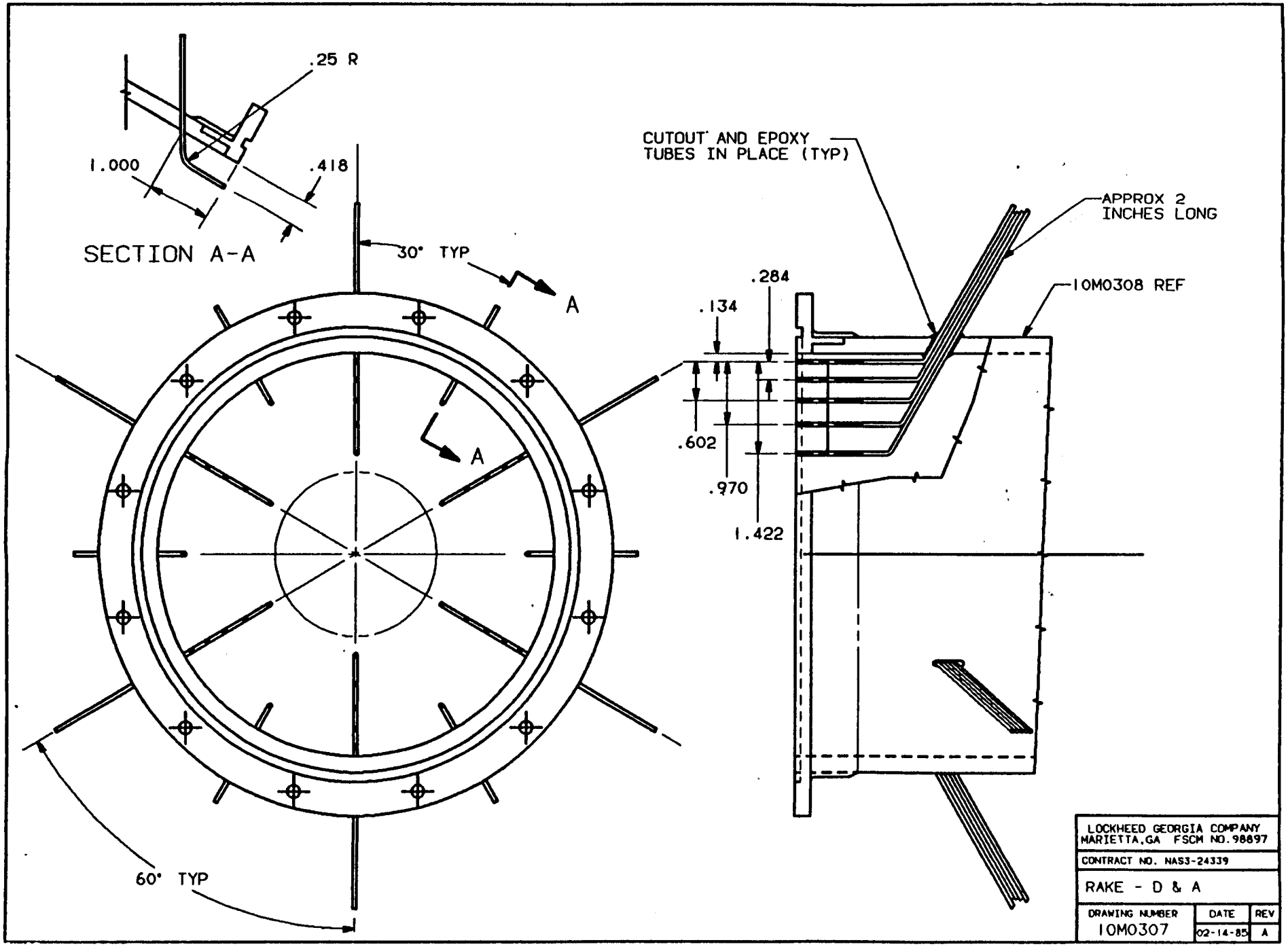

70

LOCKHEED GEORGIA COMPANY MARIETTA, GA FSCM NO. 98897		
CONTRACT NO. NAS3-24339		
RAKE - D & A		
DRAWING NUMBER 10M0307	DATE 02-14-85	REV A

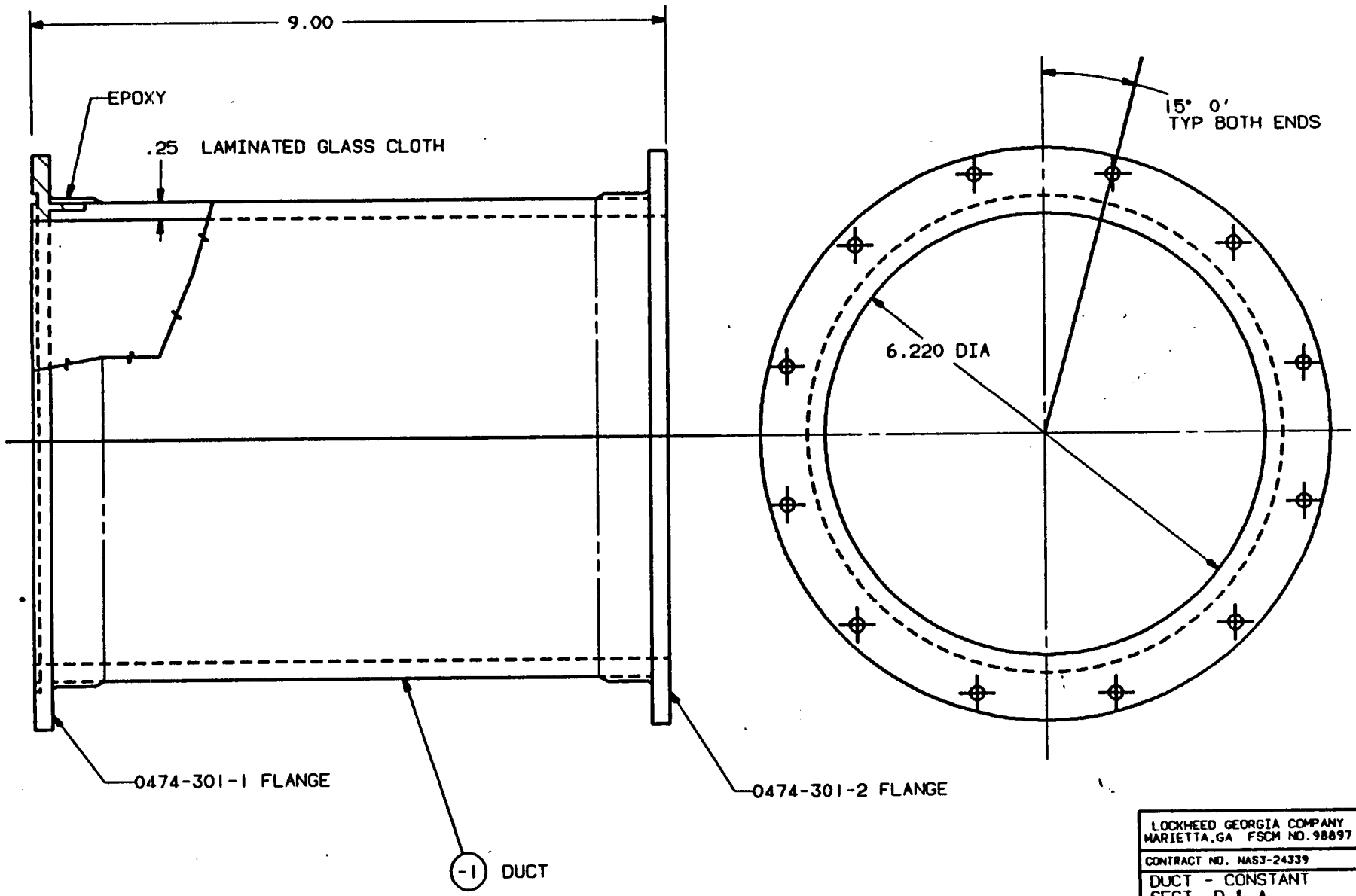

LOCKHEED GEORGIA COMPANY MARIETTA,GA FSCM NO.98897		
CONTRACT NO. NAS3-24339		
DUCT - CONSTANT SECT. D & A		
DRAWING NUMBER	DATE	REV
10M0308	02-14-85	A

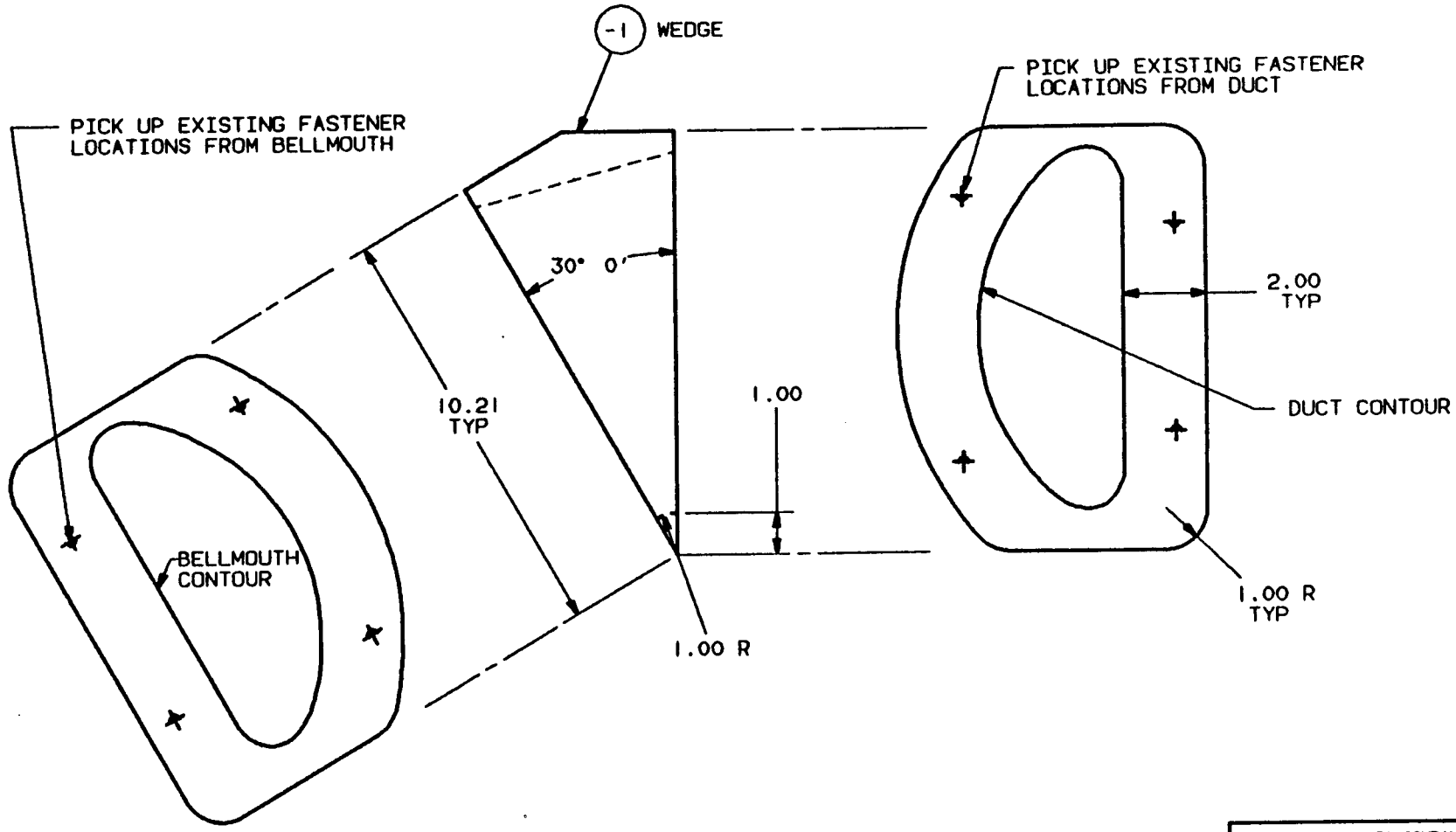

LOCKHEED GEORGIA COMPANY MARIETTA,GA FSCM NO.98697		
CONTRACT NO. NAS3-24339		
BELLMOUTH WEDGE		
DRAWING NUMBER 10M0309	DATE 02-14-85	REV A

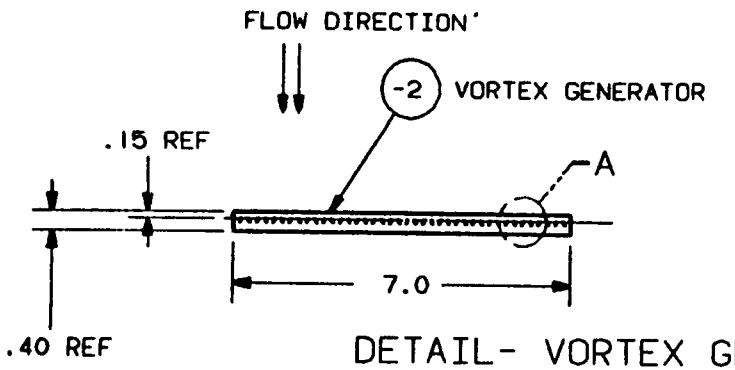

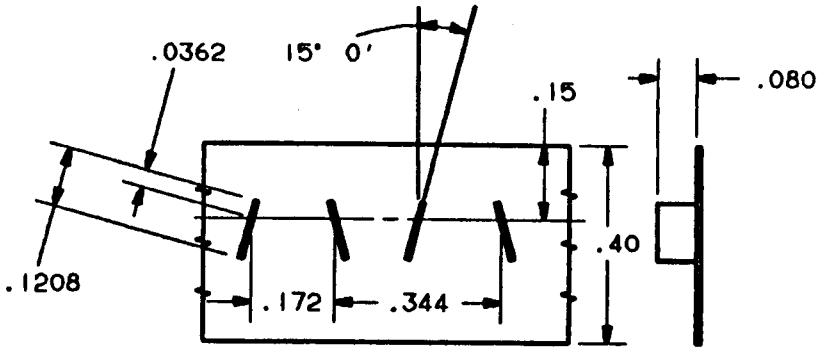

DETAIL- VORTEX GENERATOR

MAKE FROM .010 BRASS SOLDERED TOGETHER

INSTALL ON FLOOR OR DUCT AT PARTING LINE OF DUCT AND BELLMOUTH (BOND IN PLACE WITH INSTANT GLUE AND FAIR WITH WAX)

VIEW A

DIMENSIONS TYPICAL

SCALE 10/1

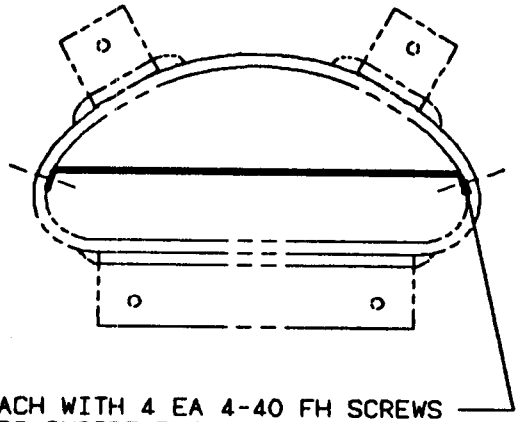

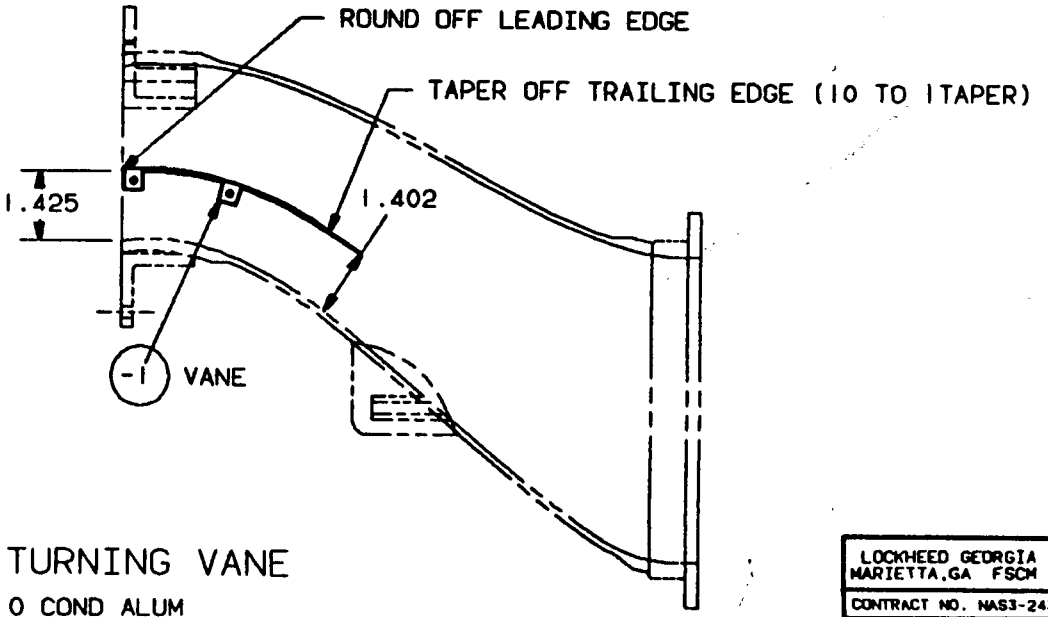

DETAIL-FLOW TURNING VANE

MAKE FROM .050 0 COND ALUM

LOCKHEED GEORGIA COMPANY MARIETTA,GA FSCM NO.98697		
CONTRACT NO. NAS3-24339		
INLET DUCT VORTEX GENERATOR & VANE		
DRAWING NUMBER	DATE	REV
10M0310	02-14-85	A

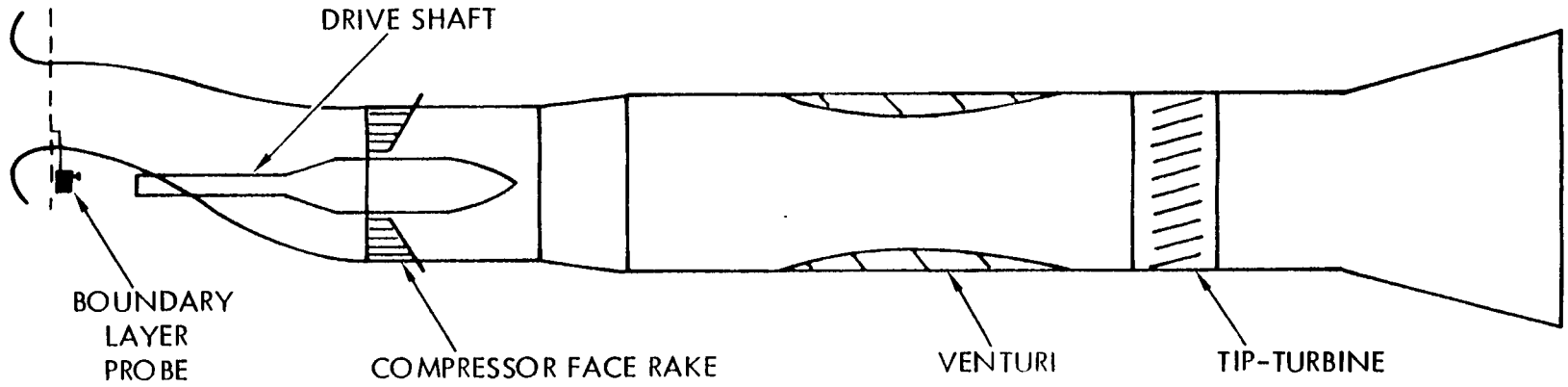

SK-1. Inlet Model Test Rig Assembly

REFERENCES

1. Little, B. H., Jr., and Trimboli, W. S., "An Experimental Investigation of S-Duct Diffusers for High-Speed Prop-Fans," Paper No. Aiaa-82-1123, June 1982.

2. Allison Gas Turbine Division of General Motors, "High Lift Helicopter Engines, Model XT701-AD-700, Prime Item Development Specification No. 844-C," June 1976, U.S. Army Approved, April 1977.

3. American Society of Mechanical Engineers, "Fluid Meters, Their Theory and Application," ASME Research Publication, Fourth Edition, 1937.

4. Society of Automotive Engineers, "SAE Aerospace Applied Thermodynamics Manual," SAE Committee AC-9, Second Edition, 1969.

5. Tanner, D. D., and Wynosky, T. A., "Engine Inlet Interaction with a Prop-Fan Propulsion System," SAE Paper No. 841478, October 1984.

1. Report No.	2. Government Accession No.	3. Recipient's Catalog No.
CR-174845		

4. Title and Subtitle	5. Report Date
PTA Test Bed Aircraft Engine Inlet Model Test Report	
	6. Performing Organization Code: 535-03-12
7. Author(s): J. P. Hancock	8. Performing Organization Report No.
	10. Work Unit No.
9. Performing Organization Name and Address: Lockheed-Georgia Co.	11. Contract or Grant No.
	13. Type of Report and Period Covered
12. Sponsoring Agency Name and Address	14. Sponsoring Agency Code

15. Supplementary Notes

Lewis Research Center Project Mgr.: E. J. Graber

16. Abstract

The inlet duct test for the Propfan Testbed Assessment (PTA) program was completed in November 1984. The basic test duct was designed using the Lockheed QUADPAN computational code. Test objectives were to experimentally evaluate, modify as required, and eventually verify satisfactory performance as well as duct/engine compatibility. Measured total pressure recovery for the basic duct was 0.993 with no swirl and 0.989 for inflow with a 30 degree simulated swirl angle. This compared to a predicted recovery of 0.979 with no swirl. Measured circumferential distortion with swirl, based on a least-square curve fit of the data, was 0.204 compared to a maximum allowable value of 0.550. Other measured distortion parameters did as well or better relative to their respective maximum allowable values. The basic duct configuration with no refinements is recommended for the PTA inlet as a minimum cost installation.

17. Key Words (Suggested by Author(s))	18. Distribution Statement
	[redacted]

19. Security Classif. (of this report)	20. Security Classif. (of this page)	21. No. of pages	22. Price*

*For sale by the National Technical Information Service, Springfield, Virginia 22161